BEHAVIOUR OF SISAL FIBER-REINFORCED CONCRETE IN EXTERIOR BEAM-COLUMN JOINTS UNDER MONOTONIC LOADING

OKEOLA Abass Abayomi

MASTER OF SCIENCE IN CIVIL ENGINEERING

(STRUCTURAL ENGINEERING OPTION)

PAN AFRICAN UNIVERSITY, INSTITUTE OF SCIENCE, TECHNOLOGY AND INNOVATION

2018

Behaviour of Sisal Fibre-Reinforced Concrete in Exterior Beam-Column Joints Under Monotonic Loading

OKEOLA Abass Abayomi

CE300-0011/17

A research thesis submitted to the Pan African University Institute of Basic Sciences, Technology and Innovation in partial fulfilment for the award of the degree of Master of Science in Civil Engineering (Structural Option) of the Pan African University.

2018

DECLARATION

I, OKEOLA Abass Abayomi, the undersigned do declare that this report is my original work and to the best of my knowledge, that it has not been presented for a degree in any other University or Institution.

Signature: …… Date:…….

OKEOLA Abass Abayomi

CE300-0011/17

This research thesis has been submitted for examination with our approval as University Supervisors.

Signature: …… Date:…….

Prof. (Eng.). Silvester Ochieng Aboudha

Department of Civil and Construction Engineering, University of Nairobi, Nairobi, Kenya.

Signature: …… Date: …….

Dr. (Eng.). John. N. Mwero

Department of Civil and Construction Engineering, University of Nairobi, Nairobi, Kenya

DEDICATION

To God Almighty and my ever supportive parents

ACKNOWLEDGEMENT

First and foremost, my sincere and heartfelt gratitude goes to Almighty Allah for helping me complete this fruitful study. Secondly, I will like to appreciate the African Union Commission (AUC) and AFRICA-ai-JAPAN for funding this research project. I am grateful to my dear supervisors Prof. (Eng.) Silvester Ochieng Aboudha and Dr. (Eng.) John. N. Mwero for their enormous guidance, insights and advices towards the accomplishment of this thesis. My sincere appreciation also goes to the Department of Civil Engineering of Pan African University Institute of Basic Science, Technology and Innovation (PAUISTI) and Jomo Kenyatta University of Agriculture and Technology (JKUAT) for providing me with the facilities required to carry out my experimental research work.

ABSTRACT

Concrete is the most widely used construction material because of its unique inherent properties, such as high compressive strength, good durability, fire resistivity, and low permeability. Aside from these positive properties are adverse characteristics, such as low tensile strength, brittleness, low resistance to cracking, and low impact resistance. These attributes made it necessary to investigate ways to improve the properties of concrete. Some of these deficiencies, such as low tensile strength, can be improved by incorporating optimum amount of certain fibers in concrete. Sisal is one of the numerous natural fibers that have shown great promise over the years. It possesses many advantageous properties, which include sustainability, high tensile modulus, and low cost. It is locally available in Kenya, Tanzania, and Brazil. It can be incorporated into the cementitious matrix to improve its mechanical strength, post-yield behaviour as well as inhibits crack propagation. In this study, the physical and mechanical properties of sisal fiber reinforced concrete was investigated. Durability performance in terms of strength and weight changes was reported at 45 and 90days. The concrete reinforced with sisal fiber was used to cast beam-column joints, the beam has a size of 150mmX150mm, 800mm long while the rectangular column was 150mmx200mm, 1m long. The joints were tested under monotonic load and verified using Finite element analysis. The Finite element analysis was done using Abaqus CEA where

Concrete damage plasticity was used to model the concrete and uniaxial stress strain for the steel reinforcement. Sisal fiber with an aspect ratio of 230 and tensile strength of 373N/mm^2 were added to the mix at 0.5%, 1.0%, 1.5% and 2.0% by weight of cement. A design mix ratio of 1: 1.92: 3.68 for cement: fine aggregates: coarse aggregates with a constant water to cement ratio of 0.47 was used. Physical tests carried out include workability on fresh concrete, density and water absorption on hardened concrete at 28 days. Mechanical tests carried out include compressive strength. Splitting tensile strength, Young's Modulus and Poisson's ratio. The crack pattern, ultimate load, ultimate deflection and shear capacity of beam-column joints made with sisal fiber reinforced concrete was also reported. The results shows that there was an improvement in splitting tensile strength and Young's Modulus at 1.0% fiber incorporation. Sisal fiber plays a crucial role in arresting crack propagation. There was a general decrease in the compressive strength as the fiber content increased. However the performance of beam –column joints improved for all fiber content and Abaqus CEA can be used to model the behaviour of sisal fiber reinforced beam - column joints.

TABLE OF CONTENT

LIST OF TABLES

LIST OF FIGURES

LIST OF ABBREVIATIONS AND ACRONYMS

SFRC = Sisal Fiber reinforced concrete

FRC = Fiber reinforced concrete

SSD = Saturated surface dry

FRP = Fiber reinforced polymer

NFRC = Natural fiber reinforcement concrete

a_s = distance from extreme compressive fiber to the centroid of compressive reinforcement

A_{sh} = area of shear reinforcement in the joint

b_b = width of beam

b_c = width of column

b_f = bond efficiency factor (= 0.75)

b_j = effective width of joint transverse to the direction of shear

d = effective depth of beam

d_b = diameter of beam longitudinal reinforcement

d_f = diameter of fiber

E_s = modulus of elasticity of steel

E = Modulus of elasticity of concrete

F_{ac} = axial compressive strength of concrete

F_o = increased joint compressive strength due to confinement (= $Kf_c^{'}$)

fc' = compressive strength of concrete

f_{cr} = modulus of rupture of concrete

F_{ys} = yield strength of transverse reinforcement

h_b = total depth of beam

h_c = total depth of column

h_j = effective depth of joint parallel to the direction of shear

K = $k = 1 + \frac{\rho_s f_{ys}}{f_o}$

l_f = length of fiber

N = axial compressive load of column

S	=	spacing of stirrups
$V_{(exp.)}$	=	experimental value of ultimate shear strength
$V_{(pre.)}$	=	predicted value of ultimate shear strength
$V_{(th.)}$	=	theoretical value of ultimate shear strength
v_f	=	volume fraction of fibers
X	=	neutral axis depth
ρ_s	=	volume ratio of transverse hoop reinforcement
f_y	=	yield strength of reinforcement
Γ	=	Joint shear stress expressed as a multiple of $\sqrt{f_c'}$
λ	=	capacity reduction factor (= 0.78)
σ_t	=	Tensile strain
ε_t	=	Total strain
ε_{ck}	=	Cracking strain

CHAPTER ONE - INTRODUCTION

1.1. Background of the Study

The point of intersection of beam and columns is called a beam-column joint (Muthupriya, Boobalan, and Vishnuram 2014). The joints are critical sections in RC structures, it is an area where the bond and normal stresses are considerably high (Gnanapragasam, Chitra, and Ravi 2016). The behaviour of a beam-column joint is influenced by many factors such as concrete grade, column load, and detailing arrangements of the column and beam reinforcement bars (Swar et al. 2015). The joint should therefore have sufficient strength and endurance to resist the internal forces transferred by the framing members.

Due to difficulty in rehabilitating buildings damaged at the joints in cases of structural failure or seismic forces, it is necessary to provide sufficient strength and ductility for beam-column joints even in countries not located in seismic zones. Many techniques have been suggested in making beam-column joints stronger against shear stresses and seismic forces. Such techniques included the use of extra hoops, transverse reinforcement and of recent, fibers as constituents and polymers (Kadarningsih et al. 2014; Swar et al. 2015). Fibers have shown tremendous potential in not just increasing the mechanical strength of concrete but also improving the ductility and energy absorption of beam-column joints (Muthuswamy and Thirugnanam 2014). Fibers can be selected singly or used in combination with other fibers such that the weakness of one is compensated for by the strength of another.

Synthetic and hybrid fibers such as glass and steel are mostly used in civil engineering

construction to improve the ductility of beam-column joints and also reduce reinforcement congestion and honeycombing at the joints, but due to fast depleting natural resources and huge consumption of energy involved in its production, researchers have been looking inward for green and sustainable options to replace steel (Singh and Sujana 2013). Strong vegetables fibers such as sisal, hemp and jute have looked promising in this regard. They have been used to toughen bricks and pottery since the very beginning of civilization (Singh and Sujana 2013; Vajje and Krishna 2014).

1.2. Statement of Problem

Severe reverse cyclic loading due to earthquakes causes large inelastic deformations in the beam-column joints of high-rise buildings. If the joints are not designed and detailed properly, their performance can significantly affect the overall response of the moment-resisting frames. Due to the restriction of space available in the joint block, the detailing of joint reinforcement assumes more significance than elsewhere. One of the basic assumptions of the frame analysis is that the joints are strong enough to sustain the forces (i.e., moments, and axial and shear forces) generated by the loading, and to transfer the forces from one structural element to another (i.e., from beams to columns in most of the cases). The analysis with the assumption of joint being rigid fails to consider the effects of high shear forces developed within the joint).

Over the years, numerous cases of earthquake reported in different parts of Africa (See Appendix A1) have demonstrated that even when the beams and columns in a reinforced concrete frame remain intact, the integrity of the whole structure is compromised if the joints, where these members are connected, fail. Unfortunately,

high and mid- rise structures in Africa are designed as beam-column rigid frames in accordance with the obsolete British Standard (BS8110) without seismic considerations (Eurocode 2, on the other hand addresses seismic forces). This seismic forces subject joints to moments, horizontal and vertical shear forces under seismic excitations and loads which may be higher than its capacity. Thus the beam-column joints are susceptible to failure earlier than the adjacent members due to the destruction of joint zone. This failure is mainly for the external joints. Therefore, ductility and energy absorption capacity of the beam-column joints are of paramount importance in the seismic resistance of structures

1.3. Justification

Beam-column RC joints are subjected to moments, horizontal and vertical shear forces under seismic excitations and require high ductility for energy dissipation (Swar et al. 2015). The use of additional reinforcement bars can lead to congestion and honeycombing at the joints. This can be avoided, especially when addition of natural fibers could potentially provide the joints with the required ductility and energy absorption capacity. Although, partially failed joints can be repaired, the task is reactive rather than proactive and is difficult to execute. Therefore, further research must be done to improve the performance especially the ductility capacity in beam-column joints using sustainable, locally available materials to prevent structural failure in the event of seismic activities to ensure safety of lives and properties as well as reduce cases of structural collapse.

1.4. Objectives

1.4.1. General Objective

The general objective of this study is to investigate the behaviour of sisal fiber reinforced concrete (SFRC) in exterior beam-column joints under monotonic loading.

1.4.2. Specific Objectives

1. To determine the compressive and tensile strength of sisal fiber reinforced concrete.
2. To assess the durability of sisal fiber reinforced concrete in acidic and alkaline medium.
3. To evaluate the characteristics of beam-column concrete joints reinforced with sisal fiber under monotonic loading.
4. To develop a finite element model that predicts the behaviour of beam-column sisal fiber reinforced concrete joints under monotonic loading.

1.5. Research Questions

1. What is the effect of sisal fiber on the strength of concrete?
2. What is the effect of extreme environmental condition on the strength of SFRC?
3. Can Sisal fiber improve the ductility of beam column joints?
4. Can a Finite Element model be used to predict the behaviour of SFRC beam-column joints?

1.6. Scope of Study

The study will focus only on exterior beam-column joint under monotonic loading. The performance of five beam-column joint specimens with different volume fractions of sisal fiber will be compared. All test specimens will be designed in accordance to BS 8110 (Obsolete but still used in most African countries). This project research is limited to Africa, and a case study of Kenya will be used. All materials that will be used in this study will be obtained from suitable sites in Kenya,

CHAPTER TWO-LITERATURE REVIEW

2.1. Fiber Reinforced Concrete

Fiber-reinforced concrete (FRC) is concrete containing fibrous material which increases its structural integrity. It contains short discrete fibers that are uniformly distributed and randomly oriented. Fibers include steel fibers, glass fibers, synthetic fibers and natural fibers – each of which lend varying properties to the concrete. In addition, the character of fiber-reinforced concrete changes with varying concretes, fiber materials, geometries, distribution, orientation, and densities. The mechanical behaviour of fibre reinforced concrete (FRC) depends largely on the interactions between the fibres and the brittle concrete matrix: physical and chemical adhesion; friction; and mechanical anchorage induced by complex fibre geometry or by deformations or other treatments on the fibre surface. The "first generation" steel fibres, produced by shearing thin sheets of steel, were not very efficient, because they were too smooth to bond well with the matrix. Subsequently, many different fibre geometries were developed to improve the mechanical anchorage, which is the most important of the bonding mechanisms. Surface treatments of the synthetic (mostly polypropylene) fibres have been similarly employed to improve the fibre-matrix bond.

There are two methods to categorize fibres according to their modulus of elasticity or their origin. In the view of modulus of elasticity, fibres can be classified into two basic categories, namely, those having a higher elastic modulus than concrete mix (called hard intrusion) and those with lower elastic modulus than the concrete mix (called soft intrusion).

Steel, carbon and glass have higher elastic modulus than cement mortar matrix, and polypropylene and vegetable fibres are classified as the low elastic modulus fibres. High elastic modulus fibers simultaneously can improve both flexural and impact resistance; whereas, low elastic modulus fibres can improve the impact resistance of concrete but do not contribute much to its flexural strength. According to the origin of fibres, they are classified in three categories of metallic fibers (such as steel, carbon steel, and stainless steel), mineral fibers (such as asbestos and glass fibers), and organic fibers. Organic fibers can be further divided into natural and man-made fibers. Natural fibers can be classified into vegetable origin or sisal (such as wood fibers and leaf fibers), and animal origin (such as hair fibers and silk).

2.1.1. Synthetic fiber reinforced concrete

Plain concrete is brittle, with limited ductility resulting in little resistance to cracking. The internal micro cracks present in concrete are propagated when subjected to tensile stress, resulting in brittle fracture of concrete (Prahallada, Shanthappa, and Prakash 2014) ultimately leading to insufficient energy absorption capacity under alternating loads. Steel reinforcement is sufficient in providing the required tensile strength for concrete, but it doesn’t adequately address the issue of micro cracks present in concrete. Steel fiber reinforced concrete (StFRC) is produced using the conventional hydraulic cements, fine and coarse aggregates, water, and Short discrete steel (SFs). American concrete institution (ACI 544.IR, 1996) defines SFs as discrete, short lengths of steel having aspect ratio (ratio of length to diameter) in the range of 20 to 100 with any of the several cross-section which are sufficiently small to be easily and randomly dispersed in fresh concrete mix using conventional mixing procedures. To

enhance the workability and stability of StFRC, superplasticizers (chemical admixtures) may also be added into the concrete mix

The behaviour of StFRC can be classified into three groups according to its application, fiber volume percentage and fiber effectiveness; for instance SFRC is classified based on its fiber volume percentage as follows: 1-Very low volume fraction of SF (less than 1% per volume of concrete), which has been used for many years to control plastic shrinkage and as pavement reinforcement. 2-Moderate volume fraction of SFs (l% to 2% per volume of concrete) which can improve modulus of rupture (MOR), flexural toughness, impact resistance and other desirable mechanical properties of concrete. 3-High volume fraction of SFs (more than 2% per volume of concrete) used for special applications such as impact and blast resistance structure; these include SIFCON (Slurry Infiltrated Fiber Concrete), SIMCON (Slurry Infiltrated Mat Concrete). In most cases, SFs may act as secondary reinforcement used along with conventional steel bars or pre-stressing strands as the main reinforcement. In the class of high volume fraction of SFs (more than 2% per volume of concrete), the SFs have excellent mechanical properties and can be used without other continuous reinforcement; however, these composite materials are often suited for highly specialized applications due to the limitations associated with processing and cost.

2.1.2. Natural fiber reinforced Concrete

Natural fibers as shown in figure 2.1 are of interest in recent times due to its sustainability and environmental friendly characteristics (Farghaly, Tobbi, and Benmokrane 2009). It is also very cheap and has shown encouraging mechanical properties when mixed with concrete (Samuel, Agbo, and Adekanye 2012). It serves

as a crack arrestor (Vajje and Krishna 2014) and can significantly boost the tensile strength of its composite. Some reported properties of natural fibers are presented in Table 2.1 and 2.2.

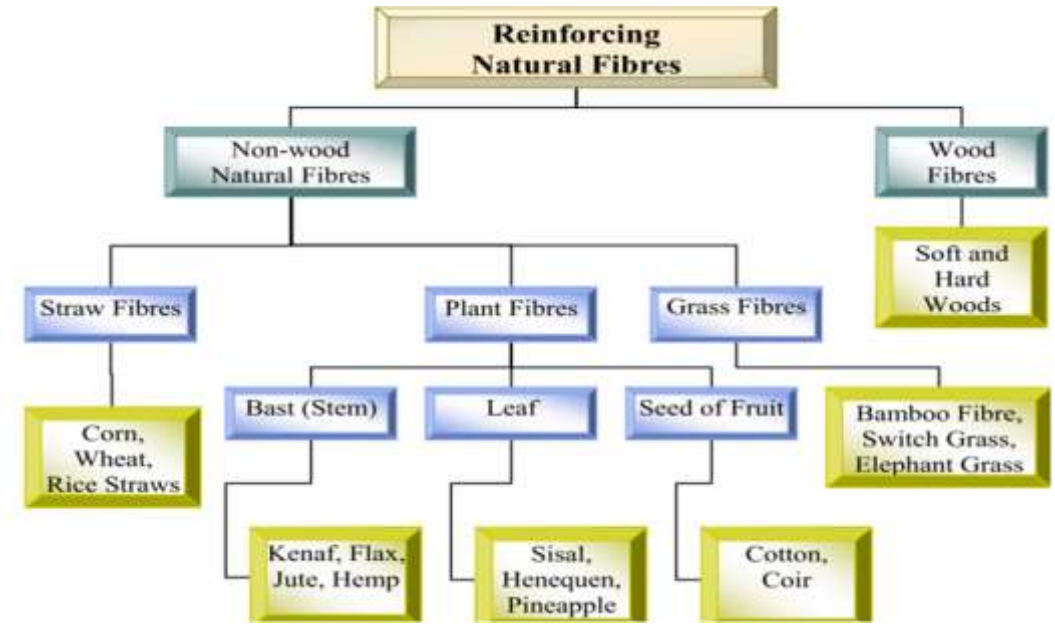

Figure 2- 1: Classification of natural fibers.

.Table 2- 1: Physical and mechanical properties of some natural fibers (Danso et al., 2014)

Fibers	Density (g/cm^3)	Tensile strength (MPa)	E (GPa)	Elongation at break (%)
Flax	1.50–1.53	450–1100	27.6	2.7-3.2
Sisal	1.45	468–640	9.4-22	3-7
PALF	1.44	413–1627	34.5-82.5	1.6
Ramie	1.50	400–938	61.4-128	1.2-3.8
Jute	1.30–1.45	393–773	13-26.5	7-8
Cotton	1.50–1.60	287–800	5.5-12.6	7-8
Coir	1.15	131–175	4-6	15-40

Table 2- 2: Chemical composition of important plant fibers (Mwaikambo 2006)

Fiber	Cellulose (%)	Hemicellulose (%)	Lignin (%
Cotton	82–96	2–6	0.5–1
Pineapple	80–81	16–19	4.6–12
Hemp	70–92	18–22	3-5
Flax	72–84	16–18	0.6-5
Ramie	68–76	13–15	0.6-1
Banana	60–65	6–19	5-10
Jute	51–84	12–20	5-13

2.1.3. Challenges with the use of Natural fibers

Natural fibers are one of the most studied materials. However, the use of these remains a challenge as question remains over their durability.

2.1.2.1. Aging and Degradation Natural fibers

Vegetable fibers in lime content environment of cement matrices undergo an aging process during which they may suffer a reduction in strength and toughness as a result of weakening of the fibers. The aging process called mineralization is due to alkali attack on the fiber (Flávio de Andrade, Mobasher, and Filho 2009).

2.1.2.2. Treatments of natural fibers for improved durability

The durability of natural fibers in concrete can be improved by matrix modification, fiber modification, and combined fiber-matrix modification (Priyadharshini and Ramakrishna 2014; Sabarish et al. 2017; Singh and Sujana 2013). Most commonly adopted treatment is the use of water repellant and alkali treatment (Ozerkan et al. 2013). The hydrophilic tendency can be addressed by finding a surface treatment of fibers to reduce the water absorption without harming the fibers matrix bond. This can be done by using moisture inhibiting chemicals such as Sulphur (Corinaldesi and

Moriconi 2004). Matrix modification can also be done by replacing ordinary Portland cement OPC with supplementary cementitious materials such as fly ash, silica fume, slag and metakaolin thereby reducing alkalinity (Singh and Sujana 2013). Sisal fiber hence, do not get deteriorate with time when we used in a low content calcium Portland cement (Sood and Sood 2017).

A marked improvement in fiber durability was also observed when using high alumina cement and natural pozzolans such as calcined waste crushed clay brick (Toledo Filho et al. 2009; Tolêdo Filho et al. 1999). The reaction between the fiber and the NaOH during alkali treatment is described by the following chemical equation: Fiber-cell-OH + NaOH → fiber-cell-O-Na^+ + H_2O + impurities. Fibers were able to preserve their flexibility and strength in areas with carbonated concrete with a pH of 9 or less (Pacheco-Torgal and Jalali 2011). However, too much reduction of the alkalinity of concrete matrix (to Ph < 10) will incur decomposition of passive layer of steel reinforcement. Ternary blends containing slag/ metakaolin and silica fume are effective in preventing fiber degradation (Pacheco-Torgal and Jalali 2011). The embrittlement of the sisal reinforced concrete composite can be avoided almost completely by immersing sisal fiber in a condensed silica fume slurry before adding them to the mix.

2.2. Properties of Sisal fibers reinforced concrete

Sisal fiber is a hard fiber extracted from the leaves of sisal plants (Agave sisalana). It is one of the most widely used natural fibers and is easily cultivated (see Figure 2.2). Nearly 4.5 million tons of sisal fiber is produced every year throughout the world (Sabarish et al., 2017). Brazil (125ktons), Mexico (120Ktons), Tanzania (26Ktons) and

Kenya (22Ktons) are the major sisal producing countries. The Chemical composition of sisal varies largely due to variation in source, age, extraction and measurement methods. The chemical composition of sisal fiber is presented in Table 2.3. Joseph et al. (1999) reported that sisal is one of strongest vegetable fibres and several studies have been reported in the literature based on its use as reinforcement in cement matrices (Mukherjee & Satyanarayana, 1984). In a study carried out by (Samuel, Agbo, and Adekanye 2012), the possibility of applying different natural fibers was investigated, sisal and flax was reported to be a good reinforcement candidates for high performance concrete composites. Studies of sisal fibre reinforced concrete carried out by Nilsson (1975) shows that sisal fibres with a length of 10- 30 mm casted into beams shows an improvement in the tensile strength in bending. It was found that toughness increased markedly when continuous fibers were used. (Sumithra Radha K.T and Dadapheer 2017) reported that addition of sisal fibres not only increases tensile strength but also increases bond strength, but decreases permeability. Sisal fiber also significantly improves the tensile modulus, and creep-resistance of the composites as fiber content increases (Zhao, Li, and Bai 2014).

Table 2- 3: Chemical Composition of Sisal Fiber (Li, Mai, and Ye 2000).

Composition	**Percentage**
Cellulose	50-80%
Hemicellulose	10-20%
Lignin	2-8%
Waxes	2%
Ash	0.8-1.1%

Figure 2- 2: Sisal fiber

2.2.1. Modulus of elasticity of Sisal fiber reinforced concrete

The modulus of elasticity of concrete (E_c) is a material property that describes the deformation parameters and geometric response of a structure when loaded (Tipka and Vašková 2018). It is a function of the stress-strain behavior of its constituent material and represents an essential property in the analysis and design of structural elements (Jurowski and Grzeszczyk 2018). Most design standards and studies propose empirical relations relying on compressive strength and concrete density to compute the modulus of elasticity of normal-weight concrete (Ispir et al. 2010). A typical example is presented in Table 4.21. However, this is not always accurate for all types of concrete, as it implies that the elastic modulus is a function of curing age, aggregate type, and water–cement ratio, which all influence compressive strength (Krizova and Hela 2015). Furthermore, concrete and FRC are anisotropic materials and thus possess different properties in different directions. Thus, it is imperative to conduct experimental studies on SFRCs to develop more reliable equations for determination of its modulus of elasticity.

Table 2-4: Some empirical relations for predicting concrete modulus elasticity.

Designation	Equation	Validity
Eurocode 2	$22(f_{cm}/10)^{0.3}$	Europe
ACI 318-08	$0.043.{p_c}^{1.5}.\sqrt{f_{cc}}$	USA
ACI 318-08	$4700\sqrt{f_{cc}}$	USA
CSA A23-3-04	$4500\sqrt{f_{cc}}$	Canada
BS8110-2	$9100{f_c}^{0.3}$	Great Britain
IS456-1979	$5688\sqrt{f_{cc}}$	Indian
TS (500)	$3250\sqrt{f_{cc}+14000}$	Turkey

2.3. Beam-Column Joints

Beam-column joint is the intersecting portion of beam and columns in reinforced concrete buildings (Sureshkumar and Rangasamy 2017). The design of the joint can be complicated and puzzling for structural engineers due to the tendency to have congestion of reinforcements at the joints especially in the design for seismic forces. Furthermore, the joints are characterised by several interactions of shears, bond, fatigue and confinement.

2.3.1 Types of beam- Column joints

The types of beam-column joints in a moment resistant frame are:

Interior joint: This is the point of intersection where four beams frames into the vertical faces of a column.

Exterior joint: This is the point of intersection where one beam frames into the vertical face of a column and two more beams frame into the column in the perpendicular direction. Exterior beam-column joints are more vulnerable to seismic forces than interior joints (Gnanapragasam, et al., 2016).

Corner joint: A corner joint is one in which beams frame into two adjacent vertical faces of a column. See figure 2.3.

2.3.2. Classification of beam-Column joints

As per ACI 352, Structural connections are classified into two categories: Type 1 and Type 2 based on the loading conditions for the connection and the expected deformations of the connected frame members when resisting lateral loads as shown in figure 2.3.

Type 1 Joints: these joints have members designed to satisfy strength requirements, with insignificant inelastic deformation. They are non-seismic joints.

Type 2 Joints: these joints have members that are required to dissipate energy through reversals of deformation into the inelastic range. These are seismic joints.

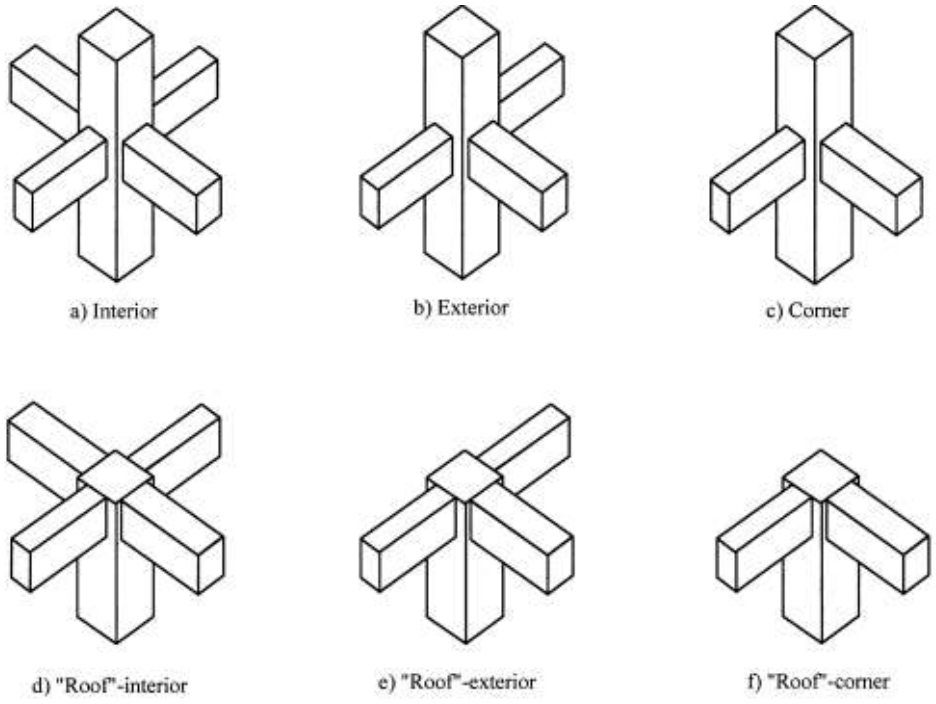

Figure 2- 3: Typical beam- column joints

Source: ACI 352R-02 (ACI-ASCE Committee 352)

2.3.3. Beam-Column Joints in frames

Beam-column joints transfer the loads and moments at the ends of the beams of multi-storey buildings into the columns. The forces acting on an interior joint due to gravity loading are shown in Figure. 2.4. The axial loads from the columns as well as tension and compression from the beam ends directly transmitted through the joint. If the two beam moments of a four-member connection are in equilibrium with one another as shown in Fig.2.4 (a), then no extra reinforcement is required.

In cases of lateral loading due to seismic forces, the equilibrating forces from beams and columns, as shown in Fig. 2.4(b) create compressive stresses and diagonal tensile forces within the joint. Cracks develop perpendicular to the tension diagonal A-B in the joint and at the faces of the joint where the beams frame into the joint. Concrete is known to be weak in tension, thus, transverse reinforcements have to be provided in such a way that they cross the plane of failure to resist the diagonal tensile forces (Uma and Jain 2006).

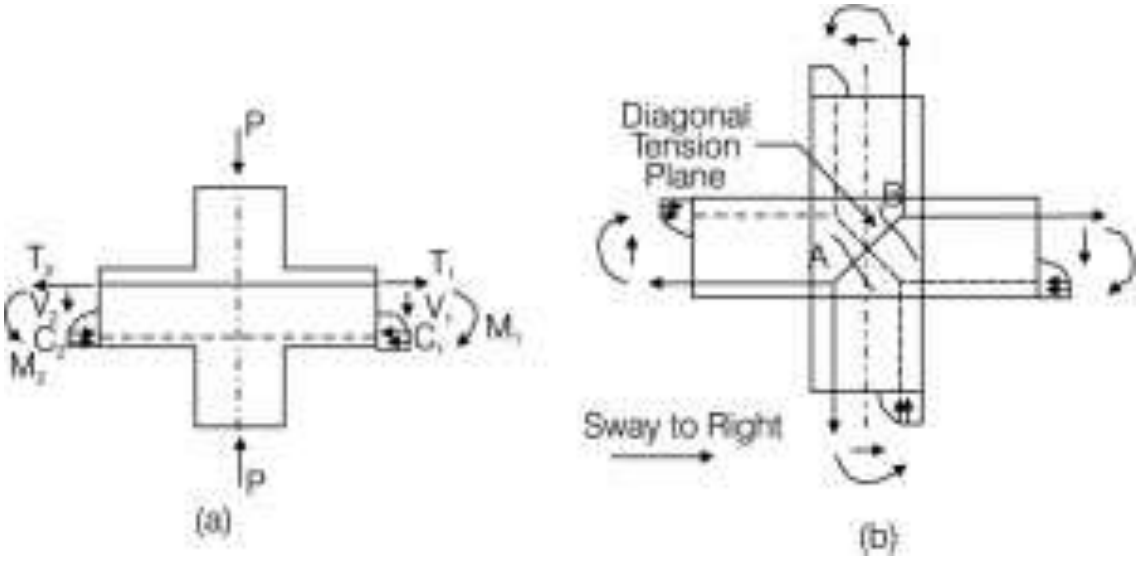

Figure 2- 4: Forces acting on beam-column joint

2.4. Design of Beam-Column Joints

The joint block area is relatively small compared to member sizes, it is important to consider localized stress distribution in the joints. A simplified force system showing the applied forces and reactions may be assumed in designing beam to column connections. The steel reinforcement for the tensile zone is also calculated on the assumption that steel reaches the design yield stress and the concrete, its designed compressive stress. Where bond failure or local bearing is anticipated, the lesser of the two capacities for flexural and local failure should be adopted based on experimental results. It is necessary to avoid bond and anchorage failure within the joints, especially at the external joints, through proper design and detailing (Sureshkumar and Rangasamy 2017).

2.4.1. Failure mechanism of beam- column joints and prevention

The prime mechanisms of failure of a beam-column joint are: Shear failure within the joint, Bond failure of beam or column passing through the joint and Anchorage failure of bars, especially in interior joints (Antonopoulos and Triantafillou 2003).

Beam-column joint of a moment resisting frame subjected to lateral forces become prone to joint shear failure due to high shear stress which appears in the joint panel as a result of opposite sign moments on both sides of the joint core (Najafgholipour et al. 2017). Inadequate transverse reinforcement in the joint and weak-column: strong-beam design, are also responsible for joint shear failures (Ghobarah and Said 2002; Masi et al. 2008). Shear failure of joints can be avoided when designing Ductile Moment Resisting Frames (DMRFs) by employing the weak-beam strong-column principle (Fernando, Providenca, and Costa 2011; Mahini, Isfahani, and Ronagh 2008)

and provision of adequate transverse reinforcement (Antonopoulos and Triantafillou 2003).

Ductility is crucial in resisting lateral forces due to seismic activities. The ductility capacity of all members are transferred to the joint, such that the damage at the joint will be substantial due to the formation of undesirable plastic hinges (Lu et al. 2012). Poor detailing without due consideration for seismic provisions also decreases joints ductility (Gnanapragasam, Chitra, and Ravi 2016). Meticulous attention to the ductility of the reinforcement within the joint region is necessary. Damaged beam-column joints after an earthquake are shown in Figure 2.5.

Figure 2- 5: Failure of corner beam-column joints in past earthquakes: (a) Izmit earthquake in Turkey 1999: (b) Abruzzo earthquake in Italy 2009

2.4.2. Experimental loading of beam-column joints for seismic forces

Many studies have been conducted to understand the behaviour of beam-column joints under different loading conditions to depict seismic conditions. Beam-column joints behaviour tested using constant axial column load and a reversing, quasi-static cyclic

load applied at the beam tip was reported by (Ghobarah and Said 2002). (Lu et al. 2012) studied the behaviour of interior RC beam-column joints with additional bars under cyclic loads. The beam-column joint behaviour under monotonic forces using different forms of reinforcements was also studied (Gnanapragasam, Chitra, and Ravi 2016; Muthupriya, Boobalan, and Vishnuram 2014). In conducting static load tests on reinforced beam-column joints, the axial load on the column must not exceed fifty percent of its capacity so as to reduce the axial loads at the joints and achieve seismic load behaviour (Gnanapragasam, et al., 2016).

2.4.3. Strong column – weak beam concept

The concept describes a practical way of how a reinforced concrete building is expected to fail in case of earthquake to reduce damages and injuries. The idea is that the beams and horizontal elements of the structure should create plastic joints without total collapses before the columns which helps the structure to dissipate the seismic energy better. The creation of these plastic joints in the beams, ensures the conservation of the initial ductility and boosts its ability to absorb bigger amount of lateral displacements.

The plastic hinges are anticipated positions where the structural damages can be allowed to occur due to inelastic actions involving large deformations (Lu et al. 2012). Most well-established country code for designing structural elements (Eurocodes, ACI, etc,), incorporates these concepts. It is achieved by simply having a strong column with more stiffness as compared to the beams resting on it. The strong-column weak-beam concept is enforced in ACI 352R-02 (2002) through Sect. 21.4.2.2.

2.4.4. Beam –Column joints reinforced with FRC

In seismic prone areas, fiber reinforced concrete are rapidly becoming an adopted technology for structural elements (Machaka, Basha, and ElKordi 2014). Steel is one of the most popular fibers for FRC. Study done using Glass- steel fiber hybrid was reported to increase the ductility of beam-column joint by a factor of 1.5 (Muthuswamy and Thirugnanam 2014). Similar experiment done using steel fibers shows that steel fiber increases the ductility of the joint (Keerthana and Reddy 2014; Romanbab, Choudhury, and Laskar 2013). Steel and polypropylene fibers used in exterior beam-column joints subjected to cyclic loading increased the strength requirements of the joints under seismic conditions. (Muthupriya, Boobalan, and Vishnuram 2014) made use of glass fibers in high performance concrete, the exterior beam-column joints were subjected to monotonic load, result showed specimens with glass fiber in HPC increases ultimate load-carrying capacity and gives lesser deflection than the control specimens.

External retrofitting of joints under different loads has also been investigated. (Antonopoulos and Triantafillou 2003) applied simulated seismic load to a poorly-detailed scaled beam joint bounded with synthetic FRP. They submitted that externally bonded FRP reinforcement is a viable solution towards enhancing the strength, energy dissipation, and stiffness characteristics of poorly detailed joints. (Esfahani and Kianoush 2005) concluded that FRP composite wraps are effective in restoring the flexural strength and ductility capacity of earthquake-damaged concrete columns.

In a recent study by (Bharti, et al., 2017), the plastic behaviour of exterior beam-column joint with different fiber reinforced concrete (FRC) was explored

experimentally under cyclic loading. Steel fiber and polypropylene fibers improved the nonlinear behaviour of beam-column joints. But in shifting towards green sustainable construction, natural fiber reinforced concrete has shown tremendous promise. Addition of natural fibers can be done externally (bonding) or internally (composites).

2.4.5. Shear strength of the joint

Tsonos et al. (1992)

The studies carried out by Tsonos et al was on the shear strength of beam-column. Based on their experimental investigations, they suggested a model based on the strut-and-tie concept. The suggested equation for predicting the joint shear strength is as presented below:

$$V = \left[\frac{\alpha\gamma}{2\sqrt{f_c}}\left(1+\sqrt{1+\frac{4}{\alpha^2}}\right)\right]^5 + \frac{5\alpha\gamma}{\sqrt{f_c}}\left(\sqrt{1+\frac{4}{\alpha^2}}-1\right)$$

This equation was developed based on the assumption that both strut and truss mechanisms depend on the core concrete strength.

Bakir (2003)

Bakir in his study considered a lot of variables and their influence on the shear joint strength. After studying the influence of all possible variables, Bakir (2003) he carried out a regression analysis on the available test data. Best regression statistics were obtained by using variables such as stirrup ratio, stirrup yield strength, concrete cylinder strength, and ratio of height of column to the diameter of beam longitudinal bars. The effect of the crossed inclined bars provided in the study was also included.

Based on these studies, following equation for the joint shear strength was obtained:

$$V = \left(\frac{b_c + b_b}{2 \times 10^6}\right) h_c \lambda \left(0.092 f'_c + 0.55 \text{In} \left(\frac{h_c}{d_b}\right) + 0.23 \frac{A_{sh} f_{ys}}{\left(\frac{b_c + b_b}{2}\right) h_c} \right)$$

Jiuru et al. (1992)

In the study carried out by Jiuru et al. (1992). A model for predicting the ultimate shear strength of the fiber reinforced joints was developed based on the assumption that even after cracking, considerable tensile stress remains in the concrete until the fibers are pulled out from the matrix. Accordingly the ultimate shear strength is given by:

$$V = V_c + V_f + V_s$$

Where $V_c$is the shear carried by the concrete, $V_f$is the shear carried by the fibers, and V_s is the shear carried by the joint stirrups. These are expressed as

$$V_c = 1 \times 10^{-5} \left(1 + \frac{N}{b_c h_c f_{ac}}\right) b_j h_j f_{ac}$$

$$V_f = 2 \frac{l_f}{d_f} v_f b_j h_j$$

$$V_s = f_{ys} \frac{A_{sh}}{S} (d - a_s)$$

2.5 Load-deflection behaviour of beam column joints

The ability of beam-column joints to be ductile and dissipate energy is a function of the applied load and corresponding deflection the area under the load-deflection curve is the energy absorption capacity of the joint. The load carrying of beam-column joint

can be improved with an increase in the length of anchorage bars leads to an increase in the maximum load carrying capacity and displacement(Bharti, Chidambaram, and Kwatra 2017). The ultimate load and deflection also gives an indication of the structural stiffness Structural stiffness controls natural period and hence seismic forces. The latter are lower for longer periods, that is, for small stiffness, but then displacements and deformations may become excessive. In addition ensuring adequate safety factors against collapse, seismic criteria should aim at controlling deformations, because they are directly responsible for damage to non-structural elements, impact with adjacent structures, panic and discomfort. Stiffness is also the main variable controlling safety against instability (Najafgholipour et al. 2017). Lateral displacements and internal forces produced by horizontal ground motion are amplified by interaction between gravity loads and the displacements mentioned(Lu et al. 2012).

Thus, it is essential that an earthquake resistant structure should be capable of deforming in a ductile manner when subjected to lateral loads in several cycles in the elastic range. Ductility of a structure is its ability to undergo deformation beyond the initial yield deformation, while still sustaining load(Buyukozturk 2004).

2.6. Research Gap

With reference to the literatures reviewed, Natural and synthetic fibers have proven a suitable material in concrete to improve some properties of concrete. Synthetic fibers however are expensive and not sustainable. The construction industry is therefore looking towards sustainable natural fibers (Sood and Sood 2017). Natural fibers enhances the energy absorption capacity and ductility of elements under unanticipated loading (Singh and Sujana 2013; Sivaraja and Kandasamy 2009). So far, the work done

on NFRC has been mainly concentrated on its mechanical strength (Girimath et al. 2017; Ramesh, Palanikumar, and Reddy 2013; Sabarish et al. 2017; Samuel, Agbo, and Adekanye 2012; Singh and Sujana 2013; Sivaraja et al. 2010; Tol et al. 2000) and not on its application in structural elements especially where high ductility is required such as in Beam-Column Joints (Tolêdo Filho et al. 1999). The researchers that studied behaviour of joints reinforced with fibers used either synthetic fibers mostly steel and glass (Muthupriya, Boobalan, and Vishnuram 2014) or used the Fibers to retrofit failed joints (Ghobarah and Said 2002). Despite the high ductility and sustainability tendency of natural fibers there is limited research on its behaviour in beam-column joints. This research therefore aims to investigate the behaviour of beam-column joints made of SFRC under monotonic loading.

CHAPTER THREE –MATERIALS AND GENERAL METHODS

This chapter deals with the material and methods that were used in this research. The main parameters to be studied are physical properties, mechanical strengths (compressive and split tensile strength of SFRC), yield load, crack load, ultimate load, and deflection at yield and ultimate load and strains at the joints.

3.1. Materials

3.1.1. Cement

The type of cement used in this study was Ordinary Portland cement CEM 1 42.5 which is a high strength cement characterized by low alkali content. It has a minimum compressive strength of 42.5MPa at 28 days. This cement is manufactured in accordance to the requirements of EN 197-1 (European Norm) standards.

3.1.1.1 Specific gravity of Ordinary Portland Cement

The weight of the empty Le chaterlier flask was recorded as “A”. Kerosene was poured until it reached 250ml point, this was noted as “B”. Cement was slowly added with a straw, ensuring that it falls directly inside the flask without making contact with the body. The volume of the Cement and kerosene was taken as “C”. The difference in B and C gives the volume displaced. The weight of the amount of cement added was taken “D”. The ratio of D to the displaced cement volume gives the specific gravity. The tests were done twice and the average taken as the specific gravity.

3.1.1.2. Chemical Properties of Cement

The chemical composition of OPC CEM I 42.5N was obtained using an X-ray fluorescence. The non-destructive test was done at the Kenya Ministry of mining by placing samples of the cement in an XRF spectroscopy machine. The chemical content

of the cement was obtained by measuring the X-ray emitted (See Figure 3.1) from the cement when it is excited by a primary X-ray source. Each of the elements present in the sample produces a set of characteristic fluorescent X-rays.

Figure 3- 1: X-Ray Fluorescence Spectroscopy Machine

3.1.2. Fine aggregates (Sand)

River Sand used was obtained locally from available sources in Kivaa, Kenya. In this study, sand conforming to ASTM C33 was used. The aggregates that passes the 4.75mm standard sieve size and containing no more coarser material was considered as sand. Six (6) physical property tests were carried out on the procured fine aggregates (sand). These tests were: particle size analysis, fineness modulus, specific gravity, water absorption, density and silt content.

3.1.2.1. Sieve Analysis and Fineness modulus of Fine Aggregates

1000g of granite samples was weighed for testing, samples were taken in accordance to ASTM D75. Sieve sizes 4.75 mm, 3.71mm, 2.36 mm, 1.18mm, 0.6mm, 0.3mm and

0.15 mm were arranged in descending order with fitting lid at the top and pan at the bottom. Sieve analysis tests was done in accordance with ASTM C136.

3.1.2.2. Specific Gravity and Water Absorption of Fine Aggregates

500g of samples of fine aggregate was taken in accordance ASTM D75.Test was done in accordance with ASTM C128-01 (Standard Test Method for Density, Relative Density (Specific Gravity), and Absorption of Fine Aggregate).

3.1.2.3. Bulk Density ("Unit Weight") and Voids in Fine Aggregate

Test was done in accordance with ASTM C29-97 (Standard Test Method Bulk Density Unit Weight and Voids in Aggregate) .The sample was obtained in accordance with Practice of ASTM D 75.

3.1.2.4. Silt content of Fine Aggregates

The silt content of the fine aggregate was conducted in accordance with British Standards. 500g samples of the sand were taken and washed thoroughly by allowing flowing water to pass through the specimen in a 0.13mm sieve. The weight was recorded as M1, after which it was oven dried at 100°C for 24hours and allowed to cool at room temperature. The oven dried sample was recorded as M2. The difference in the masses M3 gives the amount of silt.

$$\text{Percentage of Silt} = \frac{M3}{M1} \times 100\% \qquad 3.8$$

3.1.3. Coarse aggregates

The coarse aggregate used was crushed granite from a quality quarry. The aggregates which are retained on a 4.75mm standard test sieve sizes are known as coarse aggregates. Aggregates that conform to ASTM C33 specification was used in this

study. The coarse aggregate was limited to a maximum size of 20mm. The aggregates were used in saturated surfaced dry condition. Five (5) physical property tests were carried out on the procured coarse aggregate (granite). Namely: Particle size analysis, Specific gravity, Water absorption, Density and Aggregate impact/crushing.

3.1.3.1. Sieve Analysis of Coarse Aggregates

5000 g of granite samples were taken in accordance to ASTM D75. Sieve sizes of 37.5mm, 25 mm, 19 mm, 12.5mm, 9.5mm, 4.75mm and 2.36 mm were arranged in descending order with fitting lid at the top and pan at the bottom. Test was done in accordance with ASTM C136-01 (Standard Test Method for Sieve Analysis of Fine and Coarse Aggregates).

3.1.3.2. Specific Gravity and Water Absorption of Coarse Aggregates

2000g of coarse aggregate was taken in accordance with ASTM D75 and immersed in water for 24hours. Tests were done in accordance with ASTM C127-01 (Standard Test Method for Density, Relative Density (Specific Gravity), and Absorption of Coarse Aggregate).

3.1.3.3. Bulk Density ("Unit Weight") and Voids in Coarse Aggregate

Test was done in accordance with ASTM C29-97 (Standard Test Method Bulk Density Unit Weight and Voids in Aggregate) which describes the method for determination of the bulk weight and voids in aggregates. The sample was obtained in accordance with Practice of ASTM D 75.

3.1.3.4. Aggregate Impact Value of Coarse Aggregate

Aggregate Impact Value (A.I.V) is a measure of resistance to sudden impact or shock which may differ from its resistance to gradually applied compressive load. Test was

done in accordance with ASTM D5874 – 16. Oven dried granite were sieved and materials retained on 10 mm sieve and passing through 14 mm sieve comprised of the test sample.

3.1.3.5. Aggregate Crushing Value of Coarse Aggregate

Aggregate Impact Value (A.C.V) can be defined as the measure of resistance to crushing when subjected to gradually apply compressive load. Test was done in accordance with ASTM C131. Oven dried granite was sieved and 2500g of materials retained on 10 mm sieve and passing through 14 mm sieve comprises the test sample.

3.1.4. Sisal fibers

Sisal Fibers were bought from a local processing company in Juja, Kenya. It was cut into a length of 30mm to reduce balling effects when mixing. The diameter of the fibers vary from 0.10mm to 0.13mm. This gives as aspect ratio of 230 to 300. The fiber was treated with silica fume slurry to ensure durability by immersing the fibers in condensed silica fume slurry for 10 minutes, then dried for 15 minutes at room temperature. Chemical analysis was carried out to obtain the cellulose, hemicellulose, and lignin content of both the treated and untreated fibers. The tensile strength, and percentage elongation was obtained using a Tensometer. It is important to understand the properties of the sisal fibers to be used in this study. Its tensile strength, tensile modulus, density, specific gravity and water absorption are investigated and reported.

3.1.4.1. Tensile Strength of Sisal fiber

The tensile strength of the sisal fibers was done using a Hounsfield Tensometer with a motor driven unit shown in Figure 3.2 in accordance with ASTM D 3822-01.The sisal fiber was subjected to tensile force up to failure and the maximum values were

obtained for three (3) treated and untreated samples and the average value recorded.

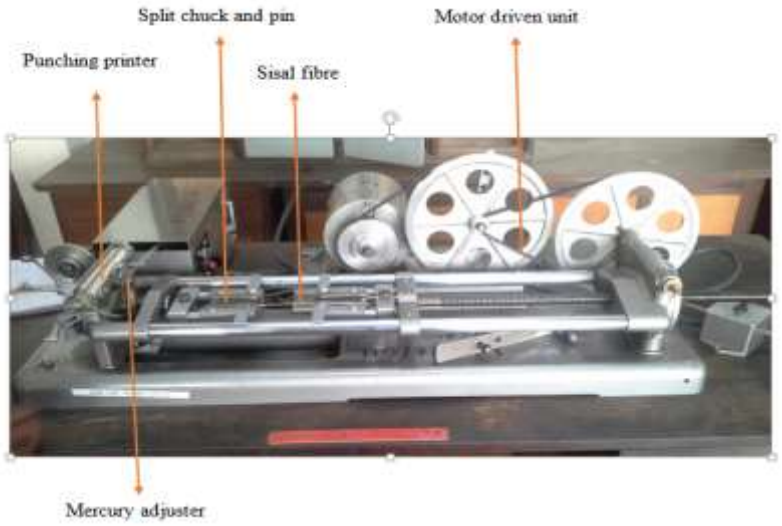

Figure 3- 2: The Hounsfield Tensometer

3.1.4.2. Density of Sisal Fiber

The mass of the plastic container was recorded as "A", after which sisal fibers of required aspect ratio was filled carefully into a container and compressed in three layers until no further fiber can be placed into the container, the mass was recorded as "B". The container was then emptied and filled with water and the mass recorded as "C". Two trials were taken and the average recorded as the density of the sisal using the equation below.

$$\text{Density of fiber} = \frac{(B-A)}{(C-A)} \times 100 \qquad 3.19$$

3.1.4.3. Water Absorption and Specific gravity of Sisal Fiber

100 g of sisal fiber was soaked in water for 24 hrs. The weight of the container, water and fiber was recorded as "A". The fiber was then removed as saturated surface dried, and the mass of the saturated surface dried sample was recorded as "B". The fiber was oven dried for 24 hours at 110°C and the mass recorded as "C". The container used

was then filled with water and the mass of the container and water was recorded as "D".

$$\text{Water Absorption} = \frac{(E-C)}{C} \times 100\% \quad 3.20$$

$$\text{Specific gravity} = \frac{C}{(E-(A-D))} \times 100\% \quad 3.21$$

3.1.4.4. Chemical Analysis of sisal fiber

This test was carried out using the direct method of cellulose, hemicelluloses and Lignin recommended by (Brindha et al.1987).

3.1.5. Water

In this study, potable water was used for mixing the materials and curing of the concrete samples.

3.1.6. Reinforcement bar (steel)

High tensile steel bars conforming to ASTMA-15-65 was adopted for this project. Longitudinal reinforcement was type T12 with a measured yield stress of 539.09MPa and T10 with a measured yield stress of 494.67MPa. Stirrups was made of mild steel type T6 with average yield stress equal to 408.95MPa.

3.2. Material Preparation

3.2.1. Concrete Preparation

Preparation of samples was done in accordance to ASTM C192-02. This was done to obtain the mechanical strength of the cubes conforming to BS EN 12390-1(2000) and cylinders in accordance with ASTM C496-04.

3.2.2. Mix Proportioning

A mix proportion was designed in accordance with ACI requirements for a target strength of 30MPa and slump of 100mm. The mix ratio is as present in Table 3.1 below was used throughout the experiment with a target mean strength of 30MPa. The design mix used had:

$$\text{Free water / cement ratio} = 0.47$$

$$\text{Free water content} = 195$$

$$\text{Assumed relative density for uncrushed aggregate} = 26\ \text{kg/m}^3$$

$$\text{Density of fine aggregate} = 730\ \text{kg/m}^3$$

$$\text{Density of coarse aggregate} = 1400\ \text{kg/m}^3$$

Designed mix ratio = 1:1.92:3.68

The fine aggregates, coarse aggregates and sisal fibers was weighed first and mixed thoroughly for about two minutes in a concrete mixer and 50% of water was added to the dry mix. The remaining 50% water, mixed with superplasticizer, was added later. Mixing was done for about 5 mins until a uniform mix was obtained.

Table 3- 1: Mix Proportions (kg/m^3)

Label	Cement	Fine	Coarse	Water	Superplasticizer	Sisal fiber
M0.0	380	730	1400	203.67	1.9	0
M0.5	380	730	1400	203.67	1.9	1.9
M1.0	380	730	1400	203.67	1.9	3.8
M1.5	380	730	1400	203.67	1.9	5.7

M2.0	380	730	1400	203.67	1.9	7.6

3.3. Methodology to obtain the physical and mechanical properties of SFRC

1. **Workability:** On each fresh mix of concrete, workability was determined using the slump cone in accordance with the requirements of ASTM C143 and compaction factor according to the terms of BS1881-103:1983. The reported slump and compaction factor values are an average of 3 measurements.

2. **Water absorption:** The water absorption tests was done using ASTM C642 as the basics. The water absorption values reported are the average obtained from 3 cubes of sizes 150mm.

3. **Density:** Measured for the cubes taken from curing water tank in accordance to ASTM C642 [22]. The density represents the mean of 3 cubes after 28 days water curing.

4. **Compression strength test:** Concrete cubes were tested according to BS EN 12390-03 and BS 1881-116 using a load-controlled universal testing machine. The average of the compression strength of 3 cubes was reported for each curing age. Cube steel mould dimensions of 150x150x150mm conforming to BS EN 12390-1(2000) was used. A total of 48 cubes was casted, cured and tested after 7 and 28 days of curing in water, compressive strength was then calculated.

5. **Split tensile test**: Cylinders were tested according to ASTM C496 using a load-controlled universal testing machine. The mean of 3 measurements was recorded as the tensile strength of each mix for each curing age.

6. **Static modulus of elasticity and Poisson ratio:** The static modulus of

elasticity and Poisson ratio was measured by using 2 bonded strain gages (PL-60-11-3LT series) placed circumferentially at diametrically opposite points at the mid-height of the cylinder specimen and connected to a data logger. A load cell connected to the same data logger was also placed above the specimen to obtain the applied load. The test was carried out in accordance with the requirements of ASTM C469.

3.4. Methodology to achieve the durability of SFRC

To test for the durability of the SFRC, the following tests was carried:

1. Chloride penetration test

2. Sorptivity test (Initial and secondary rate of water absorption)

3. Sulphate attack (Strength and weight loss)

4. Alkaline attack (Strength and weight loss)

3.4.1. Chloride Penetration Test

This test was carried out to evaluate the free chloride penetration depth in SFRC. Cylinder specimen (100 X 200mm) were ponded in a solution of 3% sodium chloride solution for a period of 28 and 56 days after an initial 28days curing in water. The grey colorimetric method which is an easy method of detecting free and water soluble chlorides was adopted. On the test day, the cylinder specimen was split longitudinally using a UTM, then 0.1M Silver nitrate ($AgNO_3$) solution was sprayed onto the freshly broken piece of concrete. In the presence of chloride, silver ions react with the chorine and produce a white precipitate of silver chloride (AgCl).

$$AgNO_3 + NaCl \longrightarrow AgCl + NaNO_3$$

Hence, chloride contaminated areas will revealed a white or purple colour while areas free of chlorine has a dark brown appearance (Javier, Lopez, and Juanzon 2017; Otsuki, Nagataki, and Nakashita 1993).

3.4.2. Sorptivity of Sisal Fiber Reinforced Concrete

The sorption test was conducted on the concrete specimen in order to characterize the rate of moisture migration of water into the concrete pores of 150 X 150mm cube specimens. As explained in the water absorption test, the specimens were oven-dried. They were then allowed to cool down to room temperature. The specimens were conditioned to maintain the moisture content and tested as per ASTM C1585-13 after 28 days of curing. After cooling, the cubes were covered with polymer while one face was placed in water on wedge supports to make sure that only the bottom surface of the specimens was in contact with the water. The test set-up for sorptivity test is shown in Figure 3.3. Weight of the cylinders were measured at regular intervals as stated in ASTM C1585-13.

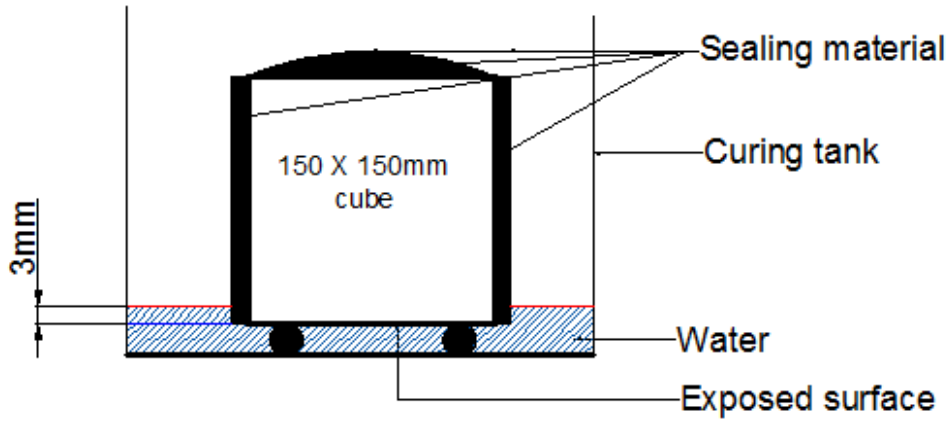

Figure 3- 3: Experimental setup for sorptivity test.

3.4.3. Sulphate Attack Test on Sisal Fiber Reinforced Concrete

During the acid resistance test, concrete cubes of size 150 X 150 X150mm cured for 28days in water were immersed in sulphuric acid solutions in separate plastic containers. The corroded test specimens were removed from the acid solutions at 7 days interval and subjected to wire-brush cleaning under running tap water to remove the corroded products. This procedure subjected new concrete surface to acid attack. The specimen were surface dried and weighed to determine the weight and strength loss at 45 and 90days. This indicates the intensity of acid attack on SFRC. A pH of 3.0 was maintained by regularly checking and adjusting the concentration. ASTM C267 was used as the basic standard for this testing procedure.

3.4.4. Alkaline Attack test on sisal fiber reinforced concrete

For alkaline attack test, concrete cube of size 150 X 150 mm were used. The specimen were casted and cured in a mould for 24 hours. After 24 hours, all the specimen were demoulded and kept in curing tank for 28days. After 28days, all specimen were kept in atmosphere for 2 days for constant weight, subsequently, the specimens were weighed and immersed in sodium hydroxide (NaOH) solution for 45 and 90 days. The pH value of the alkaline medium was 12.0. The pH value was periodically checked and maintained. After 45 and 90 days of immersing in alkaline solution, the specimens were taken out and washed in running water and weighed. The weight and compressive strength were recorded.

3.5. Methodology to achieve the behavior of SFRC in beam-column under monotonic loading.

3.5.1. Exterior beam-column joint specimen details

Based on the design presented in Appendix A2. All the tested five exterior beam-column joints has similar beam and column sizes. The column has a cross section of 150 mm X 200 mm with an overall length of 1 000 mm and the beam has a cross section of 150 mm X 150 mm with a cantilever portion of length 800 mm. Figure 3.4 shows the cross section and reinforcement configuration for the exterior beam-column joint specimens.

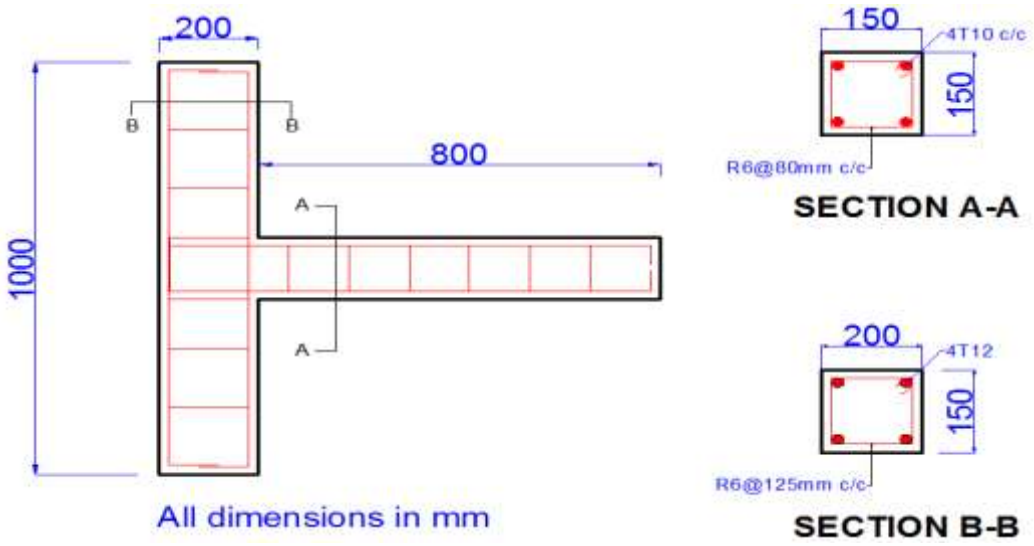

Figure 3- 4: Reinforcement details

3.5.2. Casting and testing of specimens

Marine boards were used for casting the specimens. Reinforcement cages were fabricated and were placed in the moulds with provision for concrete cover of 25mm. The mix ratio defined in section 3.2.2 were poured into moulds in layers and the moulds were vibrated for thorough compaction. After 24 hours of casting, specimens

were demoulded and cured under wet gummy bags for 28 days (Figures 3.5 a and 3.5 b).

(a) (b)

Figure 3- 5: (a) formwork and reinforcement (b) Casting stage of specimen

Specimens were tested in a rigid loading frame. Strain gauges (PL-60-11-3LT series) were also fixed at specific locations across the joints as well, a dial gauge, an LVDT and strain gauges are shown in Figure 3.6. Point A is at the top of the beam, point B, bottom of the beam. Point C is at the side of the joint while point D is at the back of the column.

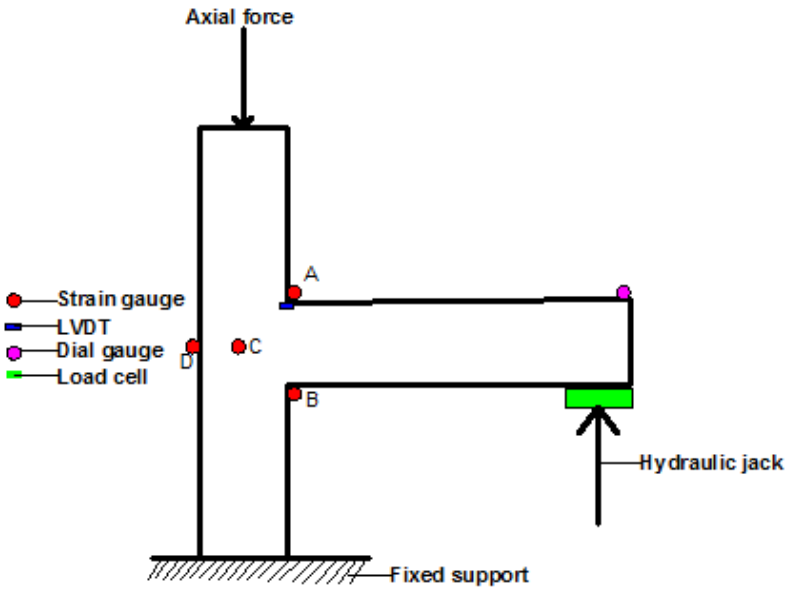

Figure 3- 6: Locations of apparatus and strain gauges on the beam-column joint

A constant load of 120 KN, which is about 20 % of the axial capacity of the column was applied to the column for holding the specimens in position. A hydraulic jack of 40 ton or 400 KN capacity was used to apply load at the beam tip. A load cell of 20 ton capacity was used to measure the applied load accurately. The gradually increasing load was applied to the end of the beam. Dial gauge was used to measure the deformation at the beam tip while, one linear variable differential transducers (LVDTs) was used to measure the deformations at the joint. The diagram of monotonic loading test set-up is shown in Figure 3.7.

Figure 3- 7: Test set-up

3.5.3. Ultimate Load, Load-Deflection Plot, Crack Formation

For each volume factions used for SFRC beam-column joints, the load at which the first crack appeared with its corresponding deflection was noted using the LVDT connected to a data logger and subsequently the load and deflection at which joint fails was recorded. The applied load was plotted against its corresponding deflection. The stiffness was obtained by obtaining a product of load and deflection.

3.6. Methodology to Achieve the Finite Element Analysis of beam-column joint under monotonic loading

The Nonlinear finite element analysis of RC beam-column joints was done by using ABAQUS CAE with joint shear failure as the governing failure mode. A 3D fine element model capable of modelling stress-strain behaviour, tensile cracking, and compressive damage of concrete and indirect modelling of steel-concrete bond was adopted. Concrete damage plasticity was used to define the non-linear behaviour of

concrete material. In modelling the material properties, the concrete material modelling and steel reinforcement modelling was defined. A mesh size of 50mm was adopted. Furthermore, boundary conditions, loading and dimensions details was defined according to the experimental set up. A uniform mesh size of 50mm was chosen over the entire element for both concrete and steel reinforcement.

CHAPTER FOUR - RESULTS AND DISCUSION

4.1. Material Characterization

4.1.1. Coarse aggregate

4.1.1.1. Sieve Analysis of coarse aggregate

The result from the test procedure are as shown in Table 4.1 below. The ultimate outcome was the percentage passing. The values were compared with those in Table 2 of ASTM C33 to observe if the aggregate falls within any specified range. The particle size distribution was drawn as shown in Figure 4.1, from which it was concluded that the coarse aggregates were nominal sized 25mm- 9.5mm meaning that most of the aggregate passed the 25mm sieve and were retained on the 9.5mm sieve. The curve also shows the envelope (lower and upper limit curves) of coarse aggregates of single sized aggregate of 25- 9.5mm referenced in ASTM C33, and since the curve for the coarse aggregates was within the envelope therefore they were found suitable for use in normal weight concrete. The shape of the coarse of the aggregates is angular which would provide a high surface-to-volume ratio, better bonding characteristics, although, would require more cement to produce a workable mix, while the surface texture was rough generating a stronger bond between the paste and the aggregate since a greater area is in contact with the cement paste creating a higher strength though it would reduce the workability and increase the paste demand.

Table 4- 1: Particle size analysis of granite

Sieve Size (mm)	Sample No (g) 1	2	3	Average	Percentage retained	Cumulative % of total	% passing	Lower Limit	Upper Limit
37.5	0	0	0	0.00	0.00	0.00	100.00	100	100
25	10	0	26	12.00	0.24	0.24	99.76	90	100
19	1056	1004	1007.5	1022.50	20.53	20.77	79.23	40	85
12.5	2095	2192	2060	2115.67	42.48	63.25	36.75	10	40
9.5	1137	1193.5	1352.5	1227.67	24.65	87.90	12.10	0	15
4.75	690	549	491	576.67	11.58	99.47	0.53	0	5
2.36	10.5	23	45	26.17	0.53	100.00	0.00	0	0
Total mass	4998.5	4961.5	4982	4980.67	4980.67				

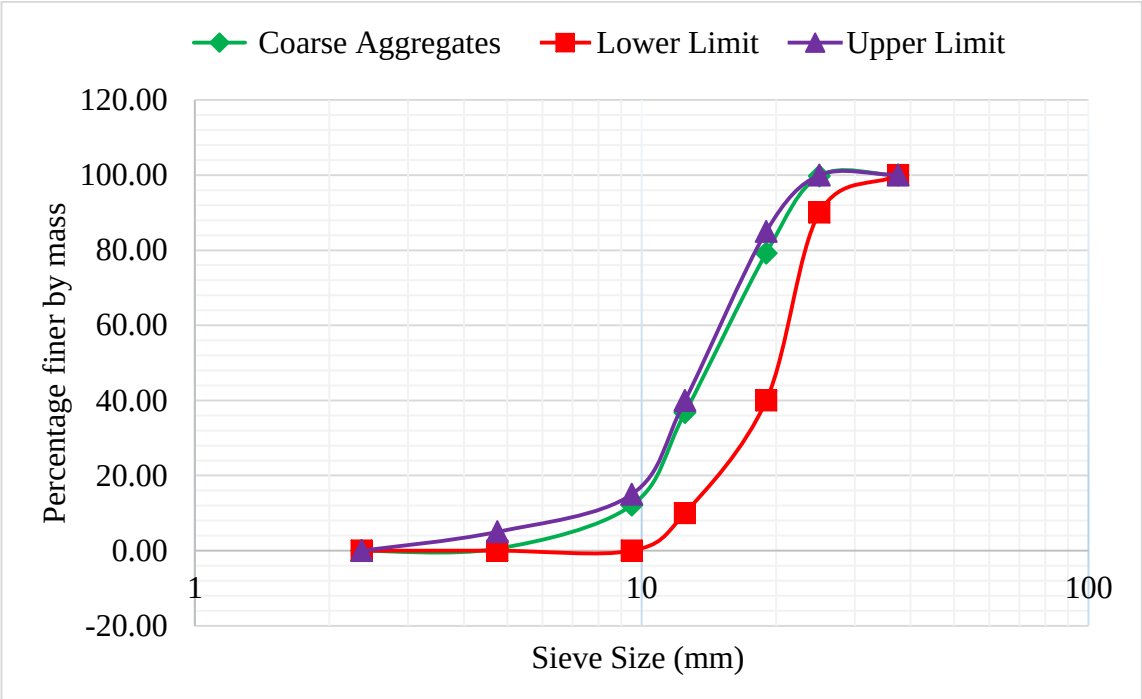

Figure 4- 1: Particle Size Distribution for coarse Aggregates.

4.1.1.2. Specific Gravity and Water Absorption of Coarse Aggregates

The results of the specific gravity laboratory test carried out on the coarse aggregate (granite) are presented in Table 4.2. The average specific gravity on oven dry basis, average specific gravity on saturated surface dried basis, apparent specific gravity and

water abortion capacity of the coarse aggregate (granite) was 2.48, 2.56, 2.70 and 3.27% respectively. The specific gravity of 2.56 falls within the specified range of 2.4 and 2.9, which indicates that the aggregate is suitable for use in normal weight concrete.

The water absorption of an aggregate indicates the quantity of water which will be absorbed by the pore structure. It is an important factor as it influences the bond between the aggregate and the cement paste, the resistance of the concrete to freezing and thawing as well as the chemical stability and resistance to abrasion. The SSD water absorption of the coarse aggregate was 3.27% which conforms to the requirement of coarse aggregates to be used in concrete which should not be more than 4.00 according to ASTM C33 standard.

Table 4- 2: Specific Gravity and Water Absorption of Coarse Aggregates

Description	Sample No			
	1	2	3	Average
Weight of sample (g)	2000	2000	2000	2000
Weight of sample + Water + Vessel (A) (g)	8983.5	9047.0	9107.0	9045.8
Weight of Water + Vessel (B) (g)	7817.5	7817.5	7817.5	7817.5
Weight of Saturated surface dry sample (C) (g)	2016.5	2015.0	2012.5	2014.7
Weight of Oven dried sample (D) (g)	1953.5	1948.5	1950.5	1950.8
S.G on Oven dry basis	2.3	2.5	2.7	2.48
S.G on SSD basis	2.4	2.6	2.8	2.56
Apparent S.G	2.5	2.7	3.0	2.70
Water absorption (%)	3.2	3.4	3.2	3.27

$$\text{Void in aggregate } = \frac{2.56-1.494}{2.56} = 41.61\%$$

4.1.1.3. Bulk Density ("Unit Weight") and Voids in Coarse Aggregate

The loose and rodded density of the coarse aggregate are summarized in Table 4.3. It

could be seen that the bulk density of the aggregates is 1494.74kg/m^3 which meets the requirement for production of normal weight concrete. It falls within the recommended range of 1200-1750kg/m^3.

Table 4- 3: Loose and Rodded density and Voids of aggregate

Parameter	Sample no 1	2	3	Average
Capacity of measure (m^3) A	0.0095	0.0095	0.0095	0.0095
Weight of measure (kg) B	4.6	4.6	4.6	4.6
Weight of measure + loose aggregates (kg) C	18.0	17.9	18.3	18.067
Weight of measure + rodded aggregates (kg) D	18.7	18.9	18.8	18.8
Loose bulk density(kg/m^3) E	1410.5	1400	1442.1	1417.54
Compacted bulk density(kg/m^3) F	1484.2	1505.3	1494.7	1494.74

4.1.1.4. Aggregate Impact Value of Coarse Aggregate

The results of the aggregate impact value carried out on the coarse aggregate (granite) are presented in Table 4.4. It can be observed that the coarse aggregate had an aggregate impact value of 8.15% which is less than 10%. Aggregate impact value between 0 - 10 percent is considered Strong. Hence, the concrete made with the aggregate can be recommended for rigid pavement construction and suitable for construction.

Table 4- 4: Aggregate impact value of granite

Parameter	Sample No 1	2	3	Average
Weight of aggregate (A) kg	638.0	623.5	635.0	632.17
Weight of fine passing 2.36mm sieve (B)	55.0	53.0	46.5	51.5
Aggregate Impact Value (AIV) (%)	8.62	8.50	7.32	8.15

4.1.1.5. Aggregate Crushing Value of Coarse Aggregate

The results of the aggregate crushing value carried out on the coarse aggregate (granite) are presented in Table 4.5. Equation 4.8 was used to obtain the aggregate crushing value. It can be observed that the coarse aggregate had an aggregate crushing value of 19.89% which is less than 30%, which is considered Strong. Hence, the concrete made with the aggregate can be recommended for construction.

Table 4- 5: Aggregate crushing value of granite

Parameter	1	2	Average
Weight of aggregate (W_1)	2500	2500	2500.00
Weight of fine passing 2.36 (W_2)	489.0	505.5	497.25
Aggregate Crushing Value (%)	19.56	20.22	19.89

4.1.2. Fine Aggregates

4.1.2.1. Sieve Analysis and Fineness modulus of Fine Aggregates

The grading curves were plotted on a semi-logarithmic graph showing the cumulative percentage passing on the abscissa while the sieve apertures plotted on a logarithmic scale. The result from the test procedure are as shown in Table 4.6 below.

Table 4- 6: Sieve analysis of fine aggregate (Sand)

Sieve size (mm)	Sample No (g)						
	1	2	3	Average	Weight	Cumulative	Total Pass
10	0	1.5	0	0.5	0.05	0.05	99.95
4.7	21	11	25	19.00	1.92	1.97	98.03
2.36	39	36	42.5	39.17	3.95	5.92	94.08
1.18	156.5	198.0	194.0	182.83	18.44	24.36	75.64
0.6	352	357.5	369.5	359.67	36.28	60.63	39.37
0.3	152	180.5	160.5	164.33	16.57	77.20	22.79
0.15	229.5	174	164	189.17	19.08	96.29	3.72
Pan	40.5	34.5	35.5	36.83	3.72	100.00	0.00
Total	990.5	993	991	991.50			
F.M						2.66	

The particle size distribution is as shown in Figure 4.2, from which it was concluded that the fine aggregates belongs to Zone 2. The curve also shows the envelope (lower and upper limit curves) of fine aggregates of Zone 2 referenced in BS 812:102: and since the curve for the sand was within the envelope therefore they were suitable for use in concrete. The fineness modulus of the sand was 2.66 which falls between the range of 2.6- 2.9 showing that the sand used was of medium type.

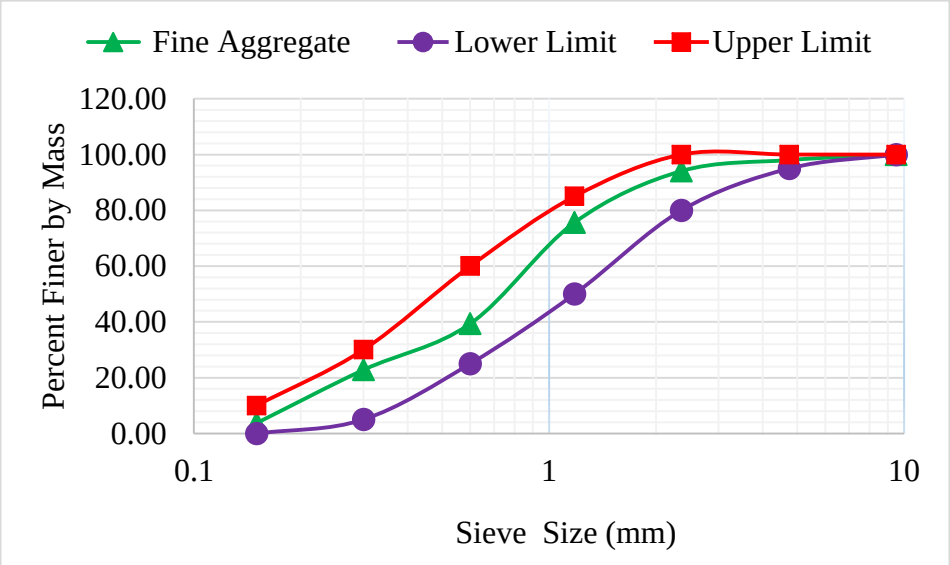

Figure 4- 2: Particle Size Distribution for fine Aggregates.

4.1.2.2. Specific Gravity and Water Absorption of Fine Aggregates

The results of the specific gravity laboratory test carried out on the fine aggregate (sand) are presented in Table 4.7. Equations 4.9 to 4.12 were used to obtain the average specific gravity, apparent specific gravity and water absorption capacity of the fine aggregate respectively. The average specific gravity on oven dry basis, average specific gravity on ssd basis, apparent specific gravity and water abortion capacity of the coarse aggregate (granite) was 2.43, 2.52, 2.68 and 3.95% respectively. The

specific gravity of 2.52 falls within the specified range of 2.4 and 2.9, which indicates that the fine aggregate is suitable for use in normal weight concrete. .The SSD water absorption of the fine aggregate was 3.95% which conforms to the requirement of a fine aggregate to be used in concrete which should not be more than 4.00 according to ASTM standard.

Table 4- 7: Sieve analysis of fine aggregate (Sand)

	Sample No			
Parameter	1	2	3	Average
Weight of aggregate + water + pycnometer(A)	1 713.5	1716.5	1720.0	1716.7
Weight of water+ pycnometer (B)	1415.0	1415.0	1415.0	1415.0
Weight of Saturated Surface Dried aggregate (C)	500.0	500.0	500.0	500.0
Weight of oven dry agg (D)	481.0	479.0	483.0	481.0
Specific Gravity on Oven dry basis	2.4	2.4	2.5	2.43
Specific Gravity on SSD basis	2.5	2.5	2.6	2.52
Apparent S.G	2.6	2.7	2.7	2.68
Water absorption	4.0	4.4	3.5	3.95

4.1.2.3. Bulk Density ("Unit Weight") and Voids in Fine Aggregate

The loose and rodded density of the fine aggregate are summarized in Table 4.8. It could be seen that the bulk density of the fine aggregates is 1576.69kg/m^3 which meets the requirement for production of normal weight concrete. It falls within the recommended range of 1200-1750kg/m^3.

Table 4- 8: Loose and bulk density of fine aggregates

Parameter	Sample No			
	1	2	3	Averag
Capacity of measure (m^3) A	0.002	0.002	0.002	0.002
Weight of measure(kg) B	1.537	1.537	1.537	1.537
Weight of measure + loose aggregates (kg) C	4.487	4.5	4.4725	4.4865
Weight of measure + rodded aggregates (kg)	4.7165	4.724	4.73	4.7235
Loose bulk density (kg/m^3)	1459.7	1466.1	1452.5	1459.4
Compacted bulk density(kg/m^3)	1573.2	1576.9	1579.9	1576.6

4.1.2.4. Silt Content of Fine Aggregates

The silt content of fine aggregates can significantly affect the strength and durability of concrete. According to Table 4.9 below, the silt content of the fine aggregate was 4.67% which is less than the 5% recommended in ASTM C 33-03.

Table 4- 9: Silt content of fine aggregates

	Sample No		
Parameter	1	2	3
Weight of Washed Sample (M1)	500	500	500
Weight of oven dried sample (M2)	484	490	456
Volume of Silt (M3)	16	10	44
Percentage of Silt (M3/M1) * 100	3.20	2.00	8.80
Silt content (%)		4.67	

4.1.3. Cement

The Specific gravity and chemical Composition of the cement was measured experimental studies, other properties were obtained from previous studies

4.1.3.1. Specific gravity of Ordinary Portland Cement

The specific gravity of the cement plays a crucial role in the design of mixes for concrete. ASTM standards recommends a range of 3.10-3.15. The calculated specific gravity of 3.12 presented Table in Table 4.10 falls within the stipulated range.

Table 4- 10: Specific Gravity of Cement

Parameter	Sample No	
	1	2
Weight of empty flask (g) A	127.5	127.5
Volume of kerosene (ml) B	251	251
Volume of kerosene + cement(ml)	280	279.75
Volume displaced (ml)	29	28.75
Weight of Cement used (g)	90	90
Specific gravity	3.10	3.13
Average Specific gravity	3.12	

4.1.3.2. Chemical Properties of Cement

The chemical content of the cement used in this study was found suitable when compared with the requirements of ASTM 150 for production of normal weight concrete as shown in Table 4.11. The Chemical composition showed that the cement contained 65% lime (Calcium oxide) which was available for pozzolanic reaction to form cementitious products in the concrete hence improving the performance of concrete. Calcium oxide is required for the formation of tri-calcium silicate and di-calcium silicate which both reacts with water to form Calcium silicate hydrate which gives concrete its strength:

Tri-calcium silicate + Water ⟶ Calcium silicate hydrate + Calcium hydroxide + heat.

Di-calcium silicate + Water ⟶ Calcium silicate hydrate + Calcium hydroxide + heat. The reaction of tri-calcium silicate is fast as it is responsible for most of the early 7days strength.

Table 4- 11: Major chemical Composition of Ordinary Portland cement CEM I.

Compound	Abbreviation	% Weight	ASTM C150 Limits
Silica	SiO_2	20.98	-
Alumina	Al_2O_3	5.67	-
Phosphorous pentoxide	P_2O_5	0.41	-
Sulphite	SO_3	3.95	≤ 3.5%
Calcium oxide	CaO	65.52	-
Iron oxide	FeO	2.37	-
Strotium	Sr	0.18	-
Magnesia	MgO	0.80	≤ 6.0%
-	LOI at 600^oC	2.85	≤ 3.0%

-	LOI at 1000^{o}C	6.30	-

4.1.3.3. Other physical properties Of Cement

Table 4- 12: Physical properties of cement (Belachew, 2017)

Physical properties	Duration	Limit of Cement	ASTM C150 Limits
Specific Gravity		3.12	-
Specific Surface (cm^2/g)		3197	≥2800
Water Demand (%)		25.65	-
Setting Time(Minutes)	Initial	160	≥45
	Final	252	≤375
Soundness(mm)		0.3	-
Compressive Strength (Mortal Prism)	At 2	19.3	≥ 12
	At 28	48.94	≥19
Colour		Grey	-

The Physical Properties of OPC are shown in Table 4.12 which conform to requirements of ASTM C150 limits and therefore suitable for the research. The specific surface area for OPC was 3197cm^2/g which also meets the ASTM C150 standards as the value was within the range of 3000 - 5000cm^2/g.

4.1.4. Sisal Fiber

4.1.4.1. Tensile strength of Sisal fiber

The tensile strength for treated and untreated single sisal fibers are as presented in Table 4.13 and Table 4.14. There was no significant variation between the tensile strength of treated and untreated sisal fibers. The untreated sisal fiber has a tensile strength of 373.360N/mm^2 while the treated sisal fibers impregnated with silica fume has a tensile strength of 373.316N/mm^2. The measured tensile strength showed little variation namely 373 ± 28 N/mm^2 which was within the range 394.2 ± 110 $N/mm^{2.}$

reported by (Zhao, Li, and Bai 2014) but a little below that reported by (Joseph et al. 1999; Ku et al. 2011) at 511- 635 N/mm^2. The elongation at breaking is expected to play a crucial role in arresting crack appearance in concrete. Sisal fibers tested has elongation values of 2.8±0.29%, this value falling within the range reported by (Zhao, Li, and Bai 2014).

Table 4- 13: Mechanical properties of untreated sisal fiber

Diameter(	Area	Force(	Strai	Strength	Modulus(M	Elongati
0.135	0.0143	5.000	0.02	349.311	14199.645	2.460
0.130	0.0133	4.737	0.03	356.872	11868.826	3.007
0.140	0.0154	6.371	0.03	413.896	13073.967	3.166
	Average	5.369	0.02	373.360	13047.479	2.878

Table 4- 14: Mechanical properties of treated sisal fiber

Diameter(mm)	Area(mm^2)	Force(N)	Strain	Strength	Modulus(Mpa)	Elongation
0.130	0.0133	4.950	0.0276	372.93	13497.33	2.763
0.145	0.0165	6.625	0.0254	401.19	15770.41	2.544
0.135	0.0143	4.950	0.0310	345.82	11166.23	3.097
	Average	5.508	0.0280	373.32	13477.99	2.801

4.1.4.2. Tensile Modulus of Sisal fiber

The tensile modulus of each strands of sisal fiber to be incorporated in the concrete is expected to impact on the mechanical properties of the concrete. The measured tensile modulus of 13.447±2.223GPa. was with the range reported by (Zhao, Li, and Bai 2014) as shown in Table 4.13 and 4.14. The linear stress- strain relationship for both treated and untreated fiber is shown in Figure 4.3 and 4.4. The addition of stiffer sisal fibers into the more compliant concrete matrix will enhance the tensile modulus and strength of the concrete, while reducing the elongation at failure of the concrete.

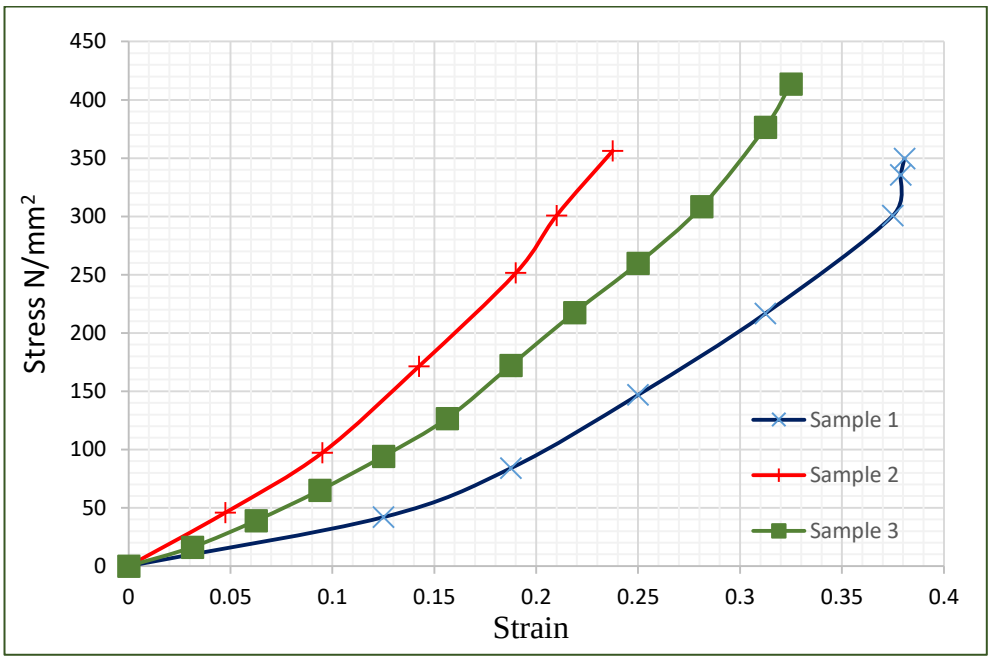

Figure 4- 3: Stress-strain curve of untreated sisal fiber

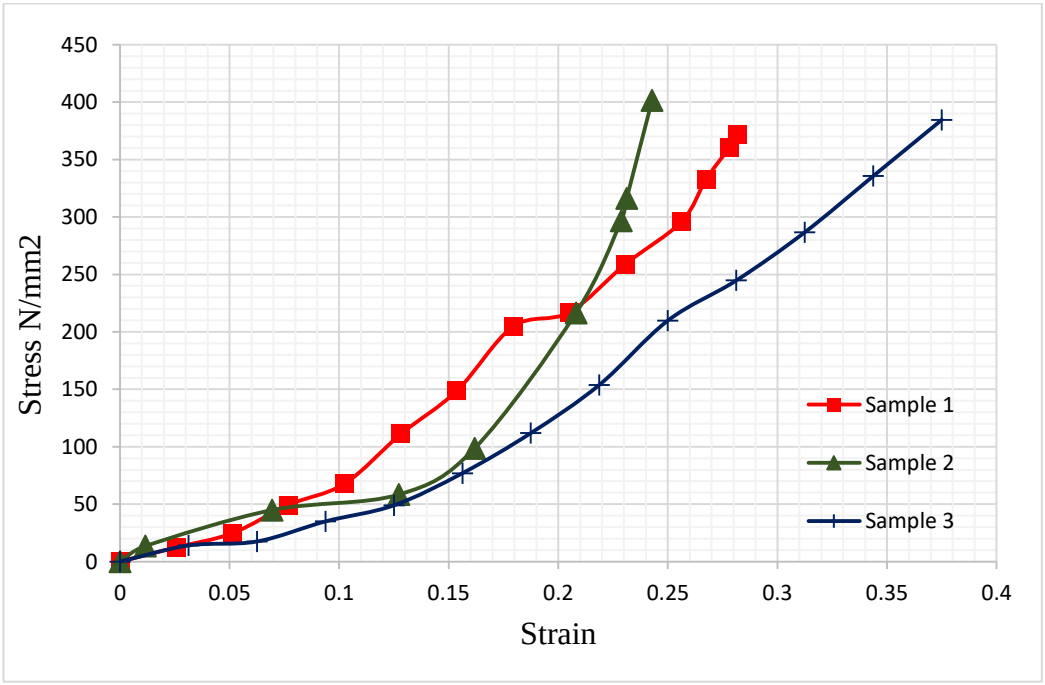

Figure 4- 4: Stress-strain curve of treated sisal fiber

4.1.4.3. Density of Sisal Fiber

The density of the sisal fiber is as shown in Table 4.15 below. The fiber has a density

of 113kg/m^3, and this is comparatively lower than the density of other constituent materials of concrete. This will reduce the density of the concrete and affect its strength.

Table 4- 15: Density of sisal fiber

	Sample No	
Parameter	1	2
Mass of container (kg) A	98	97
Mass of container + fiber (kg) B	365.5	345
Mass of container + water (kg) C	2378.5	2378.5
Density (kg/m^3)	117.3	108.7
Average density (kg/m^3)	113	

4.1.4.4. Water absorption of Sisal fiber

The water absorption of the sisal fiber is presented in Table 4.16 below, the average water absorption was found to be 43.58% which is quite high. This will affect the free water-cement ratio of the concrete mix and significantly impact the workability of the concrete. The average specific gravity however was found to be 0.729 which implies that the sisal fiber is comparatively lighter than water and will tend to float in water.

Table 4- 16: Water Absorption and Specific gravity of sisal Fiber

	Sample No	
Parameter	1	2
Weight of Sample (kg)	100g	100g
Weight of Sample + Container + Water (kg) A	2394.5	3820
Weight of Saturated Surface Dried Sample + Container (kg)	224.5	259
Weight of Oven Dry Sample (kg) C	90.7	88
Weight of Container + Water (kg) D	2389	3814
Weight of Container	97	130
Weight of Saturated Surface Dried Sample E	127.5	129
Water Absorption (%)	40.57	46.59
Specific Gravity	0.743	0.715

4.1.4.5. Chemical content of sisal fibre

The chemical content of the sisal fiber changed after treatment with silica fume. The cellulose content of the fiber samples of each variety were increased after treating with silica fume as shown in Table 4.17, a percentage rise of 9.31% was observed in the treated fiber, while hemicelluloses and lignin content decreased due to their removal from the fiber by the silica fume treatment. Significant reduction of 14.91% and 33.41% was respectively seen in the hemicellulose and cellulose content This show the efficacy of silica fume in treating natural fibers.

Table 4- 17: Chemical composition of Sisal Fiber

Composition	Untreated	Treated	Percentage change (%)
Cellulose	64.21	70.19	+9.31
Hemicellulose	20.25	17.23	-14.91
Lignin	15.53	10.34	-33.41

4.2. Effect of Sisal Fibers on the Physical and Mechanical Properties SFRC

4.2.1. Physical Properties of SFRC

4.2.1.1. Effect of Sisal Fiber on the Workability of Concrete

The ease with which fresh concrete can be transported, molded, and compacted without segregation is regarded as its workability. It is a property of freshly mixed concrete that depicts the amount of internal work needed to overcome the internal friction between the individual constituents of the concrete. It is influenced by a number of factors, which include the water/cement ratio, the aggregate/cement ratio, the particle size distribution, and shape of the constituent aggregates, as well as the

fineness and consistencies of the binder. High workability is required in congested areas, such as beam–column joins, while low workability is adopted in large sections and concrete pavements (Ismail and Al-Hashmi 2008). In this study, the design approach undertaken entails keeping all factors constant while the sisal fibers were added in increments of 0.5% by weight of cement. Results of the slump test and compaction factor are presented in Table 4.18. It shows the average slump and compaction factor values for each mix versus the percentage of sisal fiber added.

Table 4- 18: Slump and compaction factor value of SFRC.

SFRC	Slump(mm)	Compaction Factor	% Reduction in Slump	% Reduction in Compaction Factor
M0.0	92	0.93	0.00	0.00
M0.5	69	0.88	25.00	5.38
M1.0	52	0.85	43.48	8.60
M1.5	40	0.80	56.52	13.98
M2.0	20	0.73	78.26	21.51

For a constant water-cement ratio of 0.47 that was used in the mix design, there was a general decrease in the workability of fresh SFRC as reported by a consistent drop in the slump and compaction factor values as the percentages of sisal fibers were increased in the mix, as seen in Figure 4.5.

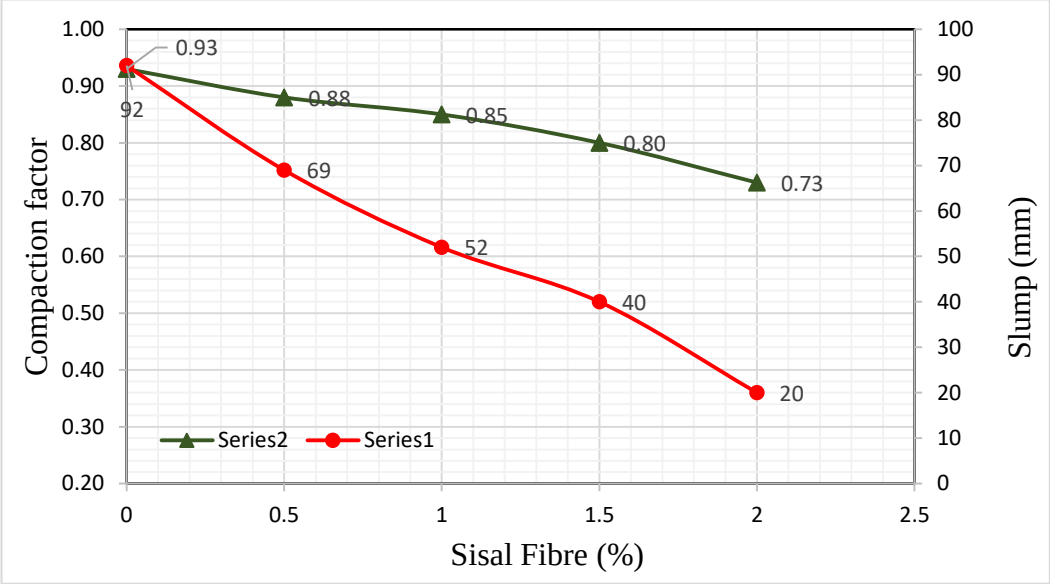

Figure 4- 5: Workability of SFRC.

The slump and compaction factor value, respectively reduced from 92 mm and 0.93 for the control mix without sisal fiber to 20 mm and 0.73 for a 2% addition. The lowest workability recorded falls in the very low range (0–25 mm) and the highest workability observed (92 mm) is classified as medium workability (50–100 mm). The decrease in the workability of fresh SFRC can be seen to be linear and proportional to the percentages of sisal fibers added to the mix. Although the mix remained workable in nature, additional efforts was required for proper compaction, especially when the fiber content exceeds 1%. A similar result was reported by (Aruna 2014; Prahallada, Shanthappa, and Prakash 2014; Sabarinathan 2017; Tolêdo Filho et al. 1999). Incremental sisal fiber addition of 0.5%, 1.0%, 1.5%, and 2.0% resulted in a slump percentage reduction of 25%, 43.48%, 56.25%, and 78.26% while the compaction factor reduced by 5.38%, 8.60%, 13.98%, and 21.51%, respectively. This reduction in the workability of concrete was ascribed to the presence of fibers in the mix tending

to lump on each other, ball, and absorb some of the free water required for lubrication and paste formation (Tolêdo Filho et al. 1999). There is also the occurrence of poor adhesion between fibers and the matrix, resulting in the inhibition of concrete flow as fiber content increases (Malhotra and Chand., 2017; Prahallada et al., 2014). Therefore, the mix required more efforts to compact.

4.2.1.2. Effect of Sisal Fiber on the Water Absorption of Concrete

The water absorption of concrete by immersion is an important property that gives an indirect indication of the pore structure of the concrete and durability performance in a corrosive environment (De Schutter and Audenaert 2004). The water absorption of SFRC in the present study is depicted in Figure 4.6. The result indicates that reinforcing concrete with sisal fibers causes a significant increase in the water absorption of concrete. As recorded, there was a sudden rise of 28.99% in the absorption of concrete by adding 0.5% sisal fiber at 28 days. Subsequent incremental of 0.5% sisal fiber resulted in little rise until 2% sisal was incorporated in the mix, resulting in a 49.18% increase in water absorption compared to the control concrete. In summary, the water absorption of concrete cubes was observed to increase with a rising percentage of sisal fiber addition in the mix. A similar result was reported by (Hidaya, Mutuku, and Mwero 2017; Rahmani et al. 2011; Regina et al. 2017), although Afroughsabet and Ozbakkaloglu reported that including additives like silica fume in concrete can help in reducing the water absorption of FRC.

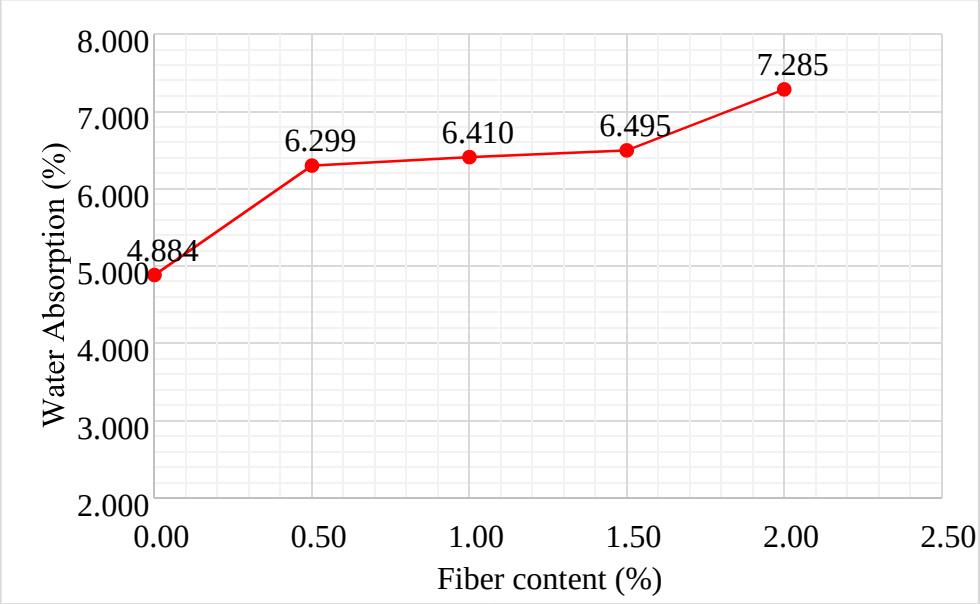

Figure 4- 6: Water absorption of SFRC.

The direct relationship between water absorption and sisal fiber percentage is a result of reduced workability, which resulted in poor compaction and increased pores. Fibers bridge the concrete pores, serving as a connecting duct for the pores and increasing permeability and porosity causing the concrete to absorb more water (Afroughsabet and Ozbakkaloglu 2015), In addition, the incorporation of fibers results in increased capillary action. Fibers can act as a water-conducting channel, increasing the water absorption of concrete (Rahmani et al. 2011). As a result, concrete becomes more susceptible to damage when exposed to a corrosive environment and hence making the concrete less durable. It is to be noted that, according to CEB-FIP, water absorption of concrete lower than 3% is classified as good, between 3% and 5% is considered average, and above 5% is poor. Hence, the control concrete falls in the average range, while concrete with sisal fiber can be said to be of poor quality.

4.2.1.3. Effect of Fiber on the Density of Concrete

The density of concrete varies as it depends on the unit weight its constituent materials, such as the amount, density, and specific gravity of the aggregates, the amount of entrapped air and water, as well as its cement content. Most standards recommend a conservative value of 2400 kg/m^3 for normal weight concrete. It is however, prudent to measure the value experimentally for accurate analysis and design purposes. In this study, it was observed that the density of concrete was generally less than 2400 kg/m^3. For all SFRC, the density increased from 7 days to 28 days due to further hydration, but the densities at each curing age tend to decrease with an increase in sisal fiber, as shown in Figure 4.7.

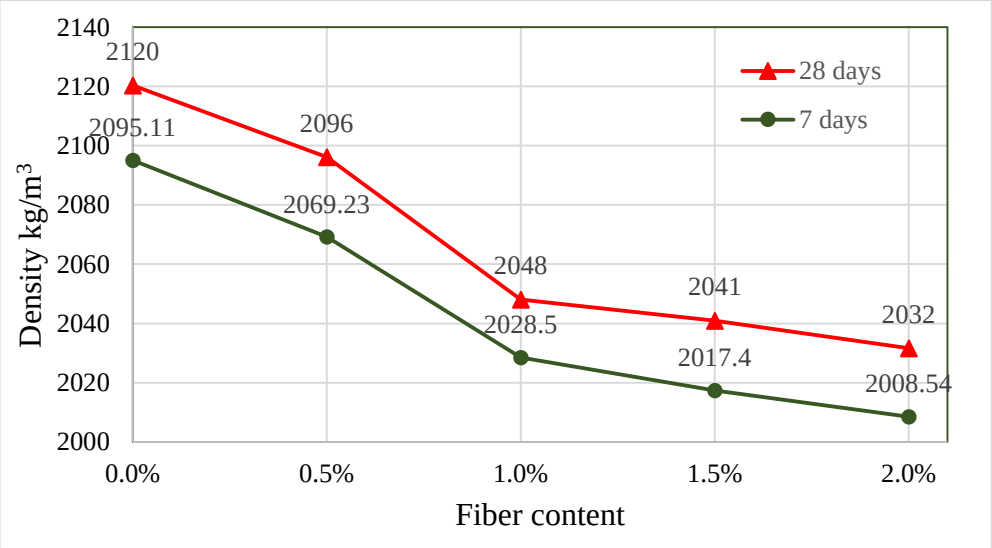

Figure 4- 7: Density of SFRC.

The result shows that M0.0 has the highest density (2120 kg/m^3), while M2.0 has the lowest density (2032 kg/m^3), which is outside the range of structural light weight concrete, hence can be classified as normal weight concrete. The density of concrete reduced at percentages of 1.14%, 3.41%, 3.74%, and 4.18% for M0.5, M1.0, M1.5,

and M2.0 as compared with M0.0 at 7 days of curing. At 28 days of curing, the percentage reductions in the density were respectively 1.24%, 3.18%, 3.71%, and 4.13%. The inverse relationship between the density and percentage of sisal fibers is a result of the lower bulk density of the sisal, which is taking the place of denser constituents, like coarse and fine aggregates (Hidaya, Mutuku, and Mwero 2017; Ismail and Al-Hashmi 2008).

4.2.2. Mechanical Properties of SFRC

4.2.2.1. Compressive Strength of SFRC

One of the most important indicators used in evaluating the performance of fiber reinforced concrete is its compressive strength. The results of the compressive strength test of SFRC at both 7 and 28 days are presented in Figure 4.8. for each curing age and increasing sisal fiber content in the concrete mix. The result shows decreasing compressive strength value below that of the control. The reduction can be attributed to the reduction in adhesive properties between the surface of the fiber and cement paste, resulting in the need for higher compacting energy and the required compressive strength (Ilya and Chea 2017). Furthermore, sisal is classified as a hydrophobic material, implying there is the tendency of it leaving behind freer water–cement, impeding strength gain.

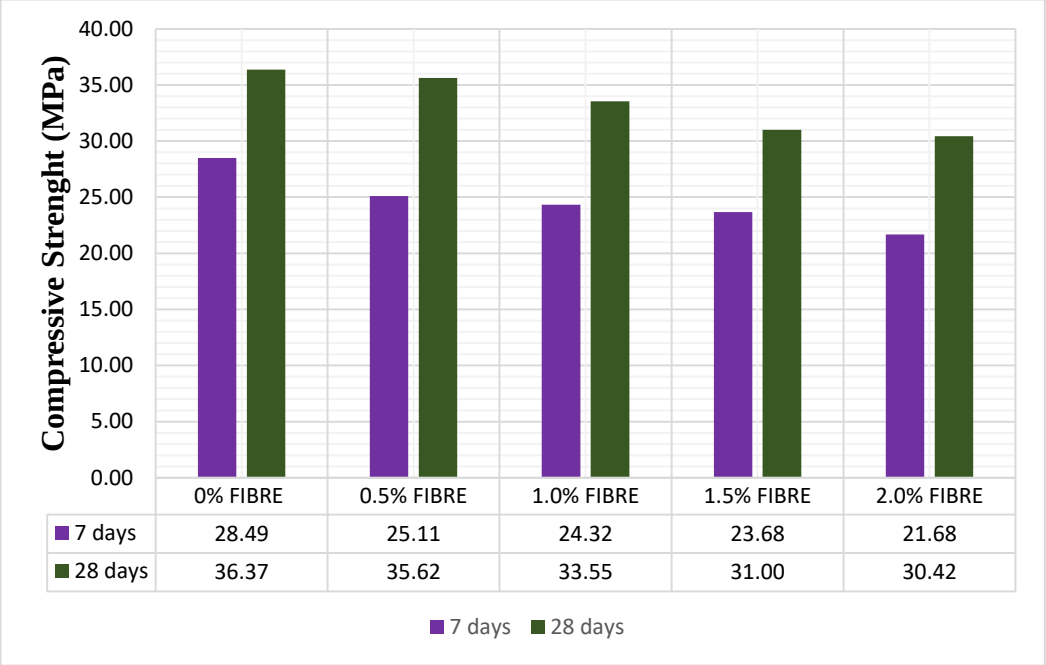

Figure 4- 8: Compressive strength of SFRC cubes.

From these results, it can be seen that M0.5 gave the least percentage reduction in compressive strength. The smallest recorded compressive strength at 28 days (30.42 MPa) was higher than the target design compressive strength (30 MPa), thus meeting the requirement for structural use according ACI committee 113. These findings are in a good agreement with the findings of (Hidaya, Mutuku, and Mwero 2017; Ismail and Al-Hashmi 2008) who showed that once the workability of fiber reinforced concrete is reduced, the compressive strength of the mix tends to decrease when compared with the reference plain concrete. A one-way ANOVA test was carried out at a 0.05 significance level and indicated that varying the percentage content of sisal has a significant impact on the compressive strength of concrete both at 7 days ($F = 19.667$, $F_{crit} = 3.478$) and 28 days ($F = 5.201$, $F_{crit} = 3.478$).

4.2.2.2. Effect of Shape on the compressive strength of SFRC

The effect of shape on the compressive strength of sisal fiber reinforced concrete is important as both cubes and cylinders can be used in obtaining compressive strength. The compressive strength of plain concrete cube was observed to be higher than that of cylinders by 27.97% and 18.04% at 7 and 28days respectively. It could be deduced from the result that cube specimen give higher compressive strength (Graybeal and Davis 2009; Hamad 2017; Nibudey et al. 2013). The specimen with the highest sisal fiber content (M2.0) gave a cube compressive strength which was 21.14% and 29.68% greater than that of the cylinders at 7 and 28 days respectively. However, these finding do not agree with that of fiber reinforced ultra-high performance concrete where the compressive strength of cylinders was reportedly higher than cubes (Kusumawardaningsih, Fehling, and Ismail 2015).

The ratio of the compressive strength of cylinder specimens (f_{cy}) to the cubes (f_{cc}) was between 0.72 and 0.54, with an average of 0.64 at 7 days as shown in Table 4.19, while the ratio of the compressive strength of cylinders (f_{cy}) to cubes (f_{cc}) was between 0.82 and 0.73 with a mean ratio of 0.79 at 28 days as depicted in Table 4.20. The difference in compression strength may be due to the applied axial force tending to align the fibers in certain planes. It tends to align the fibers parallel in cubes while in cylinders, they tend to align perpendicular to the axis of loading where they could help inhibit lateral bursting (Erdogan 2001).

From the decreasing cylinder to cube compressive strength ratio, it can be deduced that sisal fiber incorporation increases the effect specimen shape has on the compressive strength of concrete at both 7 and 28days. The ratio of the 28 days cube

compressive strength to that of cylinders was however observed to be between 1.22 and 1.37, with an average of 1.28. The higher f_{cu} is due to the development of tri-axial compression zones in cubes by virtue of the presence of restrained zones during uniaxial compression test which is absent in cylinders with an aspect ratio of 2 (Malaikah, 2005). M0.5, M1.0, M1.5 gave respective f_{cy}/f_{cc} ratio of 0.80 ,0.79 and 0.79 at 28 days which shows that the ratio of f_{cy}/f_{cc} for SFRC was in close agreement with the value 0.8 which was recommended by BS EN 12390-3.

Table 4- 19: Cube and cylinder compressive strength ratio at 7days.

Mix	Specimen	Compressive strength (MPa)	S_d	Cv	Cube: cylinder ratio	Cylinder: cube ratio
M0.0	Cube	28.49	0.62	0.02	1.39	0.72
	Cylinder	20.52	1.03	0.05		
M0.5	Cube	25.11	1.18	0.05	1.46	0.69
	Cylinder	17.25	0.15	0.01		
M1.0	Cube	24.32	1.25	0.05	1.52	0.64
	Cylinder	16.05	0.44	0.03		
M1.5	Cube	23.68	0.76	0.03	1.72	0.58
	Cylinder	13.77	0.51	0.04		
M2.0	Cube	21.68	0.90	0.04	1.87	0.54
	Cylinder	11.61	0.51	0.05		

Table 4- 20: Cube and cylinder compressive strength ratio at 28days.

Mix	Specimen	compressive strength (MPa)	S_d	Cv	Cube: cylinder ratio	Cylinder: cube ratio
M0.0	Cube	36.37	3.08	0.08	1.22	0.82
	Cylinder	29.81	0.41	0.01		
M0.5	Cube	35.62	2.54	0.07	1.25	0.80
	Cylinder	28.56	0.85	0.03		
M1.0	Cube	33.55	1.30	0.04	1.27	0.79
	Cylinder	26.37	0.76	0.03		
M1.5	Cube	31.00	1.60	0.05	1.27	0.79

	Cylinder	24.39	0.90	0.04		
M2.0	Cube	30.42	0.50	0.02	1.37	0.73
	Cylinder	22.27	0.22	0.02		

Furthermore, the variation in the effect of sisal on the compressive strength of the cube and cylinder specimen can be discerned after further curing, the disparity in the compressive strength between the two shapes grows with increase in the percentages of sisal fibers at 7 and 28 days as shown in figure 4.9 and 4.10.

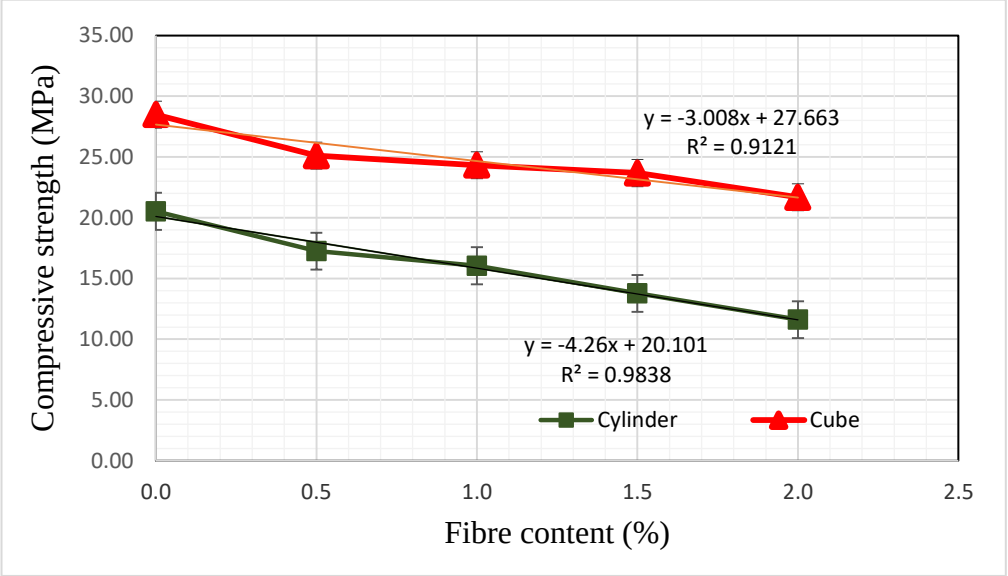

Figure 4- 9: 7 days compressive strength of SFRC cube and cylinders relationship.

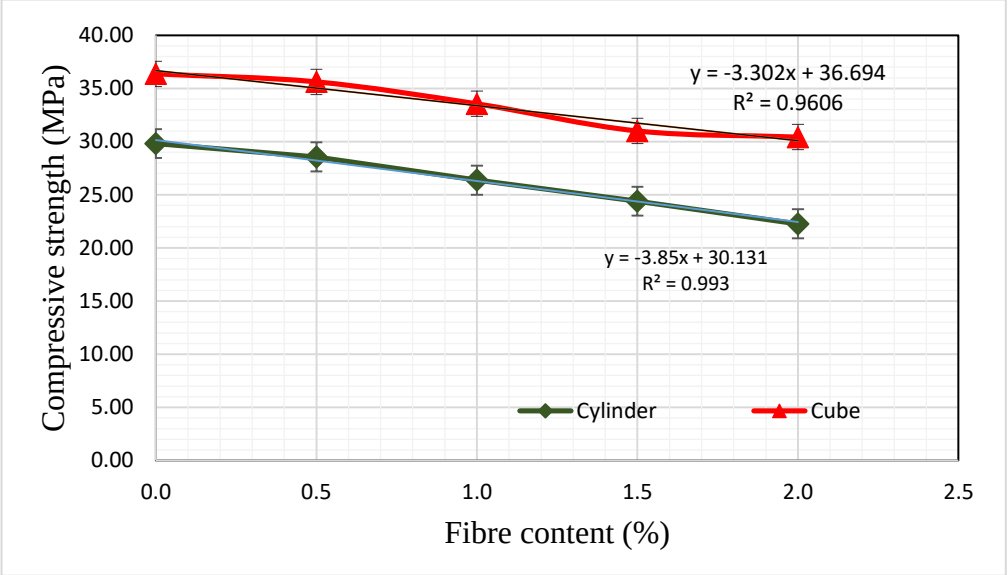

Figure 4- 10: 28 days compressive strength of SFRC cube and cylinders relationship.

Both the standard deviation and coefficient of variation increase with rising sisal fiber content at the same curing age. Certainly, incorporation of fibers reduces concrete's density, raises its water absorption and void. The increase in voids generates more interface zone between sisal and the concrete constituent's interfaces (Soto Izquierdo, Soto Izquierdo, Ramalho, & Taliercio, 2017). Consequently, SFRC has an increased number of permeable and micro crack regions than plain concrete, which further elucidate on the reduction in the compressive strength. Additionally, the greater interface zone between the fiber and concrete aggregate impacts more on the restrained zones of concrete under uniaxial compression. The tri-axial compression zones in cube specimen aids its compressive strength, however, cylinders have their unrestrained zone situated away from their ends which is further compromised by the increased interface zone as a result of fiber content. As fiber content increases, the interface zone

grows and the compressive strength of cylinders reduces, this explains the increase in the shape effect at higher fiber content. Overall, the incorporation of sisal fiber into concrete reduces its compressive strength and increases the influence shape has on the strength of concrete.

4.2.2.3. Split Tensile Strength of SFRC

This is an indirect tension test method on a concrete cylinder to obtain its tensile strength. It has long been known that the presence of fibers considerably improves the tensile strength due to the tensile stress transfer capability of the sisal fibers across concrete crack surfaces, known as crack-bridging (Chalioris, 2013). The 28 days split tensile strength value was higher than those at 7 days due to further hydration and strength gain. The results of the split tensile strength are illustrated in Figure 4.11. The data shows that sisal fibers can enhance the splitting tensile strength of concrete, but up to a limit. The split tensile strength of SFRC at each curing age increases up to 1% before declining. The maximum split tensile strength recorded was 3.463 N/mm^2 for 1.0% fiber addition. Concrete is expected to have 10% of its compressive strength as tensile strength. Thus, the finding is in close agreement with the target tensile strength of 3.5 N/mm^2 (for class 30/35). However, the least tensile strength of SFRC at 7 and 28 days was still higher than that of the control, implying that incorporation of sisal increases the tensile strength of concrete for all percentages of addition.

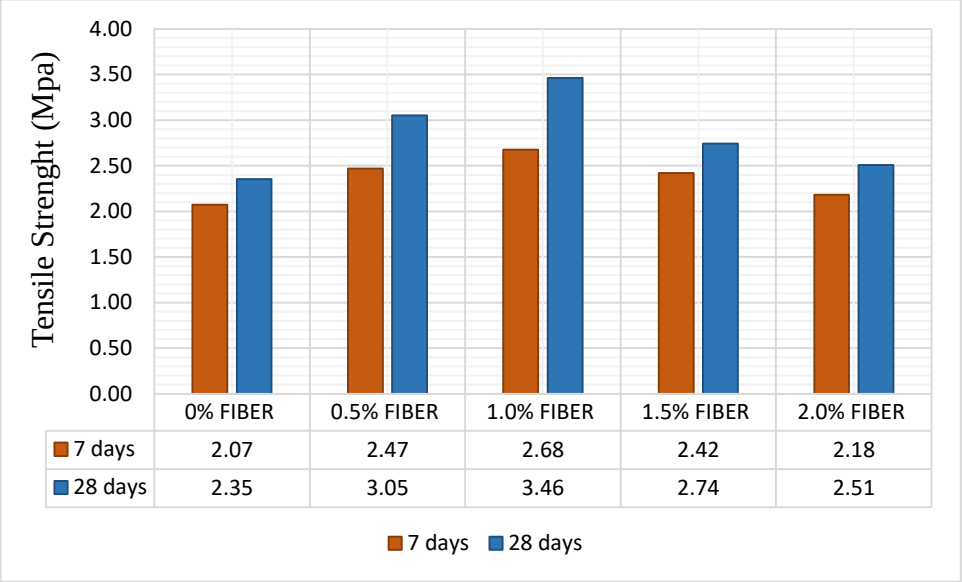

Figure 4- 11: Split tensile strength of SFRC.

A percentage increment of 19.07% and 29.14% as compared to the control was obtained for M0.5 and M1.0, respectively, while on further addition of sisal fibers, M1.5 and M2.0 showed a declining percentage increase of 16.76% and 5.18% at 7 days. Further improvement in the splitting tensile strength at 0.5%, 1.0%, 1.5%, and 2.0% fiber incorporation was noticed at 28 days of curing with a percentage increment of 29.68%, 47.17%, 16.57% and 6.63%, respectively, showing that sisal fibers can improve the split tensile strength of concrete. The observed trend in split tensile strengths of the SFRC compared favorably with those of previous works (Balasubramanian, Senthilselvan, and Sabarish 2016; Sasikumar and Thivya 2017; Sumithra Radha K.T and Dadapheer 2017). The improvement in splitting tensile strength is the ability of fibers to bridge across possible cracks and impact more ductility in the concrete as the specimens with sisal fibers didn't break into pieces, as seen in normal concrete without fiber specimens at constant stopping load. Load is transferred to the fibers at the crack site after the formation of cracks, and at this stage

different behaviour may be exhibited depending on the strength, volume fraction and aspect ratio of the fiber.

At sufficient fiber content, aspect ratio and strength, sisal fibers bridge across the possible cracks as shown in figure 6.8. Thus, sisal fibers acted as porous bridging elements across cracks, permitting the deposition of new hydration products and the subsequent infill/closure of the cracks (Tolêdo Filho et al. 1999). Furthermore, unlike the brittle failure observed in plain concrete, fibrous concrete like SFRC demonstrates a pseudo-ductile tensile behaviour and enhanced energy dissipations capacities (Karayannis 2000 and Gopalaratnam 1987). The observed trend in split tensile strengths of SFRC compared favourably with those of previous works (Sasikumar & Thivya, 2017; Sumithra K.T & Dadapheer, 2017).

The increase in the tensile strength and post cracking performance of SFRC as shown in figure 4.12 can be achieved up to a certain fiber content known as critical volume fraction; $V_{f,cr}$ (Nathan et.,al 1977; Lim and Lee 1987; Shah et.,al 1978; Sorushian 1987).

$$V_{f,cr} = \frac{f_{ct}}{n_1 n_0 \sigma_{fu}} \qquad 4.1$$

Where f_{ct} is the tensile strength of plain concrete; n_1 is the ratio of the average fiber stress to the maximum fiber stress and equals to 1, n_0 is the fiber orientation factor in the elastic range and equals to 0.405; σ_{fu} is the ultimate fiber stress. For the tested fibrous concrete mixtures, the ultimate fiber stress equals 399.44MPa and the tensile strength of plain concrete is 2.353MPa giving a critical volume fraction of 1.45%. Hence, for the post-cracking tensile behaviour of the concrete mixtures with 1.50%

and 2.0% volume of fibers, a lower tensile stress after the peak stress (tensile strength) is expected. A one-way ANOVA test at a 0.05 significance level portrayed that sisal fibers did have a significant impact on the split tensile strength of concrete at 7 days (F = 42.854, sig = 3.478), while at 28 days the sisal fibers had a lesser impact on the split tensile strength of SFRC (F = 12.872, sig = 3.478).

(a) (b) (c) (d) (e)

Figure 4- 12:.Failure modes of concrete cylinder (a) M 0.0 (b) M 0.5 (c) M1.0 (d) M 1.5(e) M 2.0

4.2.2.4. Axial Strain Ductility of SFRC

The axial strain gives an indication of the ductility properties of SFRC. An axial strain of 0.00120, 0.00112, 0.00106, 0.00105, and 0.00104 was recorded for M0.0, M0.5, M1.0, M1.5, M2.0, respectively, at 85% of the maximum stress of the concrete samples. The recorded strains represent a percentage decrease of 7.17%, 11.55%, 12.59%, and 13.55% compared to that of plain concrete. This implies that sisal fiber reduces the axial strain of concrete.

4.2.2.5. Modulus of Elasticity of SFRC

The measured E_c showed significant variation with compressive strength and sisal fiber content. As seen in Table 4.22, the E_c increases for decreasing compressive strength up to a limit, beyond which it drops. The lowest mean value of E_c was 25086.77 MPa for M0.0, while the maximum was seen in M1.0 (31654.19 MPa). A

percentage increase in E_c of 16.15% and 26.18% could be seen for M0.5 and M1.0.

Table 4- 21: Modulus of elasticity concrete.

Mix	Modulus of Elasticity (MPa)	Change in *Ec* (%)	Compressive Strength (MPa)	Yield Strain
M0.0	25086.77	0.00	32.97	0.00187
M0.5	29138.60	16.15	31.14	0.00179
M1.0	31654.19	26.18	30.23	0.00174
M1.5	28926.78	15.31	27.29	0.00172
M2.0	25379.31	1.17	24.27	0.00171

Furthermore, the addition of sisal fibers resulted in lower strains at ultimate compressive stress in comparison with the control. The longitudinal strain at maximum compressive stress was generally lower than 0.0019 for SFRC, with the maximum strain being observed in the control (0.00187). Figure 4.13 shows that M0.5 and M1.0 had better post-yield behavior, unlike the control that exhibited quasi-brittle failure.

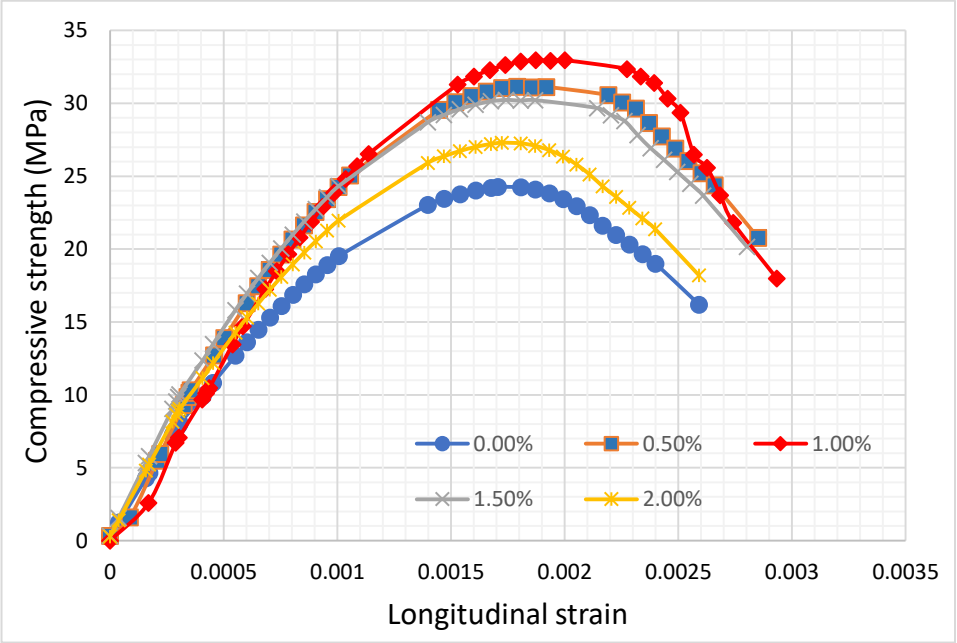

Figure 4- 13: Compressive stress and longitudinal strain of concrete.

4.2.2.6. Relationship between Modulus of Elasticity and Compressive Strength

In comparing the measured Ec for SFRC with the expressions given in the codes, the measured Ec and the predicted values from the codes are plotted in Figure 4.14. While BS 8110-2, ACI 318M-08 , ACI 318 , and CSA 123-3-04 all underestimated the value of Ec for SFRC, IS 456-1989, Eurocode-2 and TS50 better predict the Ec of SFRC. The ratio of the measured Ec of SFRC to that obtained from the equations in the three aforementioned codes that gave values close to Ec obtained during the test was computed to establish the degree of variation in the codes and computed Ec. The calculated average ratios are 0.986, 0.958, and 0.937 for IS456-1989, Eurocode-2, and TS50, respectively. From these ratios, Eurocode 2 annd IS 456 gave the highest ratios.

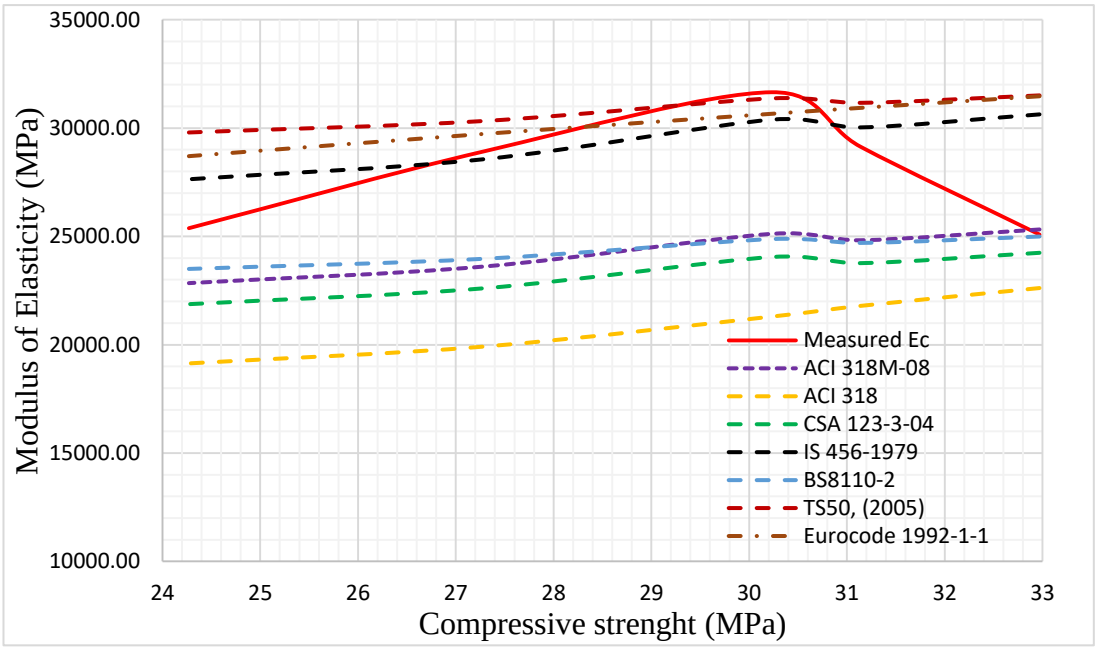

Figure 4- 14: Comparison of the measured and predicted E_c values.

For comparing the constants given by Eurocode-2 and IS 465-1989, a simple regression analysis was done on the measured Ec using the equation forms recommended by the codes as shown in Figure 4.15 and 4.16. The constants obtained

from the regression analysis are (7377.4 and 47.498) respectively which deviates from those given by the codes (5688 and 22). Considering the coefficient of determination obtained, the function, which best represents the measure Ec, is that from Eurocode-2. A power trend line was fitted for both predicted values to improve the coefficient of determination. The power equations gave a higher coefficient of determination of 0.7349 for both codes.

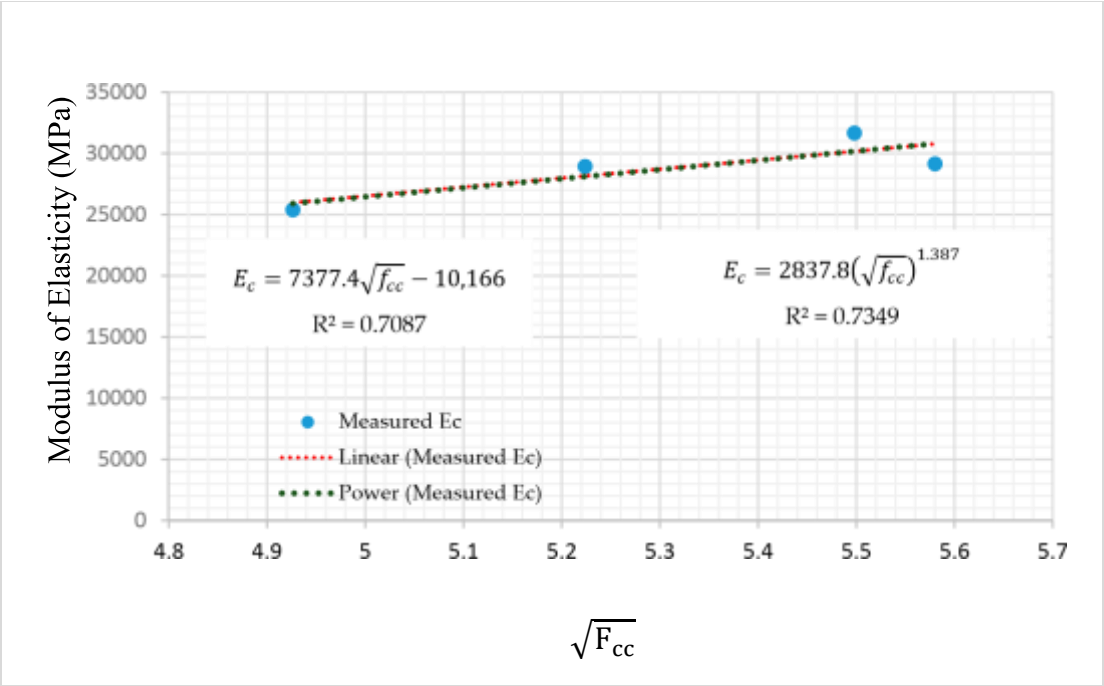

Figure 4- 15: The relationships between E_c and f_{cc} in the form of IS456-1989 equations.

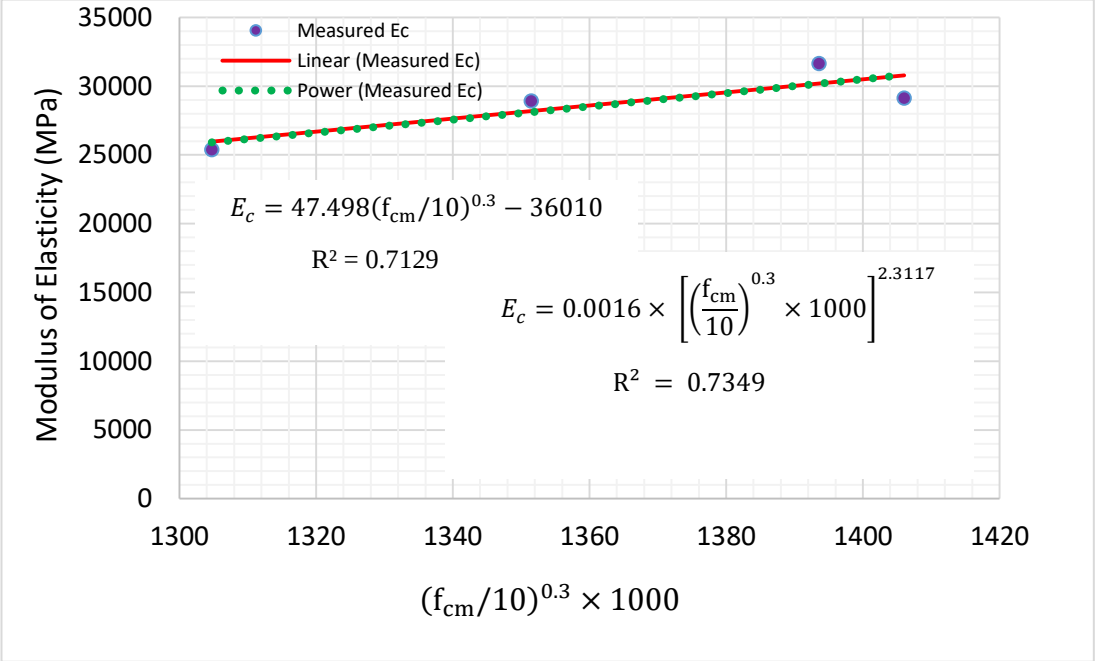

Figure 4- 16: The relationships between E_c and f_{cc} in the form of Eurocode equations.

4.2.2.7. Poisson ratio of SFRC

The ratio of the transverse strain to the axial strain known as Poisson's Ratio (ν), Figure 4.17 shows the variation of Poisson ratio with fiber content at 40% of ultimate stress.

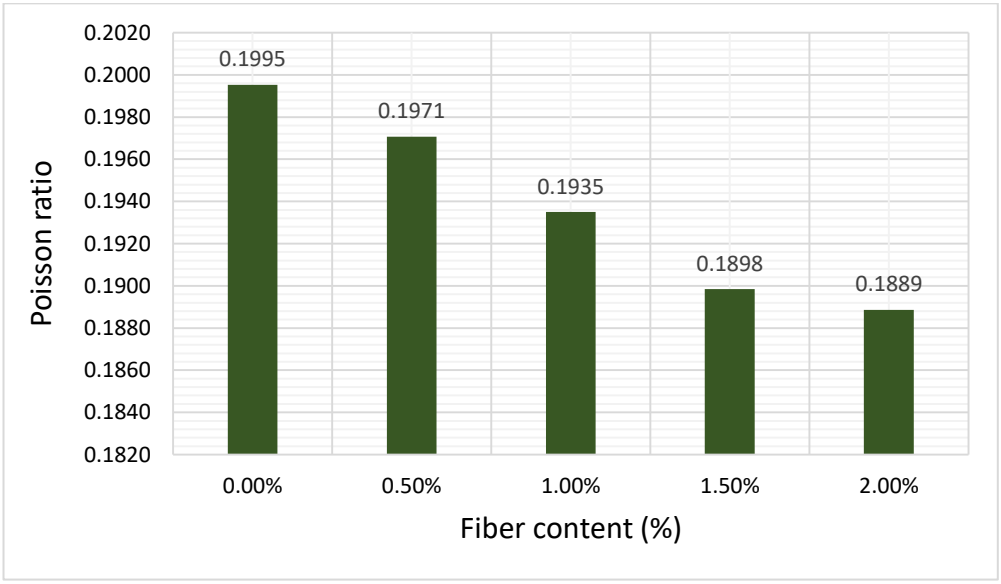

Figure 4- 17: Poisson ratio of SFRC.

The measured value of Poisson ratio ranged between 0.200 and 0.189. Plain concrete had a Poisson ratio of 0.1995, for normal strength concrete, a value of 0.2 is usually adopted (Ganesan, Indira, & Santhakumar, 2013) while SFRC showed a slight decrease in Poisson ratio as the fiber content increased. The reduction in the Poisson ratio demonstrates that the presence of sisal fibers in a concrete matrix arrests deformation, reduces expansion and stretches in all directions, resulting in less destructive external surface (Dinh, Choi, & Kim, 2016; Gao, Sun, & Morino, 1997). Similar reduction in Poisson ratio of fiber reinforced concrete was reported by (Smirnova, Shubin, & Potseshkovskaya, 2017). The relationship between Poisson's ratio and fiber content follows the equation.

$$\mu_f = \mu_c - 0.5709V_f. \qquad 4.2$$

Where μ_f is the Poisson ratio of SFRC; $\mu_c$the poisson ratio of plain concrete and V_f is the fiber content.

4.2.2.8. Failure mechanism of SFRC

Figure 4.18 shows the failure mode of cube and cylinder specimen after compression test. The stopping load for all the specimen was set at 40% of the failure load. Cracks were observed to form in the longitudinal direction before the peak stress and propagate in the lateral direction as the applied load increases. Inclined shear failure cracks were formed at the beginning of the softening phase. The crack pattern were columnar for cylinders and non-explosive for cubes. It was noticed that the cracks formed were wider with higher numbers in the specimens without sisal fibers (M0.0), whereas, they were reduced for SFRC. The least number of cracks was noticed on

M2.0.

The improved tensile strength and cracking performance of sisal fiber is important in the shear response of structural elements like concrete beams. The effect of using sisal fiber in concrete is quite similar to that of steel fibers reported by (Watanabe, Kimura, & Niwa, 2010). Thus, fibers like sisal could be promising as a non-conventional reinforcement in shear critical beams by potentially reducing shear reinforcements and altering shear brittle failure into ductile flexural ones (Chalioris, 2013). Unlike sisal however, steel fibers has already been used to partially reduce steel stirrups especially in sections where high transverse steel ratio with small spacing is required (Ding et al.,

(a) (b) (c) (d) (e)

(a) (b) (c) (d) (e)

Figure 4- 18: Failure modes of concrete after compression.(a)M0.0 (b)M0.5 (c)M1.0 (d)M1.5 (e) M2.0

4.3. The Durability of Sisal Fiber Reinforced Concrete Using Mechanical Strength and Colorimetric Method

4.3.1. Chloride Penetration Test of SFRC

As stated in the methodology, the $AgNO_3$ was sprayed onto the concrete surface. The violet region indicated the depth of penetration of chlorine as shown in Figure 4.19 while the brown and white regions indicated no signs of chloride attack.

Figure 4- 19: Measuring chloride penetration depth

Table 4- 22: Depth of chloride penetration at 28 days.

	Chloride Penetration Depth (mm)								
Specimen	1	2	3	4	5	6	7	8	Average
M0.0	17.82	20.17	15.90	19.24	20.12	18.78	21.73	21.89	19.45
M0.5	20.90	22.39	21.40	22.85	22.32	21.51	20.90	22.98	21.90
M1.0	25.34	26.00	25.43	25.45	24.82	25.76	25.39	24.49	25.33
M1.5	25.02	26.23	25.90	25.27	26.40	26.67	26.50	27.32	26.16
M2.0	28.52	27.88	29.66	30.77	29.56	29.61	30.09	29.35	29.43

Based on Table 4.23 the concrete made with 2.0% sisal fiber had the highest average depth of chloride penetration. This imply that incorporation of sisal fiber does not

lessen the diffusion of chloride ion inside the concrete thus reaching the reinforcing steel faster. This is attributed to the reduction in the cement gel (C-S-H) which was used in coating the sisal fiber when incorporated in the concrete. This gel reduction resulted in more void spaces and capillary movement in the concrete make it more permeable to chloride and chemical attack. At 56days, the depth of chloride ingress increased from what was observed at 28days. A percentage increase of 6.60%, 4.22%, 2.05%, 4.46% and 5.03% were observed in M0.0, M0.5, M1.0, M1.5 and M2.0 respectively as depicted in Table 4.24.

Table 4- 23: Depth of chloride penetration at 56 days.

	Chloride Penetration Depth (mm)								
Specimen	1	2	3	4	5	6	7	8	Average
M0.0	19.15	21.18	20.02	20.04	21.02	19.79	21.73	22.99	20.74
M0.5	23.05	23.20	22.60	23.58	22.91	22.32	21.75	23.24	22.83
M1.0	26.55	25.60	25.53	26.50	25.47	25.91	26.29	24.99	25.85
M1.5	26.82	27.42	26.97	25.87	27.49	27.57	28.10	28.39	27.33
M2.0	30.27	29.80	30.52	31.47	30.36	31.27	32.59	31.02	30.91

Collepardi et al. found that chloride penetration depth (x) varies with the elapsed time (t), following Fick's second law under unsteady state conditions for diffusion in a semi-infinite solid which states that:

$$x = 4 \times \sqrt{D.t} \qquad 4.3$$

Where D is the diffusion coefficient of chloride ions into the concrete pores filled with

water, expressed in cm^2/s. The value of D, obtained from the equation is presented in Table 4.25. The value ranged between 1.95 cm^2/s and 2.94 cm^2/s for 28 days which decreased to 0.48 cm^2/s and 1.07 cm^2/s respectively at 56 days. This shows that diffusion coefficient of SFRC reduces with exposure days.

Table 4- 24: D values and chloride depth prediction

D values		Predicted chloride depth			
28days	56days	28 days	% difference	56 days	% difference
1.95	0.48	19.61	-0.83	20.56	0.84
2.19	0.58	22.03	-0.60	23.05	-0.96
2.53	0.75	24.46	3.47	25.53	1.25
2.62	0.83	26.88	-2.74	28.02	-2.52
2.94	1.07	29.30	0.45	30.50	1.33

An attempt was made to predict the depth of penetration of chlorine in SFRC taking into consideration the fiber content and exposure days. As shown in Figure 4.20 the linear equation proposed can accurately predict the depth of penetration to 98.68% and 97.76% accuracy at 56 and 28days respectively.

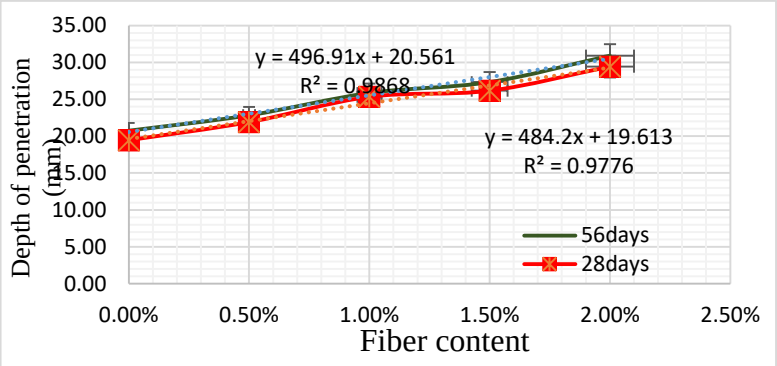

Figure 4- 20: Depth of penetration and fiber content

4.3.2. Sorptivity of Sisal Fiber Reinforced Concrete

The Sorptivity value of unsaturated concrete is an indication of its susceptibility towards water penetration. It is directly related to the micro structural and pore

properties of concrete. The plot of the Sorptivity value with square root of time is presented in Figure 4.21. It can be seen that the control cubes achieved an initial sorptivity value of 0.0263mm/s$^{1/2}$ with the value increasing for each percentages of fiber content. It was observed that increase in fiber content (from 0.5% to 2.0%) resulted in a rise in sorptivity value by 13.52%, 25.78%, 25.87%, 31.07%. This can be attributed to the sisal being a vegetable fiber with a reasonably high water absorption aiding water movement.

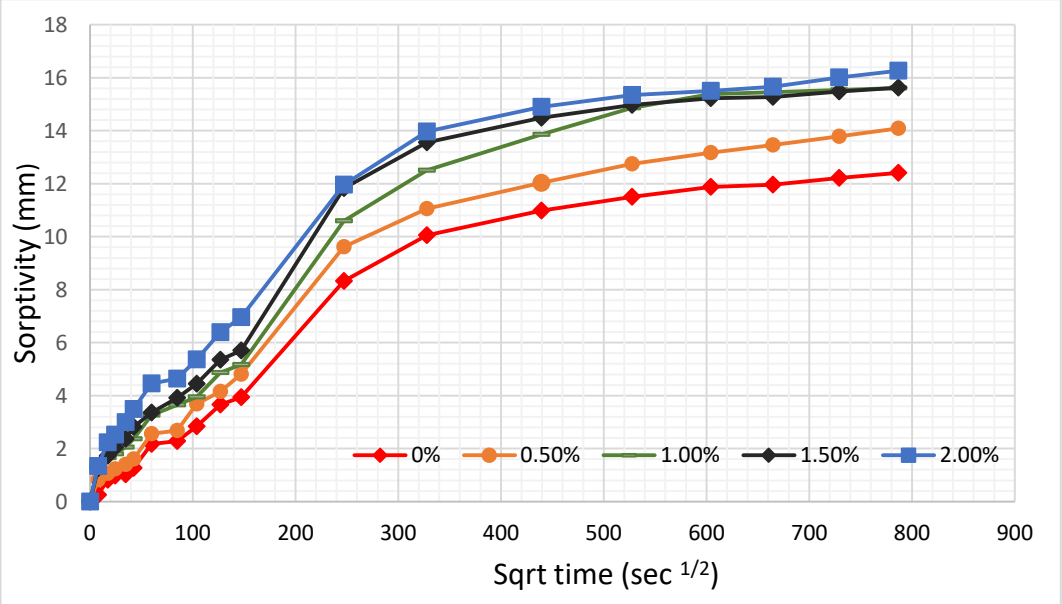

Figure 4- 21: Sorptivity of sisal fiber reinforced concrete.

The initial and final rate of water absorption (mm/s$^{1/2}$) is given as the slope of the linear regression that is the best fit to sorptivity plotted against the square root of time (s$^{1/2}$) for the first 6hours up to 7days, both are depicted in Figure 4.22. The values of the initial rate of water absorption increases from 0.0263 mm/s$^{1/2}$ to 0.0413 mm/s$^{1/2}$ as the fiber content increases due to the concrete rapidly absorbing water. The final rate of

water absorption however rose up to 0.0088 mm/s$^{1/2}$ for 1.0 % fiber from 0.0067 for 0.0% fiber content before declining, which is attributed to the higher fiber content getting saturated and no longer aiding capillary action. This indicates that SFRC have a less compacted structure due to the presence of fibers which connects the pores.

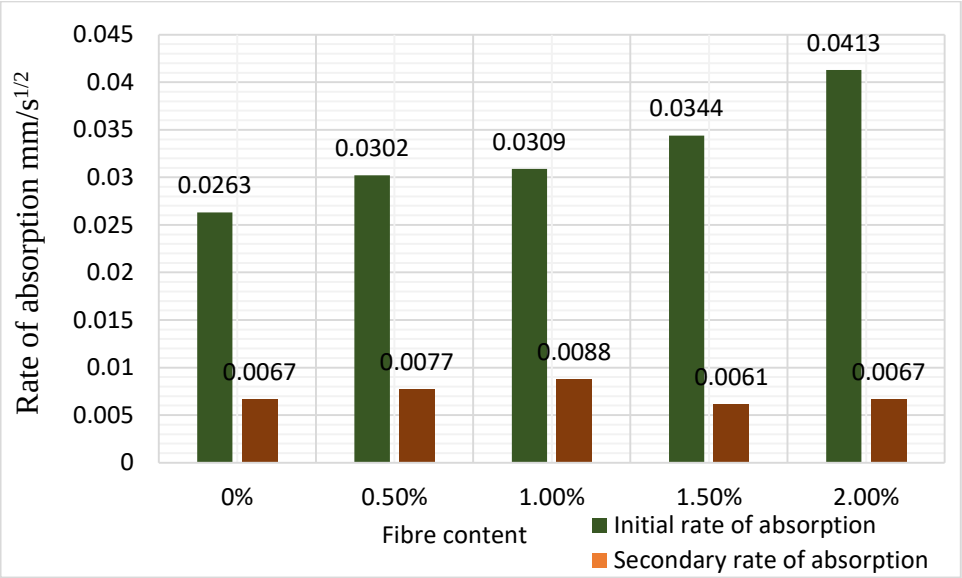

Figure 4- 22: Initial and secondary rate of absorption of SFRC.

4.3.2.1 Relationship between sorptivity and compressive strength of SFRC

In relating the compressive strength of SFRC with the initial and secondary sorptivity rate, the graph of initial and secondary sorptivity of SFRC times the square root of cube compressive strength ($Si \times \sqrt{f_{cu}}$) with respect to fiber content is presented respectively in Figure 4.24. The maximum $S_i \times f_{cu}$ is observed in 2.0% fiber content while 1.0% had the highest $S_s \times f_{cu}$. $S_i \times f_{cu}$ was observed to increase with increasing fiber content with a correlation coefficient of 0.9125 while $S_s \times f_{cu}$ increases only up till 1.0% fiber content with a relatively lower coefficient of correlation. The mathematical model for prediction of initial and secondary sorptivity

of SFRC is presented in equation 4.4 and 4.5. Based on the equations, the measured and predicted sorptivity value shown in table 4.24 depicts that equation 4.4 and 4.5 from Figure 4.23 can predict the initial sorptivity value more accurately as the percentage difference in sorptivity value was observed to be less than 5.99%, unlike secondary sorptivity that had a percentage difference as high as 22.92%. From these percentage differences, the determination of the initial sorptivity using equation 4.4 will give a near realistic value.

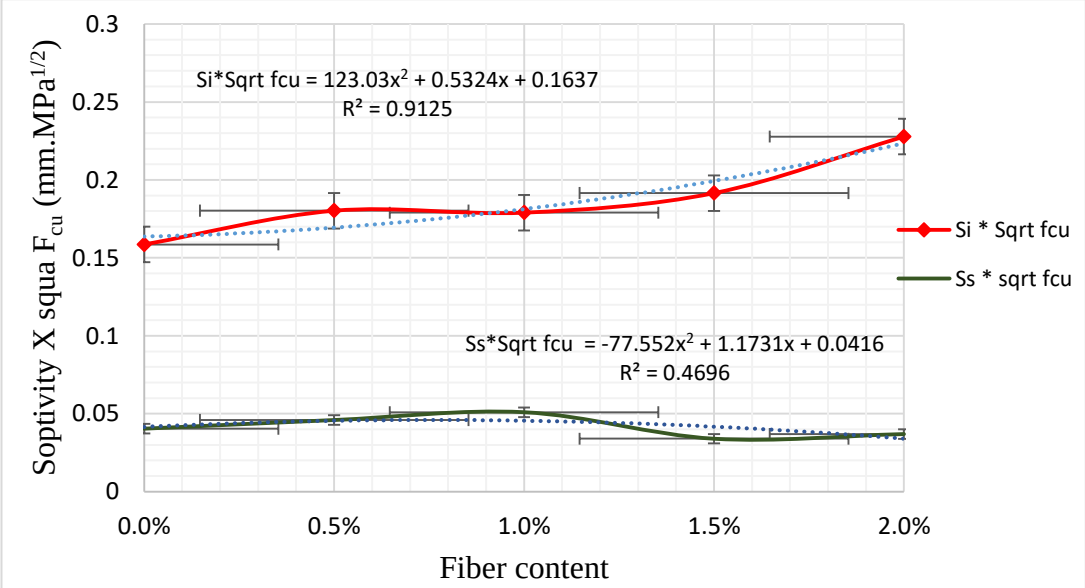

Figure 4- 23: Sorptivity and strength product vs fiber content.

$$S_i = \frac{1}{\sqrt{f_{cu}}}\left(-77.552V_f^{\,2} + 1.1731V_f + 0.0416\right) \quad 4.4$$

$$S_s = \frac{1}{\sqrt{f_{cu}}}\left(123.03V_f^{\,2} + 0.5324V_f + 0.1637\right) \quad 4.5$$

Table 4- 25: Predicted initial and secondary sorptivity of SFRC.

Fiber content	Initial sorptivity			Secondary sorptivity		
	Measured	Predicted	%	Measured	Predicted	%
0.0%	0.0263	0.0271	3.21	0.0067	0.0069	2.95
0.5%	0.0302	0.0284	5.99	0.0077	0.0076	0.93
1.0%	0.0309	0.0313	1.31	0.0088	0.0079	10.59
1.5%	0.0344	0.0358	4.09	0.0061	0.0075	22.91
2.0%	0.0413	0.0405	1.85	0.0067	0.0062	7.88

4.3.3. Effect of Sulphuric acid on SFRC

The results of the change in mass of concrete exposed to acidic medium depends on the size of the samples and cement type (such as Portland cement, sulphate resistance cement and use of SCMs), The mass change can also be significantly affected by the process of treating the reaction products, and disintegrated cement paste on the samples. Thus, the average compressive strength of the degraded samples was evaluated at the end of the exposure to the sulphuric acid solutions and compared with the initial 28 day compressive strength. Note that due to the loss of materials and surface irregularities, determining the accurate value of the strength becomes a difficult task.

After immersion in sulfuric acid solution, due to the chemical reaction between the hydration products of concrete and the surrounding acid, a calcium sulphate hydrate or a protective layer forms on the sound inner part of the concrete that has not experienced an acid attack yet. The limestone aggregates of the concrete specimens also play a part in the formation of this layer by reacting with sulfuric acid. Although the protective layer, which consists of loose particles and reaction products, is thoroughly washed after each exposure period, a visual inspection of the specimens

and crushed pieces of the concrete cylinders after the compression test indicates that the protective layer still exists and its effects on the load bearing capacity and other properties of the specimens cannot be neglected.

Bassuoni and Nehdi (2007) stated that the compressive strength of concrete specimens is affected by the properties of the concrete matrix (binder type, aggregates, w/c ratio, etc.), consolidation and curing methods, geometry and aspect ratio. The irregularities in geometry across the height of the degraded concrete cubes can result in non-uniform distribution of stresses while applying the compressive load and subsequent inconsistent results. The effects of the continuous hydration of the sound parts of the specimens and formation of a gypsum layer on the load bearing capacity of concrete samples should also not be neglected.

Figures 4.24 shows the weight loss for the fiber reinforced concrete, with and without fiber content due to corrosion of concrete by sulphuric acid. The corrosion rate is found to be affected by the duration of stay in the acid medium. Sulphuric acid attack on SFRC was more severe on concrete with 2% fiber content and reduced in the control specimen.

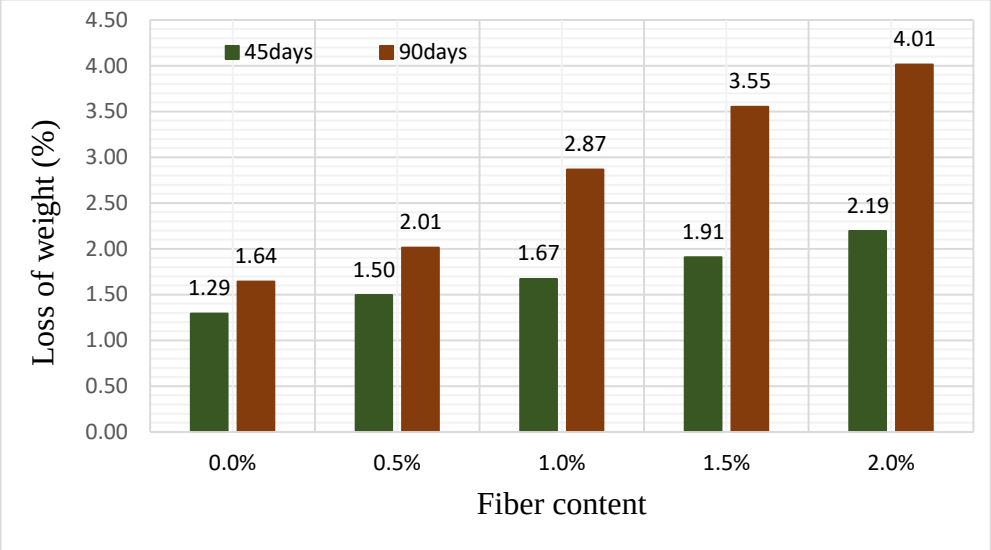

Figure 4- 24: Loss of weight of SFRC in acidic medium.

After 45 days of exposure to sulphuric acid, the weight loss for the control specimen was around 1.29%, which increased steadily until 2.19% for 2.0% sisal fiber content. However, at 90days the reduction in the weight was more significant with about 4.01% reduction observed in the SFRC with highest fiber content. This indicates that sulphuric acid attacked the hydration products of cement and the soluble corrosion products diluted the acid solution as observed with the reduced pH content. The initial corrosion rate for concrete by sulphuric acid is low and once the new surface was exposed by the removal of the corroded products and the new sulphuric acid solution was replaced the diluted acid, the rate of corrosion was increased significantly, as seen from Figure 4.25.

Figure 4- 25: Concrete cubes after 90days of exposure to sulfuric acid solution.

As per Table 4.27, due to acid attack test, percentage loss in compressive strength of control concrete specimen after 45 days is 0.96% and after 90 days percentage loss in compressive strength is 2.92%. In the case of SFRC, percentage loss in compressive strength was observed to be higher at 90 days compared to 45days for all specimen due to further corrosion. The reduction in the compressive strength generally increases as the fiber content increases. Significant reduction of 4.77% and 8.21% was respectively noted in 2.0% fiber content due to its higher void spaces. The behaviour of the specimens from the control mix in Table 4.27 is interesting to observe. M0.5, M1.0, M1.5 and M2.0 respectively experienced 3.81%, 5.31%, 7.05% and 8.21% strength loss after 90 days. The reason behind the significant loss of strength of the control samples at the end of 90days period can be the result of destruction of the concrete structure as will be shown in the visual inspection section of this chapter. It

appears that in the sulphuric acid attack, the early decomposition of calcium hydroxide and subsequent formation of layer amount of gypsum are attributed to the progressive deterioration accompanied by the scaling and softening of the matrix.

Table 4- 26: Compressive strength of cubes in acid medium.

Fiber	28days fcu water(MPa)	45days f_{cu}	% Change	90days f_{cu}	% change
0.00%	37.68	37.32	0.96	36.58	2.92
0.50%	36.04	35.43	1.68	34.67	3.81
1.00%	34.30	33.55	2.20	32.48	5.31
1.50%	32.76	31.62	3.47	30.46	7.03
2.00%	31.56	30.05	4.77	28.97	8.21

3.4. Effect of NaOH on Sisal Fiber reinforced concrete

Figure 6.9 shows the change in weight of control mix and SFRC when immersed in sodium hydroxide (NaOH) solution. The percentage weight loss, which is an indication of durability, decreases as the percentage of fiber content in concrete increases.

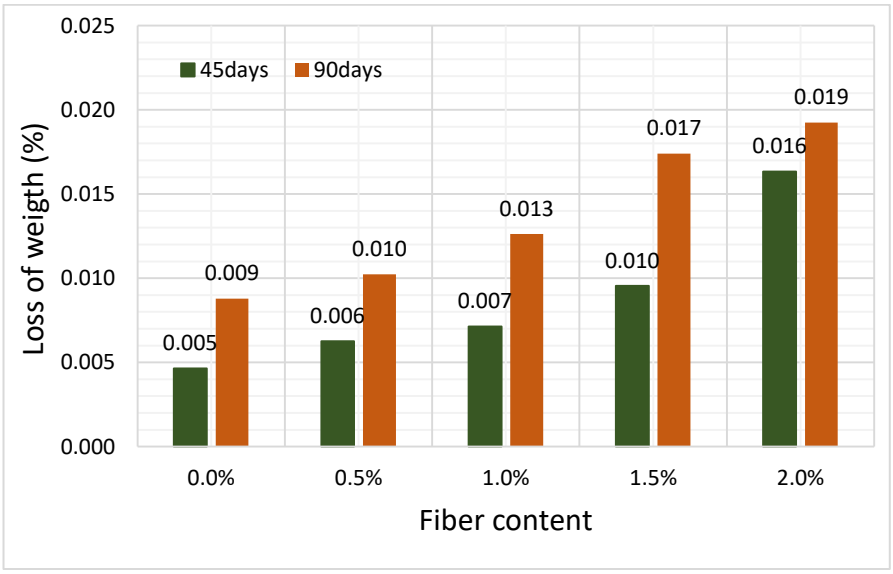

Figure 4- 26: Loss of weight of SFRC in basic medium.

The weight of SFRC due to the presence of NaOH was observed to increase as

presented in figure 4.26. The weight loss were found to be insignificant over an extended period of 45 and 90 days. The basic medium, was found to have little effect on the concrete paste as well as the surface of the concrete specimen were observed not to deteriorate as seen in Figure 4.27. The maximum recorded weight loss (0.019%) was observed in 2.0% SFRC at 90days which may be due to the to the fact that the SFRC has more voids allowing the alkaline medium to penetrate into concrete mass and also reducing the content of calcium hydroxide. Thus the percentage weight loss will increase as the percentage of fiber content increases.

Figure 4- 27: Concrete cubes after 90days of exposure to basic solution.

The specimens with no fiber content immersed in sodium hydroxide solution suffered minimal strength loss than the ones with fiber content. For example, at the end of the 45 and 90days exposure period, the M2.0 samples had a SL of 0.11% and 0.14% respectively as shown in Table 4.28. Similar increasing trend was observed with concrete exposed to sulphuric acid which can be the result of a higher penetration of sodium hydroxide which results in the significant removal of the surface layer. Hence,

the undisturbed sound inner core of the concrete will play a major part in its strength. The severity of the attack and its detrimental effect on concrete becomes more significant with increasing fiber content after 45 and 90 days of exposure whereas the strength loss wasn't as significant in the control specimen.

Table 4- 27: Compressive strength of cubes in basic medium.

Fiber	28days f_{cu} in water	45days f_{cu} (MPa)	% change	90days f_{cu}	% change
0.00%	37.68	37.64	0.11	37.63	0.14
0.50%	36.04	35.99	0.14	35.98	0.16
1.00%	34.30	34.24	0.17	34.22	0.22
1.50%	32.76	32.70	0.19	32.68	0.25
2.00%	31.56	31.49	0.23	31.47	0.29

4.4. Behaviour of SFRC Beam -Column Joints under Monotonic Load

4.4.1. Load carrying capacity

For each value volume fraction (V_f), two specimens were tested. As the difference between the two test results was found to be less than 10%, the average values of the test results was taken. The results for the test specimens are shown in Table 4.29.

Table 4- 28: Details of specimens and test results

Specimen	V_f	First crack load (kN)	Yield load (kN)	Ultimate load (kN)	Deflection at ultimate load (mm)	Stiffness at ultimate load (kN/mm)
M0.0	0.0	4.75	19.65	21.06	24.99	0.84
M0.5	0.5	5.02	20.09	22.05	25.02	0.88
M1.0	1.0	8.26	20.47	22.65	25.29	0.90
M1.5	1.5	9.13	20.85	22.70	25.83	0.88
M2.0	2.0	9.30	20.99	22.79	26.72	0.85

Yield load and ultimate load for each specimen were compared in Figure.4.28. Results shows an increase in the first crack load which rose with increasing fiber content.

Compared to the control, an increase of about 95.78% in the first crack load and 8.21% in the ultimate load for the specimens with 2.0% sisal fibers. The increase in ultimate load may be due to the following reasons. As and when the micro-cracks develop in the matrix, fibers intercepted the cracks and prevented them from propagating in the same direction (Ganesan and Indira, 2000). Hence the cracks have to take a deviated path, which requires more energy for further propagation, thus resulting in higher load carrying capacity. Fibers also played a crucial role in decreasing the deflection of the joints, specimens with fiber content performed significantly better than the mix without fibers, this resulted in improved stiffness at ultimate load for all specimen with fiber content.

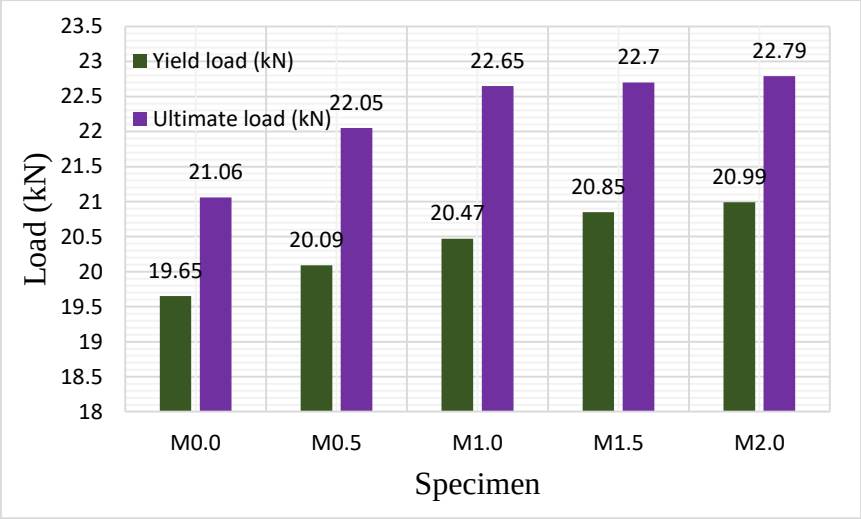

Figure 4- 28: Comparison of yield load and ultimate load of each specimen

4.4.2. Load vs deflection characteristics

A typical load-deflection plot is shown in Figure 4.29. In the load versus deflection characteristics, ultimate load and ultimate deflection were compared for each specimen. M2.0 had a higher ultimate load-carrying capacity and deflection than other

specimens with lower sisal fiber content and the control specimen. A percentage reduction of 0.12%, 1.20%, 3.36% and 6.92% was noticed in the deflection when M0.0 was compared with M0.5, M1.0, M1.5 and M2.0 respectively. Similar increase in ultimate strength of 2.24%, 4.17%, 6.11% and 6.82% was reported. It is concluded from the load versus deflection characteristics graph that specimens having sisal fiber showed better ultimate load-carrying capacity and deflection than specimens having no sisal fiber with similar reinforcements detailing.

Furthermore, it can be seen that fiber reinforced specimens showed more or less no strength degradation for the ascending portion of the load-deflection plot and that the load carrying capacity of the joints increased with increasing fiber content. The area under the load-deflection curve represents the energy absorption capacity of the specimen.

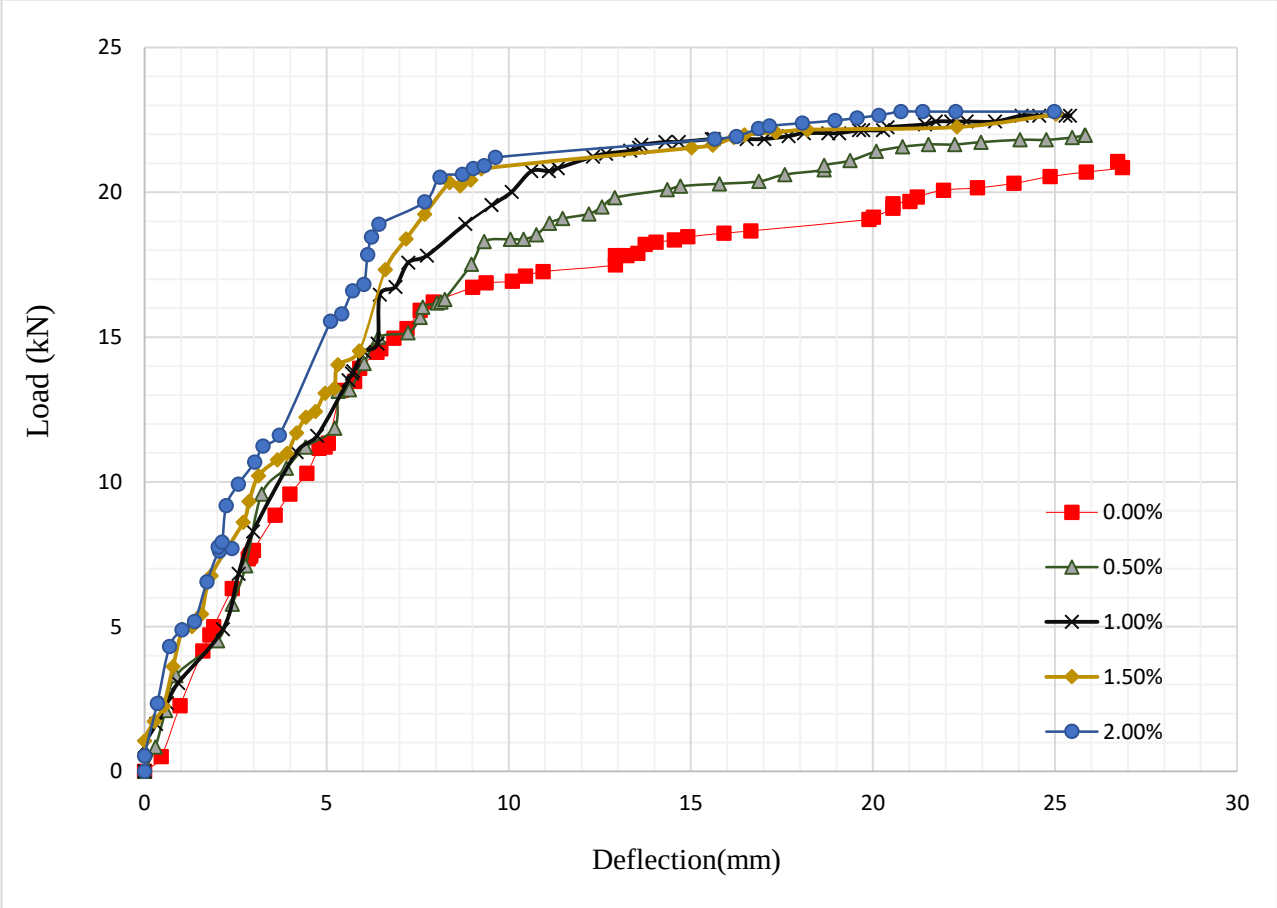

Figure 4- 29: Load vs deflection graph

4.4.3. Stiffness vs Deflection Characteristics

In the stiffness versus deflection characteristics, stiffness at ultimate load was compared with each specimen as shown in Figure. 4.30. As the stiffness of the specimen is increased, the density would be greater for the specimens, and the strength of the specimens would be high and with high ultimate carrying capacity (Figure. 4.31).

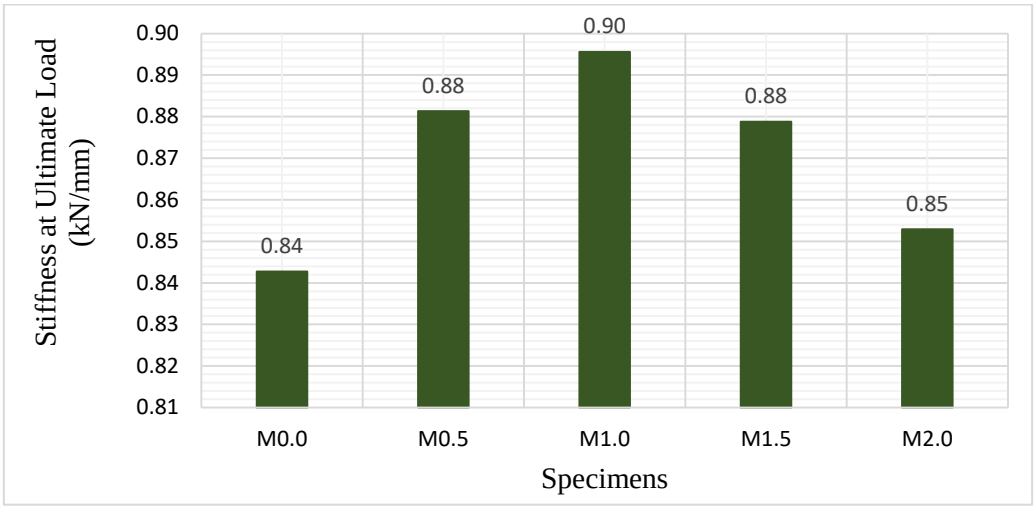

Figure 4- 30: Comparison of stiffness of each specimens

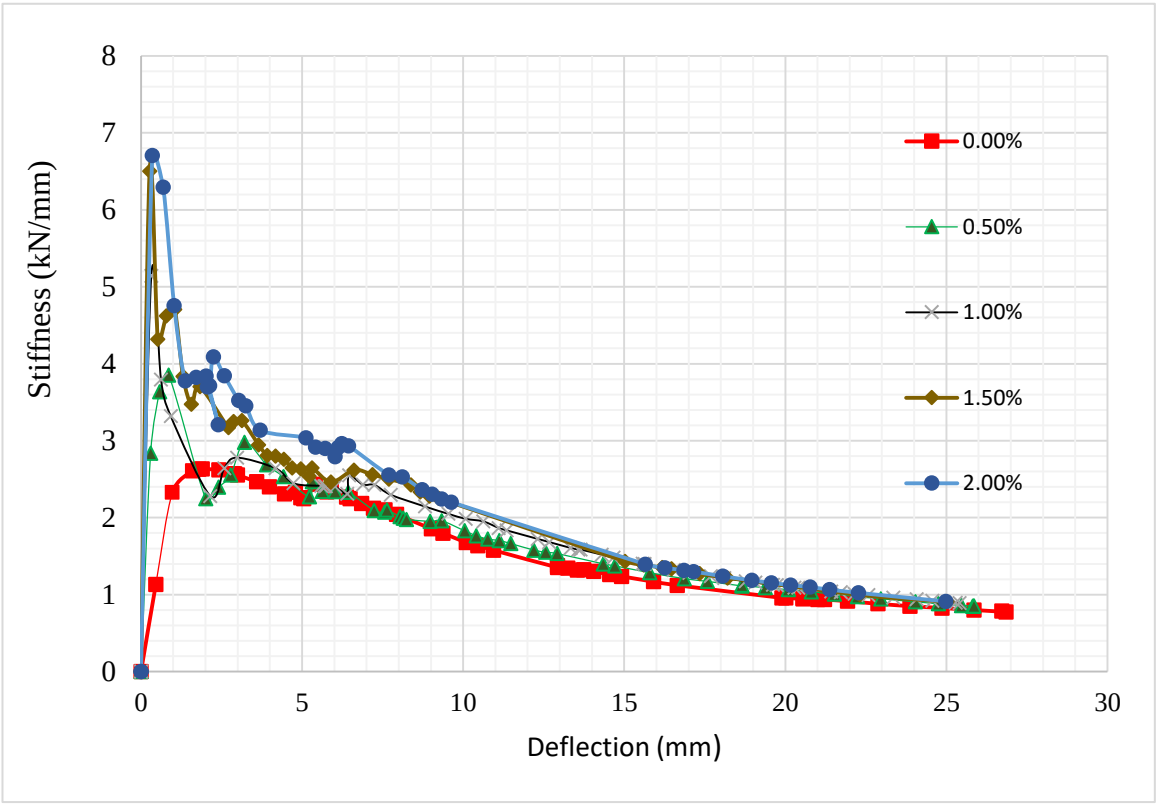

Figure 4- 31: Stiffness vs. deflection graph

4.4.4. Strain ductility of beam-column joint

The performance of a beam-column joint can be characterized by its strains and deformation. The measured strain gives an indication of the change in length as a

function of the original length. For each location on different specimens where strains were measured, a slight but noticeable reduction was noticed in the strain. Table 4.30 presents the measured strain of the specimen at ultimate load. For all specimens, the maximum strain consistently occurred at the side of the joint, followed by the bottom of the joint. The back of the joint experienced the lowest strain due to the ability of the reinforcement and fibers in providing improved ductility along the members.

Table 4- 29: Strain of specimens

	Point A	Point B	Point C	Point D
M0.0	0.00314	0.00326	0.00358	0.00242
M0.5	0.00307	0.00322	0.00356	0.00241
M1.0	0.00305	0.00321	0.00353	0.00239
M1.5	0.00303	0.00319	0.00349	0.00235
M2.0	0.00301	0.00317	0.00346	0.00232

Figure 4.32 shows the decrease in the strain of the specimen when compared with that of control. All specimen with sisal fiber experienced lower strain than the control. Reduction in strain at each location of the specimen increases as the fiber content increased. The highest reduction in strain occurred at the top of the beam-column joint (Point A), while the lowest strain reduction occurred at the bottom of the joint (Point B). This imply that the fiber plays a more crucial strain restraining function at the top of the beam than at the bottom.

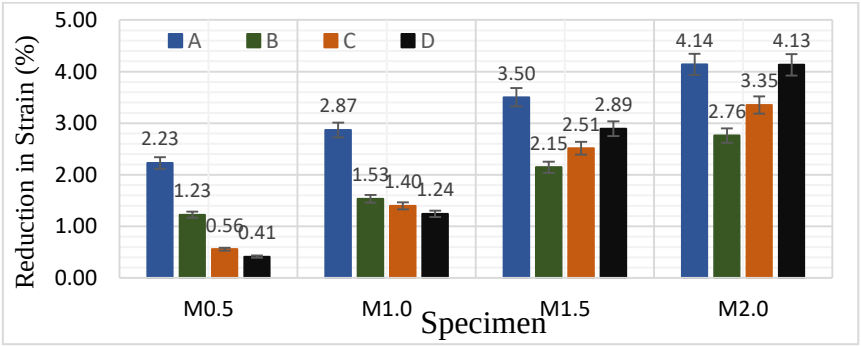

Figure 4- 32: Strain reduction is specimen

4.4.5. Crack pattern of specimens

Fibers are used in concrete for their ability to arrest crack propagation. In the tested specimen and as presented in Table 4.31, diagonal cracks were noticed more at the joint of the control specimens with 0% fiber content compared to the specimens with fibers. Major cracks reduced significantly to just 1 for M2.0 specimen representing a 75% reduction in the number of cracks formed. The pattern of cracks were consistently diagonal for all the specimens except for M0.5 that had lateral cracks. Thus, the provision of fibers at the joint reduces the congestion of reinforcement and also formations of diagonal cracks. All the cracks were observed in the beam due to design being done to make the column stronger than the beam (weak beam-strong column concept). The location of the cracks also moved further away from the beam end. The diagonal crack of M2.0 occurred within 50mm from the joint which is 72.22% smaller than the 180mm distance for the cracks observed in M0.0. Hence, all the specimens have increased load-carrying capacity, reduced diagonal cracks and distances of the crack from the beam end compared to the specimens designed without fibers (Figure 4.33).

Table 4- 30: Crack details of specimens

Specimen	Number of major cracks	Crack pattern	Distance from the joint (mm)
M0.0	4	Diagonal	180
M0.5	4	Diagonal and lateral	140
M1.0	3	Diagonal	120
M1.5	2	Diagonal	90
M2.0	1	Diagonal	50

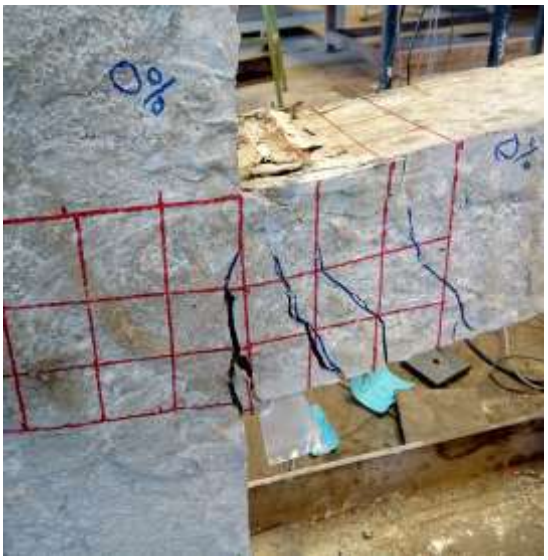

(a)

(b)

(c)

(d)

(e)

Figure 4- 33: Crack pattern (a) M0.0 (b) M0.5 (c) M1.0 (d) M1.5 (e) M2.0

4.4.6. Shear strength of the joint

Tsonos et al. (1992)

The input parameters are results are shown in Table 4.32

$$\alpha = \frac{h_b}{h_c} = \frac{150}{200} = 0.75 \qquad \gamma = \sqrt{f_c} \qquad \text{but } \sqrt{f_c} = \sqrt{kf_o} \qquad k = 1 + \frac{\rho_s f_{ys}}{f_o}$$

Table 4- 31: Shear strength of BC joint according to Tsonos et al. (1992) model

Bakir (2003)

$b_c = 150\text{mm}$ $b_b = 150\text{mm}$ $h_c = 150\text{mm}$ $\lambda = 0.78$ $A_{sh} = 113\text{mm}^2$ $f_{ys} = 399\text{mm}^2$

$d_b = 10\text{mm}$. The input parameters are results are shown in Table 4.33

Table 4- 32: Shear strength of beam-column joint according to Bakir (2003) model

Parameter	M0.0	M0.5	M1.0	M1.5	M2.0
V(N/mm^2)	9.29	9.17	8.84	8.43	8.33

Jiuru et al. (1992)

$N = 120\text{kN}$ $b_c = 150\text{mm}$ $h_c = 150\text{mm}$ $b_c = 150\text{mm}$ $b_j = 115\text{mm}$ $h_j = 115\text{mm}$

$l_f = 30\text{mm}$ $d_f = 0.115\text{mm}$ $a_s = 30\text{mm}$ The input parameters are results are shown in Table 3.34.

Table 4- 33: Shear strength of beam-column joint according to Jiuru et al. (1992) model

Specimen	V_c (N/mm^2)	V_f(N/mm^2)	V_s(N/mm^2)	V(N/mm^2)
M0.0	5.52	0.00	0.35	5.87
M0.5	5.42	0.35	0.35	6.12
M1.0	5.14	0.69	0.35	6.18
M1.5	4.81	1.04	0.35	6.20
M2.0	4.72	1.38	0.35	6.45

4. Comparison of Analytical Models with Experimental Results

The values of ultimate shear strength computed using the above equations are compared with the experimental values. Details of comparison are given in Table 4.35. It may be noted from the table that average of the ratio of V $_{(exp.)}$ to V $_{(th.)}$ is 0.77 in the case of Tsonos et al. (1992), 0.79 in the case of Bakir (2003), and 1.12 in the case of Jiuru et al. (1992). This indicates that the comparison is not satisfactory. This may be due to the following reasons. The equations considered in the comparison are meant for either normal concrete, as in the cases of Tsonos et al. (1992) and Bakir (2003), or for different fiber types, as in the case of Jiuru et al. (1992). Thus, in these equations the effect of sisal fibers was not included.

Table 4- 34: Comparison of ultimate shear strength

Specimen	$V_{(exp)}$	Calculated Values $V_{(th.)}$ (N/mm^2)			Ratio	Ratio	Ratio
	(N/mm^2)	Tsonos *	Bakir **	Jiuru ***	(W)/(X)	(W)/(Y)	(W)/(Z)
M0.0	4.63	9.25	9.29	5.87	0.50	0.49	0.79
M0.5	4.87	9.20	9.17	6.12	0.53	0.53	0.80
M1.0	7.92	9.01	8.84	6.18	0.87	0.90	1.28

M1.5	8.18	8.86	8.43	6.20	0.92	0.97	1.32
M2.0	8.95	8.77	8.33	6.45	1.02	1.07	1.39

An attempt was made to modify the model proposed by Jiuru et al. (1992). In order to account for the effect of sisal fibers in the model, a regression analysis was carried out. A parameter F was introduced to account for the combined effect of sisal fibers, compressive strength of concrete, and modulus of rupture, and is given by.

$$F = \frac{l_f}{d_f} v_f b_f \frac{f_c}{f_{cr}}$$

This parameter was related to $V_{exp}/V_{th,}$ and the plot is shown in Figure 4.34. By conducting regression analysis, the obtained modified equation gives a coefficient of correlation of 75.51%.

$$V_{exp} = V_{th}(0.0277F + 0.7449) \qquad 4.6$$

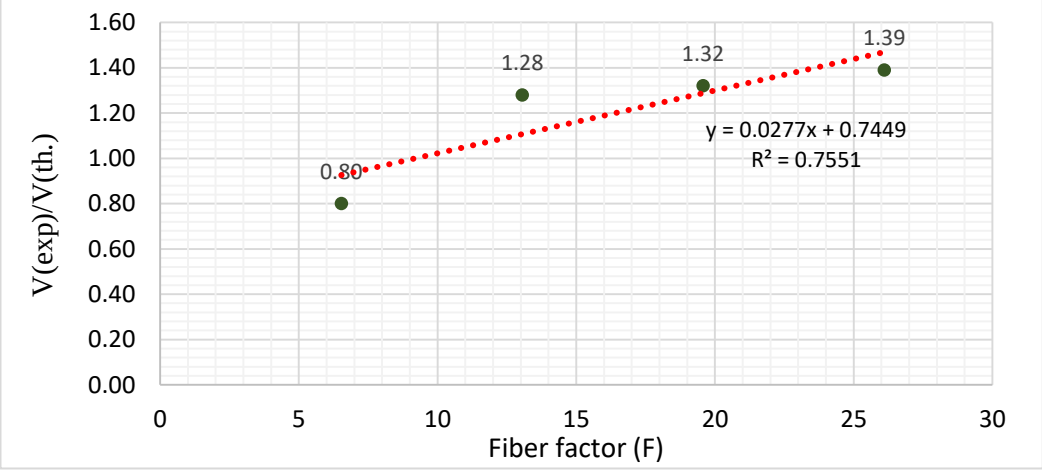

Figure 4- 34: Relationship between $V_{(exp.)}$ and $V_{(th.)}$ and fiber factor F

By replacing V_{exp} withV_{pre}, where V_{pre} indicates the predicted shear strength value,

the predicted value of shear strength is given by

$$V_{pre} = V_{th}(0.0277F + 0.7449) \quad 4.7$$

Figure 4-35 shows the comparison between the predicted and experimental values of ultimate shear strength. All the points are close to the plotted points and lie within ± 2% lines of agreement. Hence, the proposed model predicts the shear strength satisfactorily. The proposed model is however only a preliminary model that needs to be improved further with the help of a larger database.

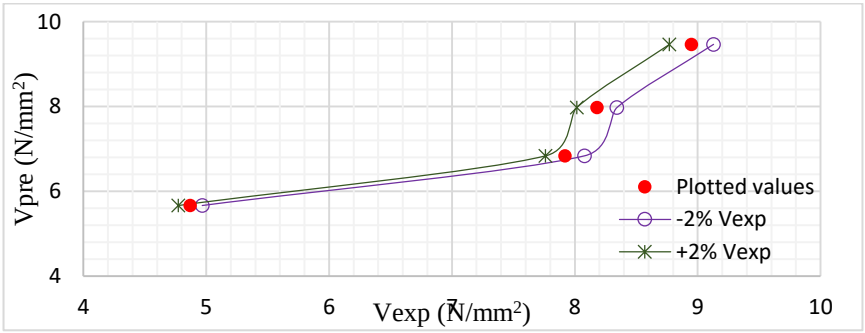

Figure 4- 35: Comparison between $V_{(exp.)}$ and $V_{(pre)}$

4.5. Finite Element Analysis of SFRC Beam-Column Joints under Monotonic Load

4.5.1. Dimensions Details and Boundary conditions

A schematic representation of the loading apparatus regarding both test connections is also presented. According to boundary conditions applied to the beam-column connection specimen, column was fixed at the bottom end and a compressive axial load was applied to the column's head using a hydraulic jack. The column axial compressive load applied to the top of the column corresponds to 20% of the axial

capacity of the column. The lateral load was applied in second step to the beam tip.

4.5.2. Meshing

A uniform mesh size of 50 mm is chosen for the concrete elements over the whole geometry as shown in Figure 4.36. The same size of mesh was also adopted for steel bars. With this configuration, the specimen has 715 elements and 1040 nodes. Details regarding element types are presented in Table 4.35.

Table 4- 35: The number and type of elements in the finite element model.

Element type	Element Shape	Geometrical order	Number of elements
C3D8R	Hexahedral	Linear	447
T3D2	Line	Linear	268

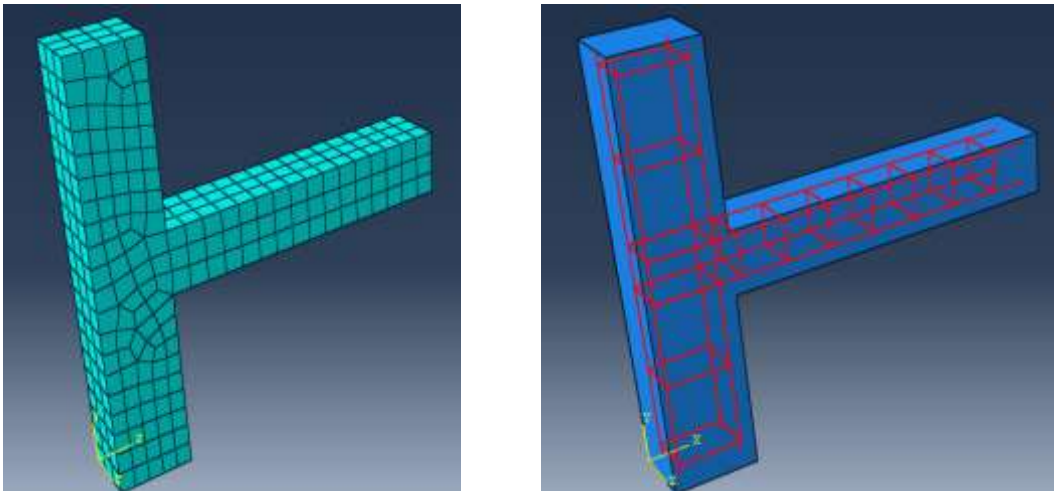

Figure 4- 36: Modeled specimens; a) Concrete element mesh joints b) Reinforcement details of joints

4.5.3. Loading, and Boundary Conditions.

Restraints were defined at both top and bottom surfaces of the specimen's column in

the test specimen according to boundary conditions addressed in the test setup and on beam and column tip surfaces. Details regarding to the geometry and boundary conditions of the RC beam-column connections which are applied to the finite element models are illustrated in Figure 4.37. Loading is introduced to the model in two separate steps in exterior beam-column connection. The column compressive axial load is applied to the column top surface in the first step which remained constant during the analysis procedure. The second step corresponds to the monotonic lateral loading of the specimen by applying the lateral displacement at the beam's end surface.

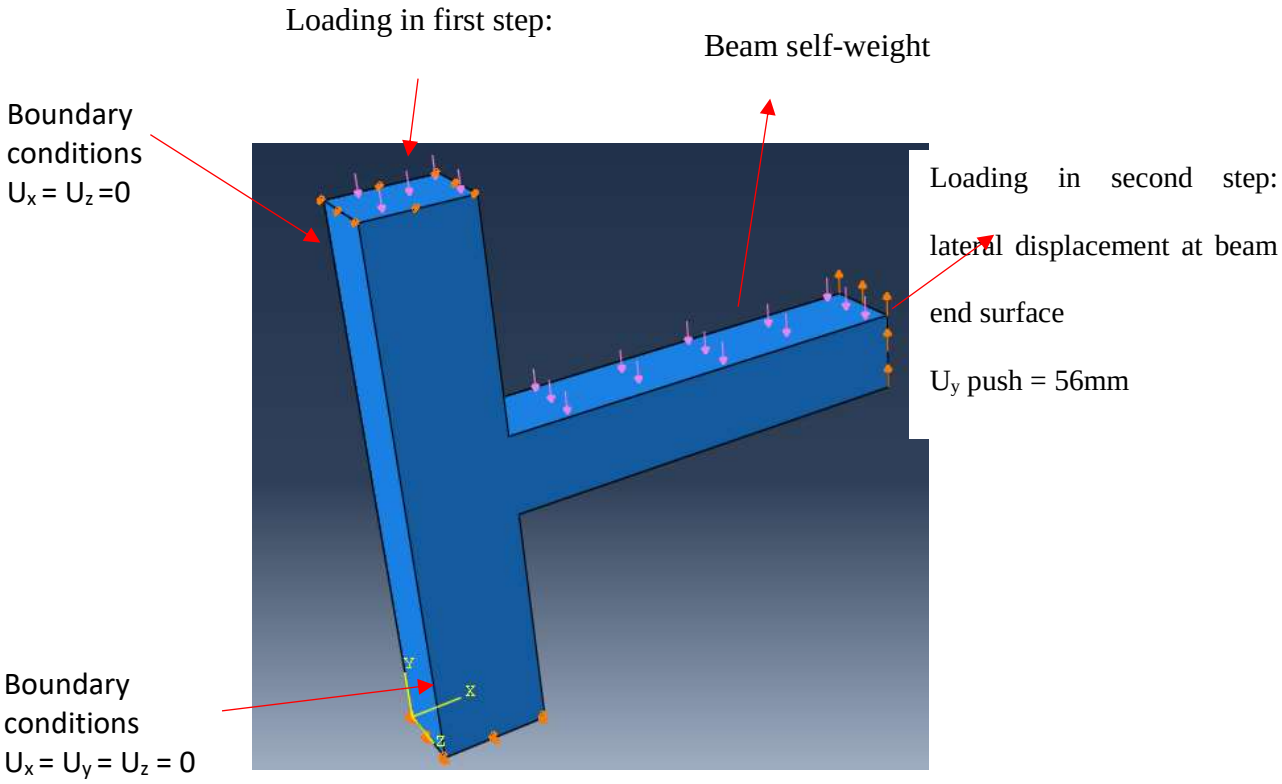

Figure 4- 37: Simulated boundary conditions and loading of specimens

4.5.4. Material Parameters

Concrete material parameters used in the presented analysis consists of concrete Young's modulus of elasticity (E_0), Poisson's ratio (v) and concrete compressive and tensile strengths. The poison's ratio value for concrete material is measured experimentally and used see 4.37. The compression behaviour parameter were also defined. The elastic strain of undamaged material ($\varepsilon^{el}{}_t$) is defined according to Equation 4.7:

$$\varepsilon^{el}{}_t = \frac{\sigma_t}{E} \tag{4.7}$$

The Cracking strain is defined as the total strain minus the elastic strain corresponding to the undamaged material according to Equation 4.8 Lubliner et al. (1989).

$$\varepsilon_{ck} = \varepsilon_t - \varepsilon^{el}{}_t \tag{4.8}$$

$$\text{Damage parameter } d_c = 1 - \frac{\text{Stress in descending part}}{\text{Stress at peak}} \tag{4.9}$$

Table 4- 36: Input concrete properties

Specimen	Mass density	Young's modulus (MPa)	Poisson ratio
M0.0	2120	25086.77	0.1889
M0.5	2096	29138.60	0.1898
M1.0	2048	31654.19	0.1935
M1.5	2041	28926.78	0.1971
M2.0	2032	25379.31	0.1995

The concrete damage plasticity input parameters were considered in the plasticity model as presented in Table 4.38.

Table 4- 37: Input concrete damage parameters

Plasticity Parameters	Notation	Parameter's value considered in the
Dilation angle	Ψ	35°
Shape factor	k_c	0.667 (default value)
Stress ratio	$\frac{\sigma_{bo}}{\sigma_{co}}$	1.16 (default value)
Eccentricity	$\in$	0.1 (default value)

The uniaxial tensile stress–strain behaviour of steel reinforcement was assumed to be elastic with Young's modulus ($E_s = 2 \times 10^5$ MPa) and Poisson's ratio ($v_s = 0.3$). The plastic behaviour is also modeled including yield stress and corresponding plastic strain. Properties of plastic phase is defined to the model using bilinear behaviour. Figure 4.38 illustrates the typical stress-strain relationship of reinforcement introduced to the numerical model. Typical reinforcement properties are also presented in Table 4.39 for the exterior beam-column connections.

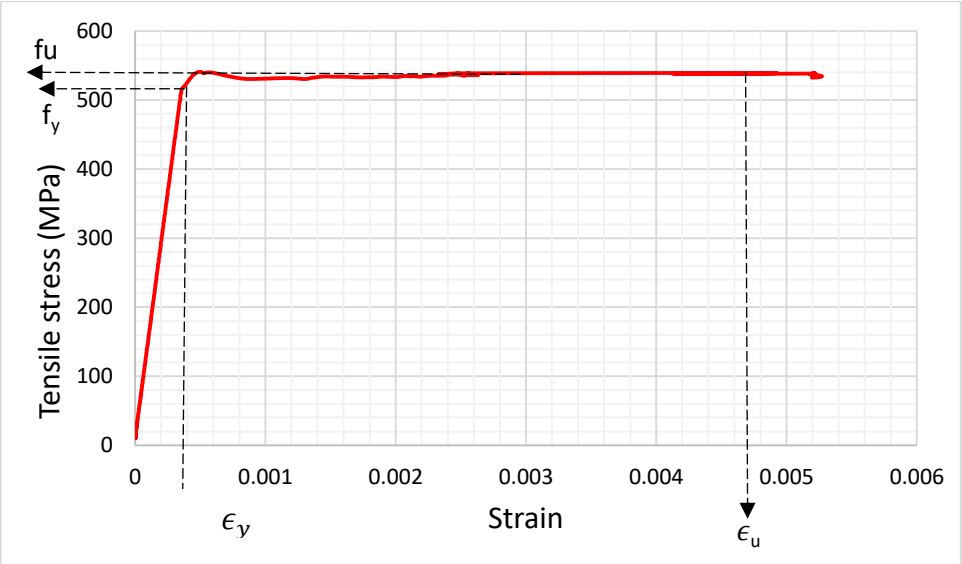

Figure 4- 38: Typical uniaxial stress-strain behaviour of reinforcements introduced to the numerical model.

Table 4- 38: Stress-strain properties of steel reinforcement

Reinforcement type	Yield strength	Ultimate strain	Plastic strain
	F_u (MPa)	E_u	p_u
Beam longitudinal bar	494.67	0.003167	0
Column longitudinal bar	539.09	0.000533	0
Stirrups	408.95	0.002875	0

A range between 31° to 42° of the dilation angle parameter is recommended for concrete material according to series of fundamental studies performed by different authors (Lee and Fenves (1988), Wu et al. (2006) and Voyiadjis et al. (2009)). According to them, an average of 35^o can reasonably capture the lateral load-deformation curve and the failure mode.

4.5.5. Finite element analysis results

The FEA results of the RC beam-column connections subjected to lateral loading is presented in terms of load-displacement curves which are monitored at the joint of the specimen. Comparison between force-displacement curves predicted by simulation and experimental results of connection specimens are presented in Figure 4.39.

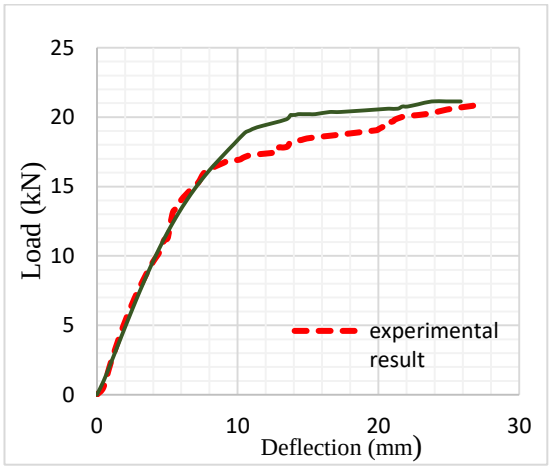

(a)

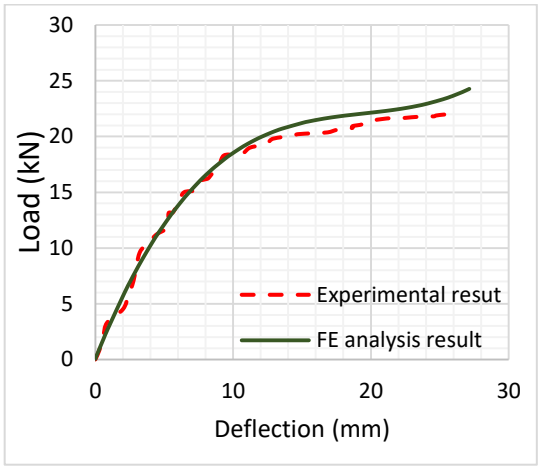

(b)

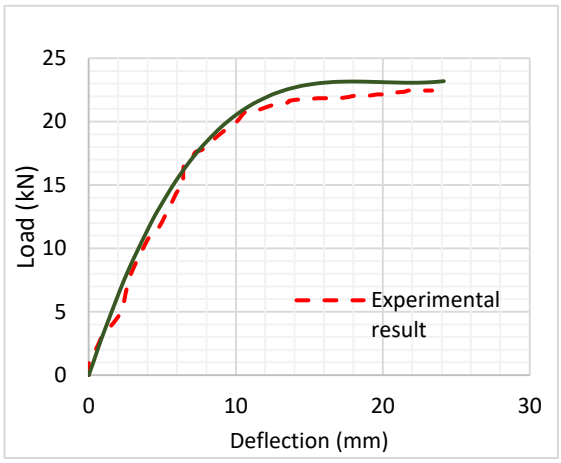

(c)

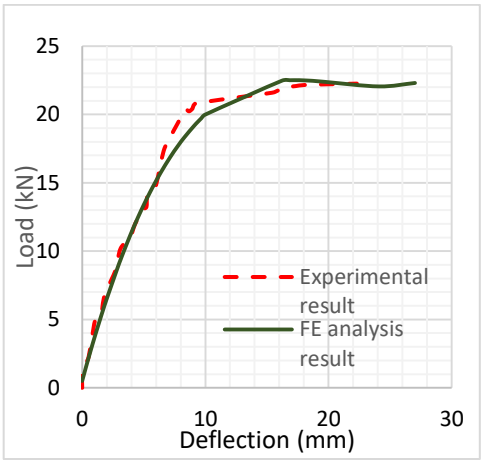

(d)

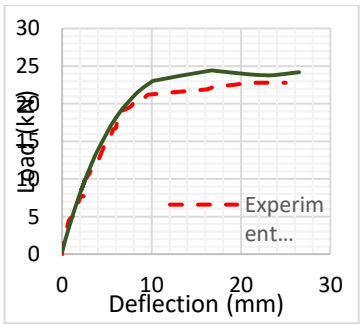

(e) Figure 4- 39: Lateral load-displacement response of FEA (a) M0.0 (b) M0.5 (c) M1.0 (d) M1.5 (e) M2.0

Peak lateral loads and displacements predicted by the numerical simulation and reported by experimental test results are presented in Table 4.40.

Table 4- 39: Ultimate lateral loads and displacements obtained from FEA and experiments

Specimen	Experimental result		Finite Element analysis result	
	Ultimate load (kN)	Deflection at ultimate load (mm)	Ultimate load (kN)	Deflection at ultimate load (mm)
M0.0	21.06	24.99	21.13	25.15
M0.5	22.05	25.02	22.30	25.85
M1.0	22.65	25.29	23.19	26.48
M1.5	22.70	25.83	24.18	27.02
M2.0	22.79	26.72	24.28	27.15

At the end of FEA procedure there was a rise of 0.33%, 1.12%, 2.33%, 6.12% and 6.13% in ultimate strength of M0.0, M0.5, M1.0, M1.5, M2.0 compared to the control specimens. Similar increase was observed in the deflections for all specimens.

The finite element analysis shows that the initial response is similar to that of the test results while the post yield behaviour slightly differs. This may be due to effects of some assumed variables such as the choice of concrete tensile and compressive properties, or the uncertainties often involved with experimental efforts such as probable existence of material deficiencies and also the inherent differences which exist between the presence and orientation of fibers. It should however be noted that the prediction at ultimate load is not accurate and non-conservative.

CHAPTER FIVE- CONCLUSIONS AND RECOMMENDATION

5.1. Conclusions

5.1.1. Physical and mechanical properties of SFRC

- The workability of fresh concrete reduces once sisal fiber is added to the mix.
- Sisal fiber cannot improve the compressive strength of concrete, although it significantly improves the split tensile strength of concrete and makes it lighter by reducing its density.
- The numerical relationship between cube and cylinder compressive strength presented in British standard can be applied to SFRC
- However, computing the modulus of elasticity of SFRC is somewhat difficult and cannot be predicted accurately with empirical relation.

5.1.2. Durability of SFRC

- The sorptivity of SFRC increases with increased fiber content.
- Sulphuric acid attack on SFRC is very severe and results in significant weight and strength loss.
- Sodium hydroxide has a negligible effect on both the strength and weight loss of SFRC.
- The structural and non-structural application of fiber reinforced concrete should be applied to regions of pH to 7.0 as it is properties are adversely affected by extreme pH mediums.

5.1.3. SFRC in exterior beam-column joints under monotonic loading

- SFRC beam-column joints undergo higher displacements under higher load without developing wider cracks.

- Addition of fibers could improve the dimensional stability and integrity of the joints.
- It is possible to reduce the congestion of steel reinforcement in the beam-column joints by replacing part of ties in the columns by sisal fibers.

5.1.4. FEM of beam-column joints under monotonic loading

Finite element analysis model can be used to predict RC beam-column joint behaviour and can be further investigated and validated for different types of joints.

5.2. Recommendations

5.2.1. For Application

1. 1% sisal fibers can be used in the production of structural concrete.

2. Sisal fibers should be used in the production of structural concrete in extreme environment with high end pH such as sewage and sea construction.

3. Sisal fibers should be used to improve the shear performance and ductility of beam-column joints under monotonic loading.

5.2.2. For further Research

1. Documentation should be done on the effect of the various aspect ratios of the sisal fibers on the properties of concrete.

2. Studies should be done on the effect of other chemicals on other mechanical properties of SFRC.

3 Investigations should be made on how the beam- column joints will perform under cyclic loading.

4. Further studies should be conducted on the effect of varying different input parameters on the output of the software.

5. The ability of the software to accurately predict crack pattern and formation under monotonic and cyclic loading should be further studied.

REFERENCES

1. ACI 211-2. (2002) Standard Practice for Selecting Proportions for Normal, Heavyweight, and Mass Concrete; American Concrete Institute: Farmington Hills, MI, USA.

2. ACI Committee 113. (2009) Manual of Concrete Inspection; American Concrete Institute: Farmington Hills, MI, USA.

3. ACI Committee 318. (2008)Building Code Requirements for Structural Concrete and Commentary; American Concrete Institute: Farmington Hills, MI, USA.

4. Afroughsabet, V.; Ozbakkaloglu, T. (2015) Mechanical and durability properties of high-strength concrete containing steel and polypropylene fibers. Constr. Build. Mater. 94, 73–82.

5. Ali, M.; Liu, A.; Sou, H.; Chouw, N. (2012) Mechanical and dynamic properties of coconut fiber reinforced concrete. Constr. Build. Mater. 30, 814–825.

6. Aruna, M. (2014) Mechanical Behaviour of Sisal Fiber Reinforced Cement Composites. World Acad. Sci. Eng. Technol. doi:10.5281/zenodo.1091698.

7. ASTM C 29. (1997). Standard Test Method for Bulk Density ("Unit Weight") and Voids In Aggregate; ASTM International: West Conshohocken, PA, USA.

8. ASTM C 33. (2003). Standard Specification for Concrete Aggregates; ASTM International: West Conshohocken, PA, USA.

9. ASTM C 127. (2001). Standard Test Method for Density, Relative Density (Specific Gravity), and Absorption of Coarse Aggregate; ASTM International: West Conshohocken, PA, USA.

10. ASTM C 128. (2001). Standard Test Method for Density, Relative Density (Specific Gravity), and Absorption of Fine Aggregate; ASTM International: West

Conshohocken, PA, USA.

11. ASTM C 131. (2003). Standard Test Method for Resistance to Degradation of Small-Size Coarse Aggregate by Abrasion and Impact in the Los Angeles Machine; ASTM International: West Conshohocken, PA, USA.

12. ASTM C143. (2003). Standard Test Method for Slump of Hydraulic-Cement Concrete; ASTM International: West Conshohocken, PA, USA.

13. ASTM C150. (2004). Standard Specification for Portland Cement; ASTM International: West Conshohocken, PA, USA.

14. ASTM C192. (2002). Standard Practice for Making and Curing Concrete Test Specimens in the Laboratory; ASTM International: West Conshohocken, PA, USA.

15. ASTM C267 – 01. (2013). Standard Test Methods for Chemical Resistance of Mortars, Grouts, and Monolithic Surfacings and Polymer Concretes. ASTM International: West Conshohocken, PA, USA.

16. ASTM C469. (2002). Standard Test Method for Static Modulus of Elasticity and Poisson's Ratio of Concrete in Compression; ASTM International: West Conshohocken, PA, USA.

17. ASTM C496. (2004). Standard Test Method for Splitting Tensile Strength of Cylindrical Concrete Specimens; ASTM International: West Conshohocken, PA, USA.

18. ASTM C642. (2006). Standard Test Method for Density, Absorption, and Voids in Hardened Concrete; ASTM International: West Conshohocken, PA, USA.

19. ASTM C1585. (2013). Measurement of Rate of Absorption of Water by Hydraulic-Cement Concretes; ASTM International: West Conshohocken, PA, USA.

20. ASTM C 1602. (2012). Standard Specification for Mixing Water Used in the

Production of Hydraulic Cement Concrete; ASTM International: West Conshohocken, PA, USA.

21. ASTM D 75. (2003). Standard Practice for Sampling Aggregates; ASTM International: West Conshohocken, PA, USA.

22. ASTM D 5874. Standard Test Methods for Determination of the Impact Value (IV) of a Soil; ASTM International: West Conshohocken, PA, USA, 2016.

23. Bakir, P.G. (2003). "Seismic resistance and mechanical behaviour of exterior beam-column joints crossed inclined bars", Structural Engineering & mechanics, Vol. 16, N0 4, pp. 493-517

24. Balasubramanian, M.; Senthilselvan S.; Sabarish, K.V. (2016). Experimental Investigation on Strength and Durability Properties of Sisal Fiber Reinforced Concrete, Int. J. Chem. Sci, 14, 241–246.

25. Bassuoni, M. T., and Nehdi, M. L. (2007). Resistance of self-compacting concrete to sulphuric acid attack with consecutive pH reduction. Cement and Concrete Research. 37: 1070-1084.

26. Belachew A., Oyawa. W. Shitote, S.M. (2017). "Experimental Investigation on Compressive Strength of Recycled Reactive Powder Concrete Containing Glass Powder and Rice Husk Ash" Journal of Civil Engineering Research. 7(4): 124-129. DOI: 10.5923/j.jce.20170704.03.

27. Brindha ,D. Vinodhini,S. Alarmelumangai k and N.S.Malathy .(1987). "Physico-Chemical Properties of Fibers from Banana Varieties after Scouring. Indian Journal of Fundamental and Applied Life Vol. 2 (1) January- March, pp.217 -221.

28. BS 1881-103. (1993). Testing Concrete: Method for Determination of Compacting Factor; British Standards Institution: London, UK.

29. BS 1881-116. (1983).Testing Concrete: Method for Determination of Compressive Strength of Concrete Cubes; British Standards Institution: London, UK.

30. BS 8110-02. (1985). Structural Use of Concrete. Code of Practice for Special Circumstances; British Standards Institution: London, UK.

31. BS EN 12390-03 (2009). Testing Concrete: Compressive Strength of Test Specimens; British Standards Institution: London, UK.

32. Chalioris, C.E. (2013), "Steel fibrous RC Beams subjected to cyclic deformations under predominant shear", Engineering Structures, 49(1), 104-118.

33. Chanko, B.; Sunilaa, G. (2017). Performance of Concrete with PET fibers. Int. J. Eng. Sci. Invetion Res. Dev. 3, 725–728.

34. Chavan, S.; Rao, P. (2016). Utilization of Waste PET Bottle Fibers in Concrete as an Innovation in Building Materials. Int. J. Eng. Res., 5, 304–307.

35. Collepardi, M. Marcialis, A. Turriziani R. (1972), Penetration of chloride ions into cement pastes and concretes, J. Am. Ceram. Soc. 55 (10). 534–535.

36. Design of Concrete Structures. A23.3-04. (2015). Available online: http://sfotoohi.ir/wp-content/uploads/2015/06/CSA-A23.3-04.pdf (accessed on 30 May 2018).

37. Dinh, N.-H., Choi, K.-K., & Kim, H.-S. (2016). Mechanical Properties and Modeling of Amorphous Metallic Fiber-Reinforced Concrete in Compression. International Journal of Concrete Structures and Materials, 10(2), 221–236. https://doi.org/10.1007/s40069-016-0144-9.

38. Erdogan, T. Y. (2001). Materials of Construction. A Comparative Evaluation of Plain and Steel Fiber Reinforced Concrete Ground Slabs (Mastes Thesis).

39. Euro-International Committee for Concrete. (1989) Diagnosis and Assessment

of Concrete Structures-State of Art Report; CEB-FIP: Lausanne, Switzerland.

40. European Committee for Standardization. (2005). Eurocode 2: Design of Concrete Structures-Part1: General Rules and Rules for Buildings; National Standards Authority of Ireland: Dublin, Ireland.

41. Ganesan, N., Indira, P. V., & Santhakumar, A. (2013). Engineering properties of steel fiber reinforced geopolymer concrete. Advances in Concrete Construction, 1(4), 305–318. https://doi.org/10.12989/acc2013.1.4.305.

42. Gao, J., Sun, W., & Morino, K. (1997). Mechanical properties of steel fiber-reinforced, high-strength, lightweight concrete. Cement and Concrete Composites, 19(4), 307–313. https://doi.org/10.1016/S0958-9465(97)00023-1.

43. Ghaffar, A.; Tatwawadi, R.S.; Darda, J. (2014). Steel Fiber Reinforced Concrete. Int. J. Eng. Trends Technol, 9, 791–797.

44. Gopalaratnam VS, Shah SP. (1987). Tensile failure of steel fiber-reinforced mortar. J Eng Mech ASCE;113:635–52.

45. Graybeal, B., & Davis, M. (2009). Cylinder or Cube : Strength Testing of 80 to 200 MPa Ultra-High-Performance Fiber-Reinforced Concrete. ACI Materials Journal, 105(6), 603–609.

46. Gnanapragasam, A Arul, G Chitra, and S Robert Ravi. (2016). “Study on Strengthening of RC Beam Column Joint Using Hybrid FRP Composites.” Scientific Research publishing 7: 2846–56.

47. Hamad, A. J. (2017). Size and shape effect of specimen on the compressive strength of HPLWFC reinforced with glass fibers. Journal of King Saud University - Engineering Sciences, 29(4), 373–380.

48. Hidaya, N.; Mutuku, R.N.; Mwero, J.N. (2017). Physical and Mechanical Experimental Investigation of Concrete incorporated with Polyethylene Terephthalate

(PET) Fibers. Eur. Int. J. Sci. Technol, 6, 31–41.

49. Ilya, J.; Chea, C.C. (2017). Mechanical behaviour of fiber reinforced concrete using soft–drink. In Proceedings of the Global Congress on Construction, Material and Structural Engineering, 28–29 August 2017; IOP Conference Series: Washington, DC, USA.

50. IS 456-1979. (1989). Plain and Reinforced Concrete-Code of Practice; Bureau of Indian Standards: New Delhi, India.

51. Ismail, Z.Z.; Al-Hashmi, E.A. (2008). Use of waste plastic in concrete mixture as aggregate replacement. Waste Manag.28, 2041–2047.

52. Ispir, M.; Dalgic, K.D.; Sengul, C.; Kuran, F.; Tasdemir, M.A.; Ilki, A. (2010). Modulus of Elasticity of Low Strength Concrete, In Procceedings of the 9th International Congress on Advances in Civil Engineering, Trabzon, Turkey, 27–30 September.

53. Javier, A. R. ., Lopez, N. E., & Juanzon, J. B. (2017). Compressive strength and chloride penetraton tests of modified type IP cement concrete with ash. Sustainable Civil Engineering Structures and Construction Materials, 171(171), 543–548. https://doi.org/10.1016/j.proeng.2017.01.369.

54. Jiuru, T., Chaobin, H., Kaijian, Y. and Yongcheng, Y. (1992). "Seismic behaviour and Shear Strength of Framed Joint Using Steel-Fiber Reinforced Concrete", Journal of Structural Engineering, ASCE, Vol.118,No 2,pp.341-358.

55. Joseph, Kuruvilla (1999."A Review on Sisal Fiber Reinforced Polymer." Revista Brasileira de Engenharia Agrícola e Ambiental 3(3): 367–79

56. Jurowski, K.; Grzeszczyk, S. (2018). Influence of Selected Factors on the Relationship between the Dynamic Elastic Modulus and Compressive Strength of

Concrete. Materails, 11, 477.

57. Kadarningsih, R., Satyarno, I., Muslikh, & Triwiyono, A. (2014). Proposals of beam column joint reinforcement in reinforced concrete moment resisting frame: A literature review study. Procedia Engineering, 95(Scescm), 158–171. https://doi.org/10.1016/j.proeng.2014.12.175

58. Karayannis CG. (2000). Nonlinear analysis and tests of steel–fiber concrete beams in torsion. J Struct Eng Mech. 9(4):323–38.

59. Krizova, K.; Hela, R. (2015). Evaluation of static modulus of elasticity depending on concrete compressive strength. World Acad. Sci. Eng. Technol. Int. J. Civ. Environ. Eng. 9, 654–657.

60. Ku, H., H. Wang, N. Pattarachaiyakoop, and M. Trada. (2011). "A Review on the Tensile Properties of Natural Fiber Reinforced Polymer Composites." Composites Part B: Engineering 42(4): 856–73.

61. Kusumawardaningsih, Y., Fehling, E., & Ismail, M. (2015). UHPC compressive strength test specimens: Cylinder or cube? Procedia Engineering, 125, 1076–1080.

62. Lee, J., Fenves, G.L. (1998). Plastic-Damage Model for cyclic loading of concrete structures. Journal of Engineering Mechanics. 124(8) .892-900.

63. Lim TY, Paramasivam P, Lee SL. (1987). Analytical model for tensile behavior of steel–fiber concrete. ACI Mater J. 84(4):286–98.

64. Lubliner, J., Oliver, J., Oller, S., Oñate, E. (1989). A plastic-damage model for concrete, International Journal of Solids and Structures 25: 299-329.

65. Malaikah, A.S., (2005). Effect of specimen size and shape on the compressive strength of high strength concrete. Pertanika J. Sci.Technology. 13 (1), 87–96.

66. Malhotra, S.; Chand, J. (2005).Experimental investigation on high strength concrete with the addition of steel fiber. Int. J. Civ. Eng. Technol. 8, 1130–1140.

67. Mishra, S.; Deodhar, S.V. (2013). Effect of Rice Husk Ash on Concrete. Int. J. Eng. Res. Appl, 3, 1718–1723.

68. Muthupriya, P., S. C. Boobalan, and B. G. Vishnuram. (2014). "Behaviour of Fiber-Reinforced High-Performance Concrete in Exterior Beam-Column Joint." International Journal of Advanced Structural Engineering 6(3).

69. Muthuswamy, K. R., & Thirugnanam, G. S. (2014). Structural behaviour of hybrid fiber reinforced concrete exterior Beam- Column joint subjected to cyclic loading. International Journal of Civil and Structural Engineering, 4(3), 262–273. https://doi.org/10.6088/ijcser.201304010026.

70. Nathan GK, Paramasivam P, Lee SL. (1977). Tensile behavior of fiber reinforced cement paste. J Ferrocem ; 7(2):59–79.

71. Nibudey, R. N., Nagarnaik, P. B., Parbat, D. K., & Pande, A. M. (2013). Cube and cylinder compressive strengths of waste plastic fiber reinforced concrete. International Journal of Civil and Structural Engineering, 4(2), 174–182.

72. Nilsson, l.(1975).Reinforcement of concrete with sisal and other vegetable fibres. Stockholm: Swedish Council for Building Research, 68p. Document No D-14

73. Otsuki, N., Nagataki, S., & Nakashita, K. (1993). Evaluation of the AgNO3solution spray method for measurement of chloride penetration into hardened cementitious matrix materials. Construction and Building Materials, 7(4), 195–201. https://doi.org/10.1016/0950-0618(93)90002-T.

74. Pacheco-Torgal, F.; Jalali, S. (2011). Cementitious building materials reinforced with vegetable fibers: A review. Constr. Build. Mater. 25, 575–581.

75. Pauw, A.(1960).Static Modulus of Elasticity of Concrete as Affected by Density; American Concrete Institute: Farmington Hills, MI, USA.

76. Prahallada, M.C.; Shanthappa, B.C.; Prakash, K. (2011). Effect of Redmud on the Properties of Waste Plastic Fiber Reinforced Concrete, an Experimental Investigation. Int. J. Civ. Eng. 2, 25–34.

77. Rahmani, T.; Kiani, B.; Sami, F.; Fard, B.N.; Farnam, Y.; Shekarchizadeh, M. (2011). Durability of Glass, Polypropylene and Steel Fiber Reinforced Concrete. In Proceedings of the International Conference on Durability of Building Materials and Components, Porto, Portugal, 12–15 April.

78. Rai, A.; Joshi, Y.P. (2014). Applications and Properties of Fiber Reinforced Concrete. Int. J. Eng. Res. Appl. 4, 123–131.

79. Regina, C.; Stephany, S.; Henrique, B.; Ferreira, M.; Fonseca, S.; Souza Oliveira, C.A.; Teixeira, R.; Araújo Gouveia, L.L.(2017). Comparative Study about Mechanical Properties of Strutural Standard Concrete and Concrete with Addition of Vegetable Fibers. Mater. Res. 20, 102–107.

80. Requirements for Design and Construction of Reinforced Concrete Structures; Turkish Standardization Institute. (2003) Ankara, Turkey.

81. Sabarinathan, S. (2017). A Study on Mechanical Properties of Sisal Fiber Reinforced Concrete. SSRG Int. J. Civ. Eng. 2, 16–20.

82. Sasikumar P.; Thivya, J. (2017). An Investigation of Sisal Fiber Concrete Using Quarry Dust. Int. J. Innovative Res. Sci. Eng. Technol.6, doi:10.15680/ijirset.2017.0604109.

83. Shah SP, Stroeven P, Dalhuisen D, Van Stekelenburg P.(1978). Complete stress-strain curves for steel fiber reinforced concrete in uniaxial tension and

compression In : Proceedings RILEM symposium on testing and test methods of fiber cement composites, The Construction Press, Lancaster; p. 399–408.

84. Shamskia N. (2012). The influence of pet fibers on the properties of fresh and hardened concrete. J. Struct. Eng. Geotech.2, 13–17.

85. Singh, S., & Sujana, S. (2013). Study of Sisal Fiber As Concrete Reinforcement Material In Cement Based Composites. International Journal of Engineering Research and Technology, 2(4), 1828–1832.

86. Smirnova, O. M., Shubin, A. A., & Potseshkovskaya, I. V. (2017). Strength and Deformability Properties of Polyolefin Macrofibers Reinforced Concrete, 12(20), 9397–9404.

87. Soto Izquierdo, I., Soto Izquierdo, O., Ramalho, M. A., & Taliercio, A. (2017). Sisal fiber reinforced hollow concrete blocks for structural applications: Testing and modeling. Construction and Building Materials, 151, 98–112. https://doi.org/10.1016/j.conbuildmat.2017.06.072.

88. Sumithra, K.T.R.; Dadapheer, A.S. (2017). Experimental Investigation on the Propreties of Sisal Fiber Reinforced Concrete. Int. Res. J. Eng. Technol. 4, 2774–2777.

89. Swar, S.K, S.K Sharma, H.K Sharma, and S Kumar. (2015). "Structural Characteristics of HPDSP Concrete on Beam-Column Joints." International Journal of Civil, Environmental, Structural, Construction and Architectural Engineering 9(9): 1181–86.

90. Tipka, M.; Vašková, J. (2017). Modulus of Elasticity in Tension for Concrete and Fiber Reinforced Concrete. Sol. St. Phen. 259, 35–40.

91. Tolêdo Filho, R.D.; Joseph, K.; Ghavami, K.; England, G.L. (1999). The Use of Sisal Fiber As Reinforcement in Cement Based Composites. Rev. Bras. Eng. Agríc. Ambient. 3, 245–256.

92. Tsonos, A.G., Tegos, I.A. and Penelis, G.G. (1992). “Seismic Resistance of Type 2 exterior beam-column joints reinforced with inclined bars”, ACI structural Journal, Vol.90, No 1, pp. 3-12.

93. Vajje, S., & Krishna, M. (2014). Study on Addition of the Natural Fibers into Concrete Saandeepani. International Journal of Scientific & Technology Research, 2(3), 445–456. https://doi.org/10.1061.

94. Voyiadjis, G.Z., Taqieddin, Z.N. (2009), Elastic plastic and damage model for concrete materials: Part I – Theoretical formulation. Int J Struct Changes Solids – Mech Appl,1(1):31–59.

95. Watanabe, K., et al. (2010), “Synergetic effect of steel fibers and shear reinforcing bars on the shear-resistance mechanisms of RC linear members”, Construction and Building Materials, 24(12), 2369-2375.

96. Wu, J.Y., Li, J., Faria, R. (2006). An energy release rate-based plastic-damage model for concrete, Int J Solids Struct 43(3):583–612.

97. Zhao, Xuefeng, Robert K.Y. Li, and Shu-Lin Bai. (2014). “Mechanical Properties of Sisal Fiber Reinforced High Density Polyethylene Composites: Effect of Fiber Content, Interfacial Compatibilization, and Manufacturing Process.” Composites Part A: Applied Science and Manufacturing 65: 169–74.

APPENDIX A1

Table A.1: Some reported cases of building collapse in Africa due to earthquake

Country	Date	Magnitude	Lives lost	Structures damaged
Mozambique	22/02/2006	7	4	294
DR Congo	07/08/2015	5.8	3	17
Egypt	22/11/1995	7.3	8	65
Botswana	03/04/2017	6.5	-	-
South Africa	05/08/2014	6.3	1	> 600
Rwanda	03/02/2008	6.2	>25	17

Source: Wikipedia

Table A.2: Destructive earthquakes in Algeria since 1980

Earthquake	Date	Magnitude	Dead	Injured	Homeless	Structures destroyed*
El-Asman	10 /10/980	10	5000	20000	120000	7000
Constantine	27/10/1985	8-9	5	300	-	-
Chenoua	29/10/1989	8	35	700	50000	4095
Beni Chougrane	18/08/1994	8	172	292	10000	715
Temouchent	22/12/1999	7	25	174	25000	600
Boumerdes	21/05/2003	9	2287	11000	100000	19000

* A housing unit with a multi-storey building is typically counted as on structure

Source: Algerian Ministry of Housing

APPENDIX A2

Design of exterior cantilever beam

A cantilever beam of span 0.8m carrying a slab of length 3m and thickness of 150mm and live load of 1.5kN/m^2. The beam has a width of 150mm and overall depth of

200mm. The concrete grade of 35N/mm^2 and the longitudinal yield steel 10mm diameter and mild steel of 6mm for the links. Using a concrete cover of 25mm. A typical pan view is shown in Figure 7.1.

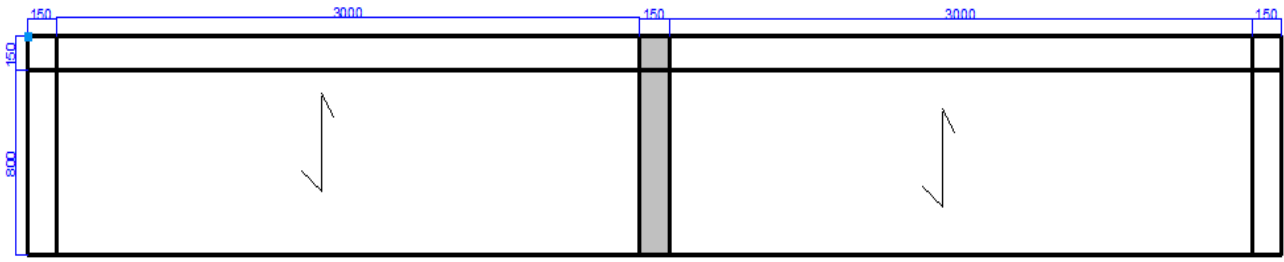

Figure A 1: Plan view of a building section

Check for deflection

$$\frac{L}{d} \leq 7 \text{ (Table 3.9 BS8110} - 1)$$

$$d \leq \frac{L}{7} = \frac{800}{1.3 \times 7} = 87.91\text{mm}$$

$$\text{Overall depth} = d + Cc + \emptyset + \partial = 87.91 + 25 + 10 + 6$$

$$= 128.91\text{mm(adopt 150mm thickness)}$$

$$\text{Actual effective depth } = h - C_c - \emptyset - \partial = 150 - 25 - 10 - 6 = 109\text{mm}$$

Slab load

$$\text{Self weight } = 24 \times 0.15 = 3.6\ \text{KN/m}^2$$

$$\text{Partion and finishes} = 1.0\ \text{KN/m}^2$$

$$G_k = 4.60\text{KN/m}^2$$

$Q_k = 1.5\ KN/m^2$

Slab load $= 1.4G_k + 1.6Q_k = (1.4 \times 4.60) + (1.6 \times 1.5) = 8.84\ kN/m$ per m width

Total Slab load $= 8.84 \times 2.5 = 22.10\ KN/m$

Beam load

Beam own Load $= 0.15 \times 0.15 \times 24 \times 1.4 = 0.756\ KN/m$

Beam finishes $= 1.4 \times 0.5\ = 0.7KN/m$

Load on beam $= 22.10 + 0.756 + 0.7 = 23.56\ KN/m$

Fixed end moment $= \frac{wl^2}{2} = \frac{23.56 \times 0.8^2}{2} = 7.54\ KN.m$

Ultimate moment of resistance $M_u = 0.156f_{cu}bd^2 = 0.156 \times 30 \times 150 \times 109^2 = 8.34KN.m$ (Section 3.4.4.4 BS 8110-1)

Fixed end moment $= 7.54\ KN.m <$ Ultimate moment of resistance

$= 8.34\ KNm$

(Design tensile reinforcement only)

Design

$k = \frac{M}{f_{cu}bd^2} < 0.156$

$k = \frac{7.54 \times 10^6}{30 \times 150 \times 109^2} = 0.141 > 0.156$ (Design for tension reinforcement only)

$$z = d\left[0.5 + \sqrt{0.25 - \frac{k}{0.9}}\right] = d\left[0.5 + \sqrt{0.25 - \frac{0.141}{0.9}}\right] = 0.81d < 0.95d, Ok$$

$$z = 0.81 \times 109 = 88.29mm$$

Depth to Neutral Axis

$x = \frac{d-z}{0.45} = \frac{109-88.29}{0.45} = 46.02mm < 0.5d\ (0.5 * 109 = 54.5mm)$ Tension steel reinforcement will have yielded

$$A_s = \frac{M}{0.95f_y z} = \frac{7.54 \times 10^6}{0.95 \times 600 \times 88.29} = 149.83\ mm^2$$

Minimum percentage of reinforcement in beams (Table 3.25 section C BS 8110-1)

$$A_{smin} = 0.2\%bh = \frac{0.20}{100} \times 150 \times 150 = 45mm^2$$

Maximum percentage of reinforcement in beams (Section 3.12.6. BS 8110-1)

$$A_{smax} = 4\%bh = \frac{4}{100} \times 150 \times 150 = 900mm^2$$

$A_{smin} < A_s < A_{smax}$

Area of one steel bar $= \pi r^2 = \pi \times 5^2 = 78.54\ mm^2$

$$\text{Number of bars} = \frac{149.83}{78.54} = 1.91 \approx 2$$

Minimum Spacing between reinforcemens (depth)

$$= (150 - (2 \times 10) - (2 \times 25) - (2 \times 6))/1 = 68\ mm$$

Minimum Spacing between reinforcemens(width)

$$= \frac{150 - (2 \times 10) - (2 \times 25) - (2 \times 6)}{1} = 68 \text{ mm}$$

Minimum distance between bars > max aggregate size+ 5mm (Clause 3.12.11.1 BS 8110-1)

68mm mm > 25 mm : 68 mm > 25 mm OK

Provide 2T10 (157.08mm^2) at the Top of the Beam

Provide 2T10 (157.08mm^2) at the Bottom of the Beam

Check for shear

Concrete shear stress$= \frac{100A_s}{bd} = \frac{100 \times 157.08}{150 \times 109} = 0.96$

Allowable concrete shear stress $V_C = \frac{0.79}{1.25} \times \left(\frac{100A_s}{bd}\right)^{\frac{1}{3}} \times \left(\frac{400}{d}\right)^{\frac{1}{4}} \times \left(\frac{f_{cu}}{25}\right)^{\frac{1}{3}}$ (Table 3.8, BS 8110-1) $= \frac{0.79}{1.25} * (0.96)^{\frac{1}{3}} * \left(\frac{400}{109}\right)^{\frac{1}{4}} \left(\frac{30}{25}\right)^{\frac{1}{3}} = 0.914 \text{ N/mm}^2$

$0.5V_C = 0.5 \times 0.914 = 0.457 \text{ N/mm}^2$

$V_C + 0.4 = 0.914 + 0.4 = 0.437 \text{ N/mm}^2$

Shear force: $V = \frac{wl}{2} = \frac{23.56 \times 0.8}{2} = 9.42\text{KN}$

Shear stress: $\Delta = \frac{V}{bd} = \frac{9.42 \times 10^3}{150 \times 109} = 0.576 \text{ N/mm}^2$

$0.5V_C < \Delta < (V_C + 0.4)$

$0.457\text{N/mm}^2 < 0.576\text{N/mm}^2 < 1.314\text{N/mm}^2$

$$\text{Spacing} = S_v = \frac{A_{sv} 0.95 f_{yz}}{0.4 b_v} = \frac{2 * (\pi * 3^2) * 0.95 \times 250}{0.4 \times 150} = 223.83 \text{ mm}$$

Section 3.4.5.5 of BS8110: 1 stipulates that spacing of links should not exceed $0.75d = 0.75 \times 109 = 81.75$mm.

$S_v > 81.75mm$

Provide "two legged" R 6mm @80 mm c/c

A4. Design of short braced column

The design of longitudinal and links of a 150 X 200mm column 500 mm long, short braced column carrying an axial load of 300kN and a moment of 7.54 KNm from the cantilever beam. The concrete grade of 35N/mm^2. High yield steel for main reinforcements and mild steel for links steel grade is 460N/mm^2 with a concrete cover of 25mm.

Design

Effective height of column $l_e = \beta l_o$

Top End condition =1 bottom end condition =3

$\beta = 1.6 \quad l_o = 500$mm

$l_e = 1.6 \times 500 = 800$ mm

$\frac{l_e}{h} = \frac{800}{150} = 5.33 < 10$ (unbraced column) **COLUMN IS SHORT**

Crack control in column (Section 3.8.6 BS8110 − 1)

$300\text{kN} > 0.2 f_{cu} A_c = 0.2 \times 35 \times 150 \times 200 = 210kN$

The fixed end moment from the beam along x-x=7.54 kN.m.

$$\frac{\mathrm{M}}{\mathrm{b\ h^2}} = \frac{7.54\ \times 10^6}{200 * 150^2} = 1.68\mathrm{N/mm^2}$$

Load from upper floors = 300 KN

Load from Beam = 9.42 KN

$$N = 300 + 9.42 = 309.42\ KN$$

$$\frac{N}{b\ h} = \frac{309.42 \times 10^3}{200 \times 150} =\ 10.314\ N/mm^2$$

$$d = \mathrm{h} - \mathrm{C_c} - \emptyset - \partial = 150 - 25 - \frac{12}{2} - 6 = 113\ \mathrm{mm}$$

$$\frac{d}{h} = \frac{113}{150} = 0.753$$

$\frac{A_{sc}}{b\ h} = 1.3\%$ From Chart 31, BS8110-3

$$A_{sc} = \frac{1.3 \times 200 \times 150}{100} = 390\ mm^2$$

$$No\ bars = \frac{390}{\frac{\pi}{4} * 12^2} = 3.45\ \approx 4$$

PROVIDE 4T12 (452.39mm^2)

Links

Diameter of links should be $= \frac{\emptyset}{4} = \frac{12}{4} = 3\mathrm{mm}$ which is

$< \mathrm{than\ 6mm\ (Minimum)}$

Use 6 mm

Spacing $= 12 \times 12 = 144 \approx 140$ mm

PROVIDE R6 @ 125mm

APPENDIX B

Laboratory results for all the combinations

Table A- 1: Slump results

Specimen	Slump(mm)	Compaction factor	Wet density(kg/m^3)
M0.0	92	0.93	2573.50
M0.5	69	0.88	2463.45
M1.0	52	0.85	2454.27
M1.5	40	0.80	2442.16
M2.0	20	0.73	2439.50

Table A- 2: Water absorption at 28 days curing time.

Fiber content	Trial 1(%)	Trial 2(%)	Trial 3(%)	Average (%)
M0.0	4.809	4.915	4.928	4.884
M0.5	6.665	6.216	6.017	6.299
M1.0	6.588	6.313	6.328	6.410
M1.5	7.048	6.268	6.169	6.495
M2.0	7.116	6.948	7.792	7.285

Table A- 3: Compressive Strength of cubes at 7 days curing time.

Fiber content	Trial 1(MPa)	Trial 2(MPa)	Trial 3(MPa)	Average(MPa)
M0.0	28.44	27.89	29.13	28.49
M0.5	23.97	26.32	25.03	25.11
M1.0	25.75	23.76	23.45	24.32
M1.5	24.56	23.21	23.27	23.68
M2.0	22.65	20.86	21.53	21.68

Table A- 4: Compressive Strength of cylinders at 7 days curing time.

Specimen	Trial 1(MPa)	Trial 2(MPa)	Trial 3(MPa)	Average(MPa)
M0.0	20.45	19.53	21.59	20.52
M0.5	17.15	17.42	17.18	17.25
M1.0	15.55	16.38	16.21	16.05
M1.5	13.38	13.58	14.35	13.77
M2.0	10.99	11.88	11.97	11.61

Table A- 5: Compressive Strength of cubes at 28 days curing time

Specimen	Trial 1(MPa)	Trial 2 (MPa)	Trial 3(MPa)	Average(MPa)
M0.0	38.09	38.21	32.81	36.37
M0.5	38.43	34.91	33.51	35.62
M1.0	33.21	34.99	32.45	33.55
M1.5	32.54	31.12	29.34	31.00
M2.0	30.29	30	30.98	30.42

Table A- 6: Compressive Strength of cylinders at 28 days curing time

Specimen	Trial 1(MPa)	Trial 2 (MPa)	Trial 3(MPa)	Average(MPa)
M0.0	30.12	29.35	29.97	29.81
M0.5	28.83	29.24	27.6	28.56
M1.0	26.73	25.498	26.89	26.37
M1.5	23.43	25.21	24.54	24.39
M2.0	22.29	22.48	22.04	22.27

Table A- 7: Splitting Tensile Strength at 7 days curing time.

Specimen	Trial 1(MPa)	Trial 2 (MPa)	Trial 3(MPa)	Average(MPa)
M0.0	2.07	2.05	2.09	2.07
M0.5	2.34	2.57	2.49	2.47
M1.0	2.71	2.67	2.65	2.68
M1.5	2.34	2.49	2.43	2.42
M2.0	2.19	2.18	2.17	2.18

Table A- 8: Splitting Tensile Strength at 28 days curing time.

Specimen	Trial 1(MPa)	Trial 2 (MPa)	Trial 3(MPa)	Average(MPa)
M0.0	2.63	2.45	1.98	2.353
M0.5	3.01	3.09	3.05	3.050
M1.0	3.23	3.45	3.71	3.463
M1.5	2.76	2.62	2.85	2.743
M2.0	2.73	2.32	2.48	2.509

Table A- 9: Density of concrete at 28 days curing time.

Specimen	Trial 1(g/cm^3)	Trial 2 (g/cm^3)	Trial 3(g/cm^3)	Average(g/cm^3))
M0.0	2.050	2.073	2.238	2.120
M0.5	2.022	2.129	2.137	2.096
M1.0	2.031	2.059	2.055	2.048
M1.5	2.018	2.049	2.056	2.041
M2.0	2.142	1.983	1.970	2.032

Table A- 10: Effect of Sisal fiber on concrete cube f_{cu} at 7 days curing time.

SUMMARY

Groups	*Count*	*Sum*	*Average*	*Variance*
0% FIBER	3	85.46	28.48666667	0.386033333
0.5% FIBER	3	75.32	25.10666667	1.385033333
1.0% FIBER	3	72.96	24.32	1.5577
1.5% FIBER	3	71.04	23.68	0.5817
2.0% FIBER	3	65.04	21.68	0.8179

ANOVA

Source of Variation	*SS*	*df*	*MS*	*F*	*P-value*	*F crit*
Between Groups	74.39744	4	18.59936	19.66784866	9.9168E-05	3.47804
Within Groups	9.456733333	10	0.945673333			
Total	83.85417333	14				

Table A- 11: Effect of Sisal fiber on concrete cube f_{cu} at 28days curing time.

SUMMARY

Groups	*Count*	*Sum*	*Average*	*Variance*
0% FIBER	3	109.11	36.37	9.5088
0.5% FIBER	3	106.85	35.61666667	6.426133333
1.0% FIBER	3	100.65	33.55	1.6996

1.5% FIBER	3	93	31	2.5708
2.0% FIBER	3	91.27	30.42333333	0.253433333

ANOVA

Source of Variation	*SS*	*df*	*MS*	*F*
Between Groups	85.13170667	4	21.28292667	5.201419766
Within Groups	40.91753333	10	4.091753333	
Total	126.04924	14		

Table A- 12: Effect of Sisal fiber On Splitting Tensile strength of concrete at 7 days

Groups	*Count*	*Sum*	*Average*	*Variance*
0% FIBER	3	6.218	2.07267	0.000500333
0.5% FIBER	3	7.404	2.46800	0.012976
1.0% FIBER	3	8.031	2.67700	0.000907
1.5% FIBER	3	7.26	2.42000	0.0057
2.0% FIBER	3	6.54	2.18000	0.0001

ANOVA

Source of Variation	*SS*	*df*	*MS*	*F*	*P-value*	*F crit*
Between Groups	0.691953067	4	0.1729883	42.85423	2.91E-06	3.47805
Within Groups	0.040366667	10	0.0040367			
Total	0.732319733	14				

Table A- 13: Effect of Sisal fiber On Splitting Tensile strength of concrete at 28 days

SUMMARY

Groups	*Count*	*Sum*	*Average*	*Variance*
0% FIBER	3	7.06	2.3533333	0.112633
0.5% FIBER	3	9.15	3.05	0.0016
1.0% FIBER	3	10.39	3.4633333	0.057733

1.5% FIBER	3	8.23	2.7433333	0.013433
2.0% FIBER	3	7.528	2.5093333	0.04384

ANOVA

Source of Variation	*SS*	*df*	*MS*	*F*	*P-value*	*F crit*
Between Groups	2.3606171	4	0.5901543	12.87196	0.00059	3.47805
Within Groups	0.4584807	10	0.0458481			
Total	2.8190977	14				

Table A- 14: Measured and computed Young's modulus

Specimen	measured Ec (MPa)	ACI 318M-08	ACI 318	CSA 123-3-04	IS 456-1979	BS8110-2	TS50, (2005)	Eurocode 1992-1-1
M0.0	25086.77	25320.29	22617.24	24242.83	30632.16	24995.62	31508.71	31467.22
M0.5	29138.60	24823.49	21795.01	23767.17	30031.14	24700.19	31165.18	30932.73
M1.0	31654.19	25118.09	21299.78	24049.24	30387.55	24875.66	31368.90	30658.73
M1.5	28926.78	23611.45	19917.29	22606.71	28564.83	23969.35	30327.06	29731.97
M2.0	25379.31	22844.91	19139.82	21872.79	27637.48	23499.38	29797.01	28704.08

Table A- 15: Sorptivity value of test specimen

Time	Sorptivity value				
$\sqrt{time}$	M0.0	M0.5	M1.0	M1.5	M2.0
0.000	0.000	0.000	0.000	0.000	0.000
7.746	0.256	0.822	1.322	1.256	1.333
17.321	0.822	1.067	1.656	1.722	2.233
24.495	0.978	1.233	1.800	2.044	2.522
34.641	1.022	1.400	2.056	2.367	3.000
42.426	1.267	1.600	2.367	2.811	3.489
60.000	2.178	2.556	3.256	3.356	4.456
84.853	2.278	2.678	3.644	3.911	4.633
103.923	2.833	3.678	3.944	4.444	5.367
126.807	3.656	4.156	4.867	5.356	6.389
146.969	3.933	4.811	5.167	5.700	6.956
246.982	8.322	9.611	10.600	11.833	11.956
327.811	10.056	11.056	12.500	13.556	13.967
439.409	10.978	12.033	13.856	14.489	14.900
527.466	11.500	12.744	14.867	14.967	15.344
604.136	11.878	13.167	15.378	15.222	15.500
664.620	11.967	13.456	15.456	15.278	15.656

729.192	12.211	13.789	15.544	15.478	16.011
786.779	12.411	14.089	15.611	15.622	16.267

Table A- 16: Weight of specimen before immersion in basic medium

Specimen	Trial 1(g)	Trial 2(g)	Trial 3(g)	average(g)
M0.0	7776	8089	7904	7923.0
M0.5	7923.5	8503.5	8109.5	8178.8
M1.0	8144	8256.2	8147.5	8182.6
M1.5	8570	8315.5	8472	8452.5
M2.0	8210.5	8412.5	8107	8243.3

Table A- 17: Weight of specimen after immersion in basic medium for 45 days

Specimen	Trial 1(g)	Trial 2(g)	Trial 3(g)	average(g)
M0.0	7776.122	8088.647	7903.128	7922.63
M0.5	7922.634	8503.18	8109.148	8178.32
M1.0	8143.14	8255.154	8147.65	8181.98
M1.5	8569.679	8314.5	8470.9	8451.69
M2.0	8209.153	8411.665	8105.143	8241.99

Table A- 18: Weight of specimen after immersion in basic medium for 90 days

Specimen	Trial 1(g)	Trial 2(g)	Trial 3(g)	average(g)
M0.0	7775.12	8088.23	7903.56	7922.30
M0.5	7922.04	8503.28	8108.67	8178.00
M1.0	8143.24	8254.14	8147.22	8181.53
M1.5	8569.15	8314.12	8469.82	8451.03
M2.0	8209.14	8411.62	8104.48	8241.75

Table A- 19: Weight of specimen before immersion in acid medium

Specimen	Trial 1(g)	Trial 2(g)	Trial 3(g)	average(g)
M0.0	8201.58	7983	8054	8079.53
M0.5	8364.5	8013.5	8248.5	8208.83

M1.0	8256.5	8167	8194.5	8206
M1.5	8105.5	8130.5	8290	8175.33
M2.0	8293	8504.5	8217	8338.17

Table A- 20: Weight of specimen after immersion in basic medium for 45 days

Specimen	Trial 1(g)	Trial 2(g)	Trial 3(g)	average(g)
M0.0	8180.5	7841	7904	7975.17
M0.5	8203.3	7950	8105	8086.10
M1.0	8194	8002	8010.5	8068.83
M1.5	7886.5	8022	8149	8019.17
M2.0	8127	8330.5	8008	8155.17

Table A- 21: Weight of specimen after immersion in basic medium for 90 days

Specimen	Trial 1(g)	Trial 2(g)	Trial 3(g)	average(g)
M0.0	8150.5	7826.5	7863	7946.67
M0.5	8160	7926	8045	8043.67
M1.0	8034	7933.5	7944.5	7970.67
M1.5	7714.5	7955.5	7985.1	7885.03
M2.0	7993	8101.5	7916	8003.50

Table A- 22: Test result for beam-column joints (M0.0)

Load (kN)	LVDT(mm)	Stiffness	Strain A	Strain B	Strain C	Strain D
0	0	0				
0.518828	0.4588	1.130837	3.44E-05	3.69E-05	1.56E-04	3.32E-04
2.270574	0.9752	2.328316	5.04E-05	4.92E-05	3.48E-04	5.90E-04
4.165862	1.5976	2.607575	8.24E-05	6.15E-05	5.64E-04	9.35E-04
4.717692	1.794	2.629705	0.000105	8.61E-05	6.24E-04	1.07E-03
5.000207	1.8976	2.635017	0.00013	9.84E-05	6.96E-04	1.23E-03
6.321441	2.4132	2.619526	0.00016	1.11E-04	8.88E-04	1.38E-03
7.341833	2.8528	2.573553	0.000194	1.23E-04	1.01E-03	1.51E-03
7.424791	2.8904	2.568776	0.000224	1.48E-04	1.02E-03	1.57E-03
7.482642	2.9168	2.56536	0.00025	1.72E-04	1.07E-03	1.61E-03
7.637904	2.9884	2.555851	0.000261	1.85E-04	1.19E-03	1.62E-03
8.850604	3.5896	2.465624	0.000276	1.85E-04	1.25E-03	1.64E-03
9.573683	3.9904	2.399179	0.000282	2.09E-04	1.31E-03	1.65E-03

10.30166	4.456974	2.311357	0.000295	2.09E-04	1.36E-03	1.66E-03
11.15565	4.788122	2.329859	0.000306	2.21E-04	1.38E-03	1.66E-03
11.19986	4.957464	2.25919	0.000308	2.21E-04	1.40E-03	1.69E-03
11.33399	5.048316	2.245102	0.000322	2.34E-04	1.44E-03	1.70E-03
13.16368	5.40891	2.433702	0.000337	2.46E-04	1.46E-03	1.73E-03
13.46981	5.769504	2.334656	0.000349	2.83E-04	1.48E-03	1.80E-03
13.91818	5.906184	2.356544	0.000397	3.94E-04	1.51E-03	1.85E-03
14.47302	6.379941	2.26852	0.000525	4.92E-04	1.54E-03	1.86E-03
14.59338	6.490692	2.248356	0.000672	7.01E-04	1.56E-03	1.89E-03
14.96245	6.851286	2.183889	0.000785	8.73E-04	1.64E-03	1.93E-03
15.29882	7.21188	2.121336	0.000861	1.17E-03	1.70E-03	1.93E-03
15.92712	7.572474	2.103291	0.000934	1.45E-03	1.76E-03	1.93E-03
16.21235	7.933068	2.043642	0.000934	1.82E-03	1.84E-03	1.94E-03
16.71575	9.01485	1.854246	0.000966	2.05E-03	2.05E-03	1.97E-03
16.87198	9.375444	1.799592	0.000968	2.48E-03	2.24E-03	2.03E-03
16.92945	10.09663	1.676743	0.000972	2.50E-03	2.26E-03	2.04E-03
17.10631	10.45723	1.635836	0.000977	2.51E-03	2.28E-03	2.04E-03
17.26253	10.94003	1.577924	0.000982	2.51E-03	2.41E-03	2.04E-03
17.49686	12.92912	1.353291	0.000994	2.53E-03	2.60E-03	2.07E-03
17.80931	12.92912	1.377457	0.001004	2.57E-03	2.80E-03	2.08E-03
17.80931	13.2451	1.344596	0.001009	2.67E-03	2.89E-03	2.09E-03
17.88742	13.5466	1.320436	0.001021	2.71E-03	2.93E-03	2.09E-03
18.19986	13.7476	1.323858	0.001063	2.78E-03	2.94E-03	2.10E-03
18.27797	14.0491	1.301007	0.001075	2.82E-03	2.96E-03	2.10E-03
18.35609	14.5516	1.261448	0.001106	2.92E-03	2.99E-03	2.12E-03
18.46221	14.91822	1.237561	0.001236	2.93E-03	3.00E-03	2.15E-03
18.59042	15.91277	1.168271	0.001277	2.95E-03	3.07E-03	2.18E-03
18.66853	16.65014	1.121224	0.001391	2.98E-03	3.19E-03	2.18E-03
19.05908	19.89096	0.958178	0.001501	3.00E-03	3.24E-03	2.25E-03
19.1372	20.01796	0.956001	0.001635	3.04E-03	3.29E-03	2.30E-03
19.44964	20.55363	0.946287	0.001742	3.05E-03	3.34E-03	2.32E-03
19.60586	20.55363	0.953888	0.00183	3.05E-03	3.38E-03	2.32E-03
19.68397	21.01249	0.936775	0.001926	3.05E-03	3.43E-03	2.34E-03
19.84019	21.21943	0.935001	0.002125	3.08E-03	3.43E-03	2.34E-03
20.07453	21.93496	0.915184	0.002411	3.09E-03	3.43E-03	2.36E-03
20.15264	22.8746	0.881005	0.002605	3.12E-03	3.44E-03	2.36E-03
20.30886	23.86915	0.850841	0.00279	3.16E-03	3.48E-03	2.36E-03
20.54319	24.8637	0.826232	0.002918	0.0031857	0.003516	0.002374
20.69942	25.85825	0.800496	0.003052	0.0032349	0.00354	0.002399
20.85564	26.8528	0.776665	0.003144	0.0032595	0.003576	0.002423
21.0663	26.723	0.788321	0.003144	0.0032595	0.003576	0.002423

Table A- 23: Test result for beam-column joints (M0.5)

LVDT (mm)	LOAD (kN)	stiffness	Strain A	Strain B	Strain C	Strain D
0	0	0				
0.297248	0.84294	2.835813866	1.6348E-05	6E-05	0.000531	0.000109
0.579712	2.10735	3.635167117	2.6156E-05	0.000109	0.000884	0.000186
0.859712	3.31155	3.851929483	3.5965E-05	0.000169	0.001106	0.00028
2.00928	4.51575	2.247446847	4.7081E-05	0.000245	0.001128	0.000404
2.411136	5.78016	2.397276636	5.8851E-05	0.000322	0.00115	0.000536
2.78208	7.10478	2.553765528	8.6315E-05	0.000491	0.001172	0.00087
3.214848	9.57339	2.977867072	0.00011051	0.000556	0.001194	0.001033
3.896256	10.47654	2.688873626	0.00014778	0.000616	0.001216	0.001228
4.420416	11.19906	2.533485536	0.00020009	0.00067	0.00126	0.001391
5.224128	11.86137	2.270497584	0.0003191	0.000719	0.001282	0.001787
5.319888	13.12578	2.467303823	0.00039299	0.000736	0.001304	0.001896
5.625984	13.18599	2.343765997	0.00053489	0.000747	0.001327	0.001943
6.02784	14.09211	2.337837434	0.00077945	0.000758	0.001371	0.002028
6.429696	14.99211	2.331698108	0.00090107	0.000796	0.001393	0.002036
7.233408	15.15402	2.095004181	0.00102008	0.000986	0.001459	0.002082
7.567728	15.67593	2.071418265	0.00111294	0.001134	0.001481	0.002106
7.635264	16.03593	2.10024565	0.00122475	0.00115	0.001481	0.002121
8.03712	16.17975	2.013127837	0.0013405	0.001172	0.001548	0.002129
8.138976	16.21548	1.992324342	0.00140719	0.001199	0.001592	0.002129
8.241792	16.30548	1.978390137	0.00149416	0.001199	0.001614	0.002145
8.97653	17.5172	1.951444489	0.00159944	0.001232	0.001636	0.002176
9.3288	18.3	1.961667095	0.00169687	0.001275	0.001658	0.002183
10.0464	18.377	1.829212454	0.00189696	0.001281	0.001835	0.002207
10.4052	18.377	1.766136163	0.00189958	0.001308	0.001857	0.00223
10.764	18.5368	1.72211074	0.00192116	0.001319	0.001924	0.002246
11.1228	18.9363	1.702475995	0.00195974	0.001455	0.001946	0.002261
11.4816	19.0961	1.663191541	0.00198328	0.001466	0.002012	0.002269
12.1992	19.2559	1.578455964	0.00198982	0.001466	0.002078	0.002277
12.558	19.4956	1.552444657	0.00200682	0.001526	0.002123	0.002277
12.9168	19.8152	1.534064164	0.00208136	0.001597	0.002167	0.002277
14.352	20.0939	1.400076644	0.00213433	0.001619	0.002189	0.002277
14.7108	20.2147	1.374140088	0.00221737	0.001711	0.002211	0.002292
15.7872	20.2946	1.28550978	0.0022298	0.001918	0.002277	0.0023
16.8636	20.3745	1.20819398	0.00227034	0.002011	0.002366	0.0023
17.5812	20.6142	1.172513822	0.00232788	0.002011	0.00241	0.0023
18.6576	20.774	1.113433668	0.00242466	0.002104	0.002543	0.0023
18.6576	20.9338	1.121998542	0.00249136	0.002115	0.002675	0.0023
19.3752	21.0936	1.088690697	0.00252798	0.002491	0.002786	0.002315
20.0928	21.4132	1.065715082	0.00263849	0.002529	0.00283	0.002315
20.8104	21.573	1.036645139	0.00278692	0.002572	0.002874	0.002323

21.528	21.6529	1.005801747	0.00283204	0.002692	0.002963	0.002323
22.2456	21.6529	0.973356529	0.0028667	0.002856	0.003118	0.002331
22.9632	21.7328	0.946418618	0.00287912	0.002878	0.003228	0.002339
24.0396	21.8127	0.907365347	0.00290724	0.002916	0.003272	0.002347
24.7572	21.8127	0.881064902	0.00293601	0.003096	0.003317	0.002354
25.4748	21.8926	0.859382606	0.00298309	0.003139	0.003361	0.002362
25.814	21.9725	0.851185403	0.00299421	0.003156	0.003405	0.00237
25.8336	21.9725	0.850539607	0.00303279	0.003221	0.003427	0.002385
25.8532	22.0524	0.852985317	0.00307987	0.003221	0.00356	0.002409
24.5655432	22.64947642	0.922001856	0.00307987	0.003221	0.00356	0.002409
25.4105496	22.64947642	0.891341461	0.00307987	0.003221	0.00356	0.002409
25.2909072	22.64947642	0.895558085	0.00307987	0.003221	0.00356	0.002409

Table A- 24: Test result for beam-column joints (M1.0)

LVDT (mm)	LOAD (kN)	stiffness	Strain A	Strain B	Strain C	Strain D
0.0	0.0	0.0				
0.00000000	0.87191286	0.00000000	0.00000000	0.00001290	0.00000000	0.00000000
0.31848000	1.63797820	5.14311166	0.00000084	0.00001290	0.00000195	0.00000650
0.62112000	2.35578085	3.79279504	0.00000084	0.00003870	0.00004720	0.00000650
0.92112000	3.05842508	3.32033294	0.00000506	0.00063210	0.00006861	0.00003248
2.15280000	4.90903170	2.28030086	0.00001096	0.00068370	0.00012652	0.00086384
2.58336000	6.82999752	2.64384272	0.00001096	0.00069660	0.00016836	0.00101972
2.98080000	8.28409121	2.77915030	0.00001349	0.00070950	0.00030948	0.00121457
4.17456000	11.02850873	2.64183740	0.00001602	0.00077400	0.00047881	0.00142890
4.73616000	11.58618558	2.44632478	0.00001855	0.00078690	0.00088367	0.00165623
5.59728000	13.51193011	2.41401719	0.00001939	0.00079980	0.00105252	0.00185108
5.69988000	13.74388510	2.41125868	0.00002192	0.00082560	0.00138243	0.00185757
5.73397200	13.82110193	2.41038881	0.00002360	0.00082560	0.00156831	0.00189005
6.02784000	14.48986858	2.40382435	0.00002529	0.00086430	0.00216148	0.00190953
6.39790560	14.77539348	2.30941099	0.00002529	0.00086430	0.00235271	0.00191603
6.45840000	16.46231706	2.54897762	0.00020232	0.00087720	0.00255660	0.00192902
6.88896000	16.73597529	2.42939069	0.00032034	0.00090300	0.00263591	0.00195500
7.24291200	17.57660175	2.42673137	0.00059853	0.00092880	0.00263883	0.00196149
7.75008000	17.81095644	2.29816420	0.00075870	0.00094170	0.00265051	0.00196799
8.81220960	18.90510051	2.14533033	0.00102256	0.00108360	0.00265148	0.00197448
9.53650080	19.55018697	2.05003778	0.00117683	0.00119970	0.00266024	0.00198098
10.07971920	20.01351900	1.98552347	0.00134206	0.00125130	0.00267727	0.00199397
10.62293760	20.72831547	1.95127904	0.00152414	0.00129000	0.00267825	0.00201345
11.10579840	20.72831547	1.86644082	0.00187989	0.00131580	0.00268117	0.00206541
11.34722880	20.82942920	1.83564019	0.00202657	0.00134160	0.00272642	0.00208490
12.31295040	21.23388414	1.72451634	0.00204765	0.00147060	0.00275270	0.00209789

12.67509600	21.33499787	1.68322180	0.00205523	0.00163830	0.00276729	0.00210438
13.33902960	21.43611161	1.60702182	0.00207884	0.00172860	0.00279211	0.00213036
13.58046000	21.53722534	1.58589807	0.00210244	0.00180600	0.00281352	0.00214335
13.64081760	21.63833908	1.58629341	0.00211930	0.00188340	0.00284515	0.00214985
14.30475120	21.73945281	1.51973652	0.00212183	0.00214140	0.00291522	0.00214985
14.66689680	21.73945281	1.48221216	0.00217831	0.00223170	0.00305147	0.00216933
15.57226080	21.84056654	1.40253023	0.00222721	0.00225750	0.00310402	0.00216933
15.63261840	21.84056654	1.39711506	0.00226514	0.00238650	0.00315122	0.00216933
16.53798240	21.84056654	1.32063066	0.00227441	0.00248970	0.00317993	0.00217583
17.02084320	21.84056654	1.28316596	0.00235366	0.00261870	0.00323589	0.00218882
17.68477680	21.94168028	1.24071005	0.00243964	0.00273480	0.00327871	0.00220181
18.10728000	22.04279401	1.21734430	0.00246578	0.00278640	0.00331034	0.00222779
18.77121360	22.04279401	1.17428710	0.00252479	0.00283800	0.00333856	0.00223428
19.07300160	22.04279401	1.15570661	0.00263943	0.00287670	0.00336143	0.00224727
19.61622000	22.14390775	1.12885702	0.00274312	0.00287670	0.00340571	0.00224727
19.73693520	22.14390775	1.12195270	0.00275745	0.00292830	0.00343053	0.00224727
20.28015360	22.14390775	1.09190040	0.00283754	0.00295410	0.00345243	0.00225377
20.40086880	22.24502148	1.09039579	0.00284260	0.00296700	0.00346362	0.00229274
21.42694800	22.34613521	1.04289865	0.00286789	0.00309600	0.00348308	0.00229923
21.72873600	22.44724895	1.03306741	0.00291172	0.00312180	0.00348649	0.00230573
22.15123920	22.44724895	1.01336312	0.00299687	0.00318630	0.00350595	0.00231222
22.57374240	22.44724895	0.99439643	0.00303311	0.00321210	0.00351666	0.00234470
23.35839120	22.44724895	0.96099294	0.00303311	0.00321210	0.00352980	0.00235119
24.08268240	22.64947642	0.94048811	0.00304829	0.00321210	0.00352980	0.00239016

Table A- 25: Test result for beam-column joints (M1.5)

LVDT (mm)	LOAD (kN)	stiffness	Strain A	Strain B	Strain C	Strain D
0	0	0				
0	1.054589	0	0.000483	7.06E-05	0.000627	0.000606
0.2669301	1.735121	6.500281	0.000857	0.000116	0.001158	0.00092
0.5217064	2.252645	4.31784	0.00132	0.000174	0.0014	0.001066
0.7825596	3.615686	4.620333	0.00196	0.000183	0.001689	0.00109
1.0434128	4.908632	4.704401	0.002482	0.000183	0.001834	0.00109
1.304266	5.005521	3.837807	0.00327	0.000191	0.001858	0.00109
1.5651192	5.437772	3.47435	0.005615	0.000204	0.001955	0.001114
1.8259724	6.760086	3.702184	0.006442	0.000204	0.002123	0.001138
2.71334207	8.607448	3.172268	0.007417	0.000224	0.00222	0.001259
2.8693852	9.321565	3.248628	0.008264	0.000262	0.002292	0.001356
3.1302384	10.21042	3.261865	0.009328	0.000287	0.002389	0.001405
3.6519448	10.76461	2.947638	0.010106	0.000349	0.002485	0.00155
3.912798	10.98431	2.807278	0.011406	0.000382	0.002582	0.00155

4.1736512	11.69326	2.801686	0.01251	0.000548	0.002654	0.001574
4.4345044	12.22996	2.757908	0.013898	0.000606	0.002654	0.001599
4.6953576	12.43326	2.64799	0.017316	0.000619	0.002678	0.001647
4.9562108	13.05776	2.634627	0.019414	0.00064	0.002703	0.001744
5.217064	13.23187	2.536267	0.020183	0.000656	0.002703	0.001841
5.307764	14.04471	2.64607	0.021059	0.00066	0.002703	0.001865
5.898464	14.52395	2.462328	0.026851	0.000669	0.002727	0.001913
6.6125399	17.31777	2.618928	0.026871	0.000685	0.002751	0.001938
7.18696023	18.39136	2.55899	0.02695	0.000689	0.002751	0.001962
7.68886231	19.23855	2.502132	0.027038	0.000694	0.002775	0.001986
8.38006027	20.33268	2.426317	0.027097	0.00071	0.002799	0.00201
8.66902787	20.22529	2.333052	0.027353	0.00071	0.002823	0.002059
8.95799546	20.42811	2.280433	0.027442	0.000814	0.002823	0.002059
9.24696306	20.80617	2.250054	0.028201	0.000876	0.002871	0.002059
15.026315	21.5347	1.433132	0.028989	0.002106	0.00292	0.002083
15.6042502	21.62449	1.385808	0.029146	0.002197	0.002968	0.002107
16.1821853	21.89386	1.352961	0.029373	0.002272	0.002992	0.002131
16.4711529	21.98365	1.334676	0.029668	0.002608	0.003065	0.002131
17.3380557	22.07344	1.273121	0.029668	0.002733	0.003282	0.002277
18.2049585	22.16323	1.217428	0.03019	0.002941	0.003378	0.002301
22.3097014	22.25303	0.99746	0.0302	0.003049	0.003475	0.002349
25.0230435	22.69606	0.907007	0.030259	0.00319	0.003499	0.002349

Table A- 26: Test result for beam-column joints (M2.0)

LVDT (mm)	LOAD (kN)	Stiffness	Strain A	Strain B	Strain C	Strain D
0	0	0				
0	0.537921	0	2.63E-05	2.99E-06	0.000217	0.002775
0.351	2.354131	6.706928	2.85E-05	3.49E-06	0.000292	0.0037
0.686018	4.319166	6.295994	2.96E-05	3.98E-06	0.000311	0.004037
1.029027	4.891303	4.753327	2.96E-05	3.98E-06	0.000321	0.004962
1.372036	5.184215	3.778483	3.07E-05	3.98E-06	0.000321	0.005551
1.715045	6.55407	3.821515	3.29E-05	3.98E-06	0.00033	0.006139
2.058054	7.612013	3.698646	3.29E-05	3.98E-06	0.000339	0.00656
2.401063	7.698024	3.20609	3.4E-05	3.98E-06	0.000339	0.006812
2.019733	7.758003	3.841103	3.51E-05	3.98E-06	0.000349	0.00698
2.131941	7.918979	3.714447	3.51E-05	3.98E-06	0.000349	0.007401
2.244148	9.176306	4.088993	4.06E-05	3.98E-06	0.000358	0.007653
2.58077	9.925995	3.846137	4.72E-05	4.48E-06	0.000358	0.007821
3.0296	10.68076	3.525468	5.27E-05	4.98E-06	0.000358	0.00799
3.254015	11.24005	3.45421	6.69E-05	4.98E-06	0.000358	0.008326
3.702844	11.61201	3.13597	0.000112	7.97E-06	0.000377	0.00841
5.117135	15.54336	3.037512	0.00015	9.96E-06	0.000396	0.00841

5.418142	15.80174	2.91645	0.000181	1.15E-05	0.000453	0.009924
5.71915	16.59544	2.901732	0.000264	2.79E-05	0.000453	0.011017
6.020158	16.81671	2.793401	0.000564	0.000157	0.000717	0.011017
6.12482	17.84978	2.914335	0.000688	0.000216	0.00181	0.012026
6.229482	18.45886	2.963145	0.000879	0.000321	0.002329	0.012026
6.438806	18.89633	2.934756	0.000958	0.00033	0.002338	0.012951
7.69475	19.66669	2.555858	0.00106	0.00051	0.002404	0.014045
8.113398	20.52591	2.529879	0.001169	0.000568	0.002432	0.017493
8.729229	20.62138	2.362337	0.001273	0.000623	0.002451	0.019427
9.030237	20.81673	2.305225	0.001343	0.0007	0.00248	0.019427
9.331245	20.921	2.242038	0.001366	0.000755	0.002498	0.019764
9.632253	21.20301	2.201251	0.001375	0.000822	0.002527	0.019932
15.65241	21.84047	1.395342	0.001378	0.001048	0.002536	0.0201
16.25443	21.93153	1.349265	0.001401	0.001187	0.002564	0.021025
16.85644	22.20473	1.317284	0.001481	0.001454	0.002583	0.021109
17.15745	22.29579	1.299482	0.001561	0.001681	0.002602	0.021193
18.06047	22.38686	1.23955	0.001715	0.001817	0.00263	0.021361
18.9635	22.47793	1.185326	0.002647	0.001997	0.002668	0.021361
19.56551	22.56899	1.153509	0.002739	0.002842	0.002772	0.02153
20.16753	22.66006	1.123591	0.002897	0.002913	0.003262	0.021698
20.76955	22.78755	1.097162	0.002938	0.003168	0.003328	0.022623
21.37156	22.78755	1.066256	0.002975	0.003169	0.003451	0.023212
22.27459	22.78755	1.023029	0.003009	0.003169	0.003451	0.023212
24.98366	22.78755	0.912098	0.003009	0.00317	0.00346	0.023212

APPENDIX C

Some of the pictures taken during the research:

Figure B- 1: BS Test siesves used for Particle size distribution of aggregates.

Figure B- 2: Slump measurement

Figure B- 3: Compaction factor measurement

Figure B- 4: Concrete cubes and cylinders specimen for testing

Figure B- 5: Compressive Testing using the UTM machine.

Figure B- 6: Splitting Tensile Testing using UTM Machine

Figure B- 7: Testing of beam-column joints set up

Figure B- 8: Testing of steel reinforcement

Figure B- 9: Heating of fibers in ethanol for chemical analysis